Flow Mechanotransduction Response in Endothelial Cell Monolayers and Platelets

Lucas H. Ting

A dissertation
submitted in partial fulfillment of the
requirements for the degree of

Doctor of Philosophy

University of Washington
2013

Reading Committee:

Nathan Sniadecki, Ph.D, Chair

Randal Ching, Ph.D

Wendy Thomas, Ph.D

Program Authorized to Offer Degree:

Mechanical Engineering

University of Washington

Abstract

Flow Mechanotransduction Response in Endothelial Cell Monolayers and Platelets

Lucas H. Ting

Chair of the Supervisory Committee:
Associate Professor Nathan Sniadecki
Mechanical Engineering

Blood flow through the cardiovascular system forms many spatiotemporally dynamic flow fields. This is due to the naturally pulsatile motion of the cardiac cycle, the inherent elastic behavior of arteries and the collapsibility of veins, and changes in activity levels throughout the day leading to changes in flow rate. Shear stress forces from the complex blood flow interact with the cells that comprise blood vessels and blood-borne cells such as platelets. Forces sensed by these cells can cause signaling to occur internally that modify and regulate morphology and cell-to-cell interactions. In this research we investigate endothelial cell monolayers and platelet response to shear stresses, while examining cytoskeletal forces, intercellular forces and complexes, and cell-to-cell protein structures. **Aim 1:** A bioreactor device was designed and fabricated to simulate physiologically relevant

shear profiles across endothelial cells grown as quasi-monolayers on micropost force sensors. The design allowed for the application of both laminar and disturbed shear regimes over time. **Aim 2:** Laminar shear was found to reinforce the natural barrier function by increasing the presence of adherens and tight junctions, while also strengthening and aligning traction forces and intercellular forces. Conversely, static and disturbed flow had lower traction and intercellular forces and lower markers of healthy cell boundary structures. **Aim 3:** Platelets also interact with shear forces, and a microfluidic device was created to expose separated platelets and platelets in whole blood to various shear rates in an effort to study clot contractility development under shear. **Aim 4:** Results demonstrated that platelets adhered to high shear gradient regimes and that increasing shear led to enhanced platelet adhesion and aggregation. Microposts placed behind shear concentration features allowed for the measurement of contractile forces, with higher shears also leading to quicker contractility onset and faster force development. Inhibition of myosin and surface integrins also revealed the critical roles that myosin-II, glycoprotein Ib, integrin $\alpha_{IIb}\beta_3$, and ADP receptor $P2Y_{12}$ have in platelet clot dynamics.

Table of Contents

List of Figures

List of Tables

Acknowledgements

I would like to make acknowledgements to my committee chair and lab PI Nathan Sniadecki for incredible guidance, support, and patience; medical student Jessica Jahn who helped developed and test the permeability and alignment image analysis programs; Sangyoon Han who helped develop and test the force analysis image analysis program; Shirin Feghhi who helped design and perform platelet experiments, Ben Shuman who helped build and prototype the device; Joon Jung who helped analyze images and gather data, Freddy Kuan-Fu Chen and Michelle Shieh for image analysis and western blotting and Marita Rodriguez for statistical analysis on circularity. I would also like to thank my supervisory committee members Mike Regnier, Randal Ching, Alberto Aliseda, and Wendy Thomas for their support and providing fresh viewpoints for this research.

I would also like to thank my family and friends for their support throughout life.

Introduction

Cardiovascular disease is the leading cause among all deaths in the United States and presents the highest cost to the health care system. Of the adult population, 36% of people are affected by it [1] and a staggering 44% of domestic deaths can be attributed to it. The economic cost is estimated at $259 billion dollars annually. [2] Among cardiovascular diseases: atherosclerosis (or atheriosclerosis), leads to potentially deadly or debilitating cardiac events such as myocardial infarction or stroke. This process is well studied and occurs through constriction of blood flow in blood vessels through the gradual buildup of macrophages, fatty lipids, and smooth muscle cells or fibroblasts into an atherosclerotic lesion within a vessel wall. Expansion of this lesion thickens and hardens the vessel wall; leading to decreases in blood flow rates and increases the blood pressure needed to circulate blood. Treatment of vessel narrowing usually involves stenting the blockage, but stenting itself introduces a foreign object into the hemodynamic flow which may cause endothelial dysfunction and possible platelet aggregation at the stent site. Further re-occlusion frequently occurs and re-stenting is usually periodically performed to address this. A better understanding of how endothelial cells and platelets are mediated by shear forces would aid in the understanding of disease progression for both atherosclerosis and platelet dysfunction diseases such as hemophilia and von Willebrand disease.

Primary Hypothesis 1: We hypothesize that different shear regimes cause mechanotransduction driven cytoskeletal remodeling which affects the protective function of endothelial monolayers.

A central theme in this research was that shear stress can induce an atheroprotective or an atheroprone state in the endothelium by affecting the organization and morphology of the cells. [3-5] When the cells are exposed to laminar flow, mechanosensory elements at the focal adhesions and junction complexes reorganize their cytoskeletal structures in alignment with the flow direction. [6] Current theories believe that this organization minimizes the intercellular gaps reducing the exposed area of the underlying extracellular matrix (ECM). Disturbed or pulsatile flow exists at bifurcations, in the downstream region of existing atherosclerosis lesions, or on surgically inserted stents. Turbulence introduced into the system causes cells to remodel with no particular direction and the cells pull apart from each other, exposing a higher amount of arterial tissue below. Leukocytes are free to adhere to exposed extracellular matrix in the intima and an atherosclerotic lesion becomes seeded. Previous studies have shown that atherosclerotic plaque and lesions have a tendency to form at regions of flow disturbance or

instabilities. [7] For these reasons, atherosclerosis risk stems from increased cell layer permeability.

This research investigated the response of endothelial cells under various flow regimes using an in-vitro system with quantitative cytoskeletal mechanics and structural analysis. Immunofluorescent staining and imaging allowed the researchers to investigate the biochemical remodeling of actin filaments and cell-cell adherens and tight junctions. By analyzing these images in MATLAB it became possible to quantify these values to ensure that observations were in fact accurate. Cellular alignment under shear was done to check that cell behavior matched what has been previously observed in literature. To quantify permeability, intra-cellular adherens junctions were quantified using β-catenin intensity across cell boundaries. Tight junctions which mediate cross-surface ion transport and cellular transmigration were investigated by marking tight junction protein zona occludens-1 to confirm the coherence of the monolayer. Lastly, the actual traction forces responsible for the morphological change of the cells were addressed. PDMS silicone micropost arrays are used to measure cellular traction forces by acting as a deformable substrate for the cells. Imaging of the top and the bottom reveal measurable deflections that are correlated with known post stiffness in order to calculate traction forces. Identification of cell boundaries is used to determine tugging forces between cells, and ultimately the average tension or intercellular force that exists in a monolayer.

Shear stress response isn't limited solely to effects on endothelial cells and has also been implicated to play a role in initiating and activating platelet. Even during formation, platelets have been observed to be formed as fragments sheared off of megakaryocyte protrusions that have extended into micro-vessels. [8] During hemostasis in the vascular system, the same shear zones and regimes affecting endothelial cells impose mechanical signaling onto the platelet [9]. Shear and drag forces physically extrudes the platelet body membrane, possibly stimulating surface receptors [10] and is also seen to increase the thrombogenicity of surfaces and make nucleating thrombi more able to capture passing platelets and grow itself. [11, 12] Shear remodeled endothelial layers that enter an atheroprone morphology may expose underlying ECM to passing blood flow; endothelial barrier breakdown creates opportunistic sites for platelets to collect. Once there, surface binding receptor complexes such as GPIb and $\alpha_{IIb}\beta_3$ create firm platelet adhesions and stabile clots while also secreting markers like P-selectin which recruit and adhere progressively more platelets. [13] Activated platelets then release their calcium and ADP stores which The classic atherosclerotic progression cascade is then thought to occur.

Primary Hypothesis 2: We hypothesize that platelet clot forces and aggregation are shear dependent.

Platelet shear response was measured as a metric for determining clot aggregation susceptibility using a microfluidic device. Rapid, live imaging of whole blood sheared through a novel PDMS microfluidic device revealed the full sequence of events responsible for platelet adhesion in high shear regimes. Shear rates ranging from physiologic to pathological, characteristic of atherosclerotic or stenosed arteries, showed the deterministic role that shear has in platelet adhesion and shape-change. Custom image analysis was developed to perform automated measurements of platelet clot force enabling an accurate measurement of contractility. The researchers also quantified platelet area to find how shear affects platelet-to-platelet adhesions. Finally, mechanisms for contractility and adhesions were probed by selective inhibition or myosin-II and antibody blocking of Glycoprotein Ib and $\alpha_{IIb}\beta_3$ to determine their role under shear.

Shear is a major contributor to vascular health. Analyzing alignment, permeability, and cellular traction forces gives us insight into the biomechanical response of vascular cells and a better overall picture of why certain sites such as bifurcations, post-clot, or post-stent regions are prone to developing or redeveloping atherosclerotic lesions. A rupturing lesion results in a highly thrombogenic wound site that attracts platelets by exposure of subendothelial proteins promoting clotting. Assessing platelet forces and clot growth is important because it signals the stability of platelet plug to ultimately heal or further complicate the vessel. This knowledge can be applied to future designs of stents by making them less prone to generating prothrombotic or atheropromoting shears. Targeting shear-related signaling molecules might also be a vector for therapy or treatment of hemostasis disorders. Novel diagnostics could also arise from the combination of shear activation of platelets and force sensing microposts to quickly determine disorders such as coagulopathy.

1. Background

1.1 Atherosclerosis

The circulatory system is a closed loop network with over 40,000 kilometers of pathway for blood to travel through. This enormous total distance and vessel surface area means that through daily activity, wear and tear of the lining of the vessels is introduced. Normal vessels are undergoing constant growth and remodeling to repair damage introduced into the system. However, imbalances in activities such as leukocyte (white blood cell) recruitment or endothelial cell remodeling can create sites of high risk, or an atheroprone state.

Blood vessels have a circular cross section that can be divided into 3 concentric rings. The outermost ring of the artery is the *adventitia* formed out of connective tissues. The middle ring is the *media*, comprised of smooth muscle cells and elastic tissues such as collagen, elastin, and proteoglycans. The innermost ring is the *intima*, a single cell thick lining of predominantly endothelial cells. These endothelial cells are collectively called the endothelium which acts as a protective barrier between blood-borne particles and the underlying arterial tissue. Damage to this layer allows the introduction of blood-borne particles into the vessel tissue.

With a cholesterol or saturated fat rich diet, small lipoproteins can accumulate in the intima tissue layer of blood vessels. [14] Prolonged residence time near an area increases the chance of aggregation and once inside the intima they can bind to proteoglycans. Once bound, the lipoproteins are susceptible to oxidation. This is potentially the progenitor for further lesion development. When the endothelium is damaged the endothelial cells release cell signalers that attract leukocytes. These cells become activated and transmigrate or diapedese through the endothelial cell junctions into the underlying arterial intima. Once there, the leukocytes interact with oxidized low density lipoprotein (LDL) and other fatty lipids and become foam cells. [15] Aggregation of many foam cells together forms a fatty streak, which can release cytokines and cell effectors enhancing recruitment. Smooth muscle cells from the arterial media may also grow and transmigrate towards the intima incorporating themselves into the enlarging fatty streak and thickening the arterial wall. [16] Inside, the smooth muscle cells divide and proliferate depositing more extracellular matrix proteins allowing for recruitment and migration of additional cells. When the smooth muscle cells die what remains is a fibrous network of extracellular matrix proteins and proteoglycans. Eventually this may result in a fibrous or calcified mass surrounding a fatty lipid core with the potential to further harden and calcify.

The atherosclerotic lesion may grow to completely occlude the vessel in time, causing problems with oxygenation of tissue downstream or abnormally increasing the pressure in redundant parallel blood vessels. Additionally the lesion can detach and be forced downstream potentially blocking another vessel. If this happens in a sensitive organ like the brain, it leads to rapid permanent damage as hypoxia triggers cells death. The research presented in this dissertation examines the cellular level interactions and responses that can drive the formation of the clot in a vessel. Atherosclerosis and endothelial permeability are closely related in onset and development of the lesions. We wanted to understand why this breakdown occurred and develop a metric to quantify this specific type of vascular damage.

1.2 Endothelial permeability

Endothelial permeability is determined by cell-cell junctions or the surface to surface contact between neighboring cells. [17, 18] If the junctional components are disassembled either in response to mechanical or biochemical factors, permeability through the cell monolayer increases allowing paracellular fluid to traverse. In a health state, endothelial cells are linked to neighboring cells through adherens, tight junctions and gap junctions. [19] Adherens junctions join cytoskeletal actin to provide mechanical strength. Tight junctions link neighboring cell membranes together to form a cellular seal that regulates fluid transport and normally prevent macrophages and lipids from transmigrating through the endothelium. [20] Gap junctions are intra-cellular connections that link cell cytoplasm together and allow molecules such as calcium to pass from cell to cell. The junctions focused upon in this research for quantification are adherens and tight junctions. Adherens junctions in particular are hypothesized to be mechanosensitive, transducing applied forces into increased recruitment of assembly proteins such as vinculin. [21, 22] Indeed, when different magnitudes of force are applied to adherens junctions, they reinforce or weaken in response. [23] During formation of the adherens junction, transmembrane cadherins link between neighboring cells and are joined to each cell's f-actin cytoskeleton by actin linking α-catenin β-catenin and γ-catenin. A weakened cell junction recruits lower amounts of catenin to the cell edges while stronger junctions necessitate more catenin to cross-link transmembrane cadherins to f-actin. For this reason we examine catenin (such as β-catenin), and tight junction structure zona-occluden-1 (ZO-1) intensity levels at cellular junctions because there is a direct correlation to endothelial cell permeability. [24]

1.3 Actin Polymerization Remodeling

The actin structure within each cell forms a complex network that is continuously remodeled on a strand and structure basis by different competing signalers. This research

considers that endothelial cell shear mechanotransductive realignment and actin structure alignment are interrelated. When cells are attached to a surface, their internal cytoskeletal forms actin strands, or f-actin, that act as tension elements in the cell; these strands transduce a tension force and are known as stress fibers. Indeed it has been shown that actin assembly occurs at actin stress fiber ends, so actin polymerization itself has a role in remodeling. The force exerted by the shear flow is sensed by integrins activating the Rho and Rac pathways, and stimulating actin to polymerize at the lamellipodia and in the cytoskeleton. [25-27] Actin response is most certainly related to this shape change, and so we examine what regulates actin filament formation to understand morphological changes.

The globular protein actin is present in abundant quantities in all eukaryotic cells and provides a multitude of important functions. Actin provides the protein framework through which cytoskeletal tension is generated. Dimensionally, actin filaments are 6 nanometers in diameter giving it a low buckling strength when compared to other cytoskeletal members such as Intermediate filaments (10 nanometers) or microtubules (23 nanometers). [28] It can be considered as a tension loadable rope within the cell while intermediate filaments and microtubules are compression elements.

Actin is a single polypeptide chain, 375 amino acids long with a molecular weight of around 42 kilo Daltons. Globular actin, also known as the actin monomer or G-actin, has two structures connected by a cleft linkage that contains binding sites for ATP and Ca^{2a+}, two important cofactors. On the surface of each G-actin lies binding sites for other G-actin. Globular actin can thus polymerize together into a filament forming filamentous actin. The strand itself is polarized as a consequence of the binding orientations of the G-actin monomers giving f-actin directionality. The two ends of actin are known as the pointed end and the barbed end, and previous literature has shown that the barbed end attracts and adds monomers are a ten-fold rate than the pointed end. Capping proteins such as CapZ or troponmodulin can bind to the barbed or pointed ends respectively, stopping the strand from growing further in that direction. In the cytoskeleton, a critical concentration of actin is two micro-molar. Above this concentration, both the pointed and barbed end will polymerize, but below this concentration (all the way to 0.2 µM) only the barbed end will polymerize. If we imagine starting with a set concentration above 2 µM of G-actin monomer in solution then a polymerizing strand will grow until the loose monomer concentration falls below 2 µM. At this point, the pointed end starts de-polymerizing while the barbed end is still capable of attracting G-actin monomer.

Effectively, the actin strand is growing at one end and shrinking at the other, moving G-actin along its length and giving it a displacing property known as *treadmilling*. Polymerization and de-polymerization can drive the stand into the cell wells, allowing the cell lamellipodia to advance toward signalers. When the f-actin strand polymerizes into the cell membrane it exerts a force on it. This is one component of cell locomotion.

Because loose G-actin will naturally polymerize there is a method that cells have developed to isolate G-actin until needed for filament formation. It's interesting to note that the actin monomer concentration in cells is many magnitudes higher than the critical concentration for polymerization. Preventing this, thymosin is a protein that weakly binds to actin monomers and stops G-actin molecules from forming filaments until needed. Other protein signals have the ability to regulate the actin assembly and modulate the structure of the filament. Profilin acts as a catalyst for actin-bound nucleotides increasing actin transfer from thymosin to the barbed actin end. Cofilin promotes disassembly of the G-actin molecules from the pointed end on actin by associating strongly with G-actin. Essentially the thymosin G-actin reserve can be consumed by up-regulation of actin polymerization via profilin and the strand can be inhibited and de-polymerized through cofilin. Other proteins affect the relative organization of the f-actin. Actin strands may be held to each other by the cross-binding protein α-actinin creating a linkage between different filaments. Fimbrin is a small protein with two actin binding domains that, when bound, causes actin to lie in parallel arrays. [29]

Certain chemicals such as the cyclic peptide phalloidin or cytochalasins affect the rate of actin polymerization. In the case of phalloidin it greatly increases the rate by binding across multiple G-actin monomers in the filament greatly reinforcing the stability and resisting de-polymerization. Cytochalasins bind to the barbed end of the f-actin strand and prevent more monomers from binding stopping further polymerization. This can freeze the actin strand in place since growth and disassembly is not chemically favorable. Phalloidin will be used in the research later on as a means of identifying actin strands after cells have been fixed.

1.4 Focal Adhesion Mechanosensing

Related to the central hypothesis of shear driven mechanotransduction is the action of force transduction through the cell. The physical shear hemodynamic creates a force at the luminal surface of endothelial cells. [30] The three cytoskeletal filaments of actin, intermediate filaments, and microtubules form interlinked tension and compression frames that transfers the force throughout the cell. Distant locations sense this applied force starting chemical activities.

Previous studies have proposed a number of possible sensing mechanisms for the force. Tension may physically change the geometry of membrane proteins or structures like the glycocalyx, open ion channels, or affect integrin dynamics sufficiently to start a signal chain. [31, 32]

When the force is transferred throughout the actin or other fibrous cytoskeleton a portion will reach the cells focal adhesions. [31] Since cells are bound to the extracellular matrix by transmembrane integrins there is a force formed at the focal adhesion. [33] Changes in force or the deformation may modulate signaling molecules or protein conformations causing the focal adhesions to align to the direction of flow. [34] Pathways such as Ras, Rac, and Rho (addressed in 1.5) become triggered affecting proliferation response, lamellipodia formation and movement, and cytoskeletal tension respectively. [35] An important response is focal adhesion kinase (FAK) which is a cytoplasmic tyrosine kinase that interacts with focal adhesion integrins to modulate the response of the focal adhesion to growth factors and integrin-ligand binding. [36] FAK serves to suppress and regulate Rho (discussed in 1.5), promoting the turnover of focal adhesions. If FAK is suppressed, then up-regulation of Rho leads to many more focal adhesions, decreasing cell migration. [37] Under shear flow it has been shown that single and monolayers of endothelial cells realign to the direction of flow. It has also been demonstrated that the cell lamellipodia protrusions are polarized to the flow and that existing focal adhesions remodel with a directional migration parallel to the flow. [36] As discussed in section 1.2 the actin substructure of the lamellipodia translates this in the direction of flow. As the focal adhesions are moved, they can also mature into larger focal adhesions. [34] New focal adhesions become formed at the leading edge lamellipodia and these are linked to the cell structure by f-actin which itself is linked to other f-actin, and intermediate filaments and microtubules through the cytoplasm.

1.5 Rho and Rac Pathways: Tension and Permeability

Two important pathways in endothelial cell permeability are within the Ras family: Rho and Rac. Rho has been shown extensively to form actin stress fibers [4] and focal adhesions in various cells for migration and for traction force generation. [26, 27] In shear, increased cell to extracellular matrix binding signals integrins to create a transient inactivation of Rho (such as with FAK); this mechanism is thought to allow cytoskeletal alignment. [38] Rac has been shown to form lamellipodia and filopodia and under shear flow leads to recruitment of leukocytes. [39] Both of these are GTPases that impact motility, gene expression, and intercellular junction organization. [19, 40] They have a deactivated state that is GDP bound and become active

when GTP binds to them. When Rho becomes phorylated by protein kinase-A, it creates the ROCK complex. ROCK both directly phosphorylates myosin light chain (MLC) and inactivates myosin phosphatase which de-phosphorylates MLC; this double action of ROCK up-regulates myosin contractility. Inhibiting ROCK by Y-27632 can effectively stop actin-myosin force generation in stress fibers in addition to suppressing activities that relate to stress fiber forces such as cofilin and actin filament stability. Conversely, the use of Calyculin-A, which is a myosin phosphatase inhibitor leads to an inability for the system to de-phosphorylate. This molecule has been used by research groups to enhance myosin activity and cell contractility. [41-43]

1.6 Previous Endothelial Shear Flow Devices

The importance of these signal pathways has led to other groups to search for methods of stimulating and recreating in-vivo conditions in-vitro. This would allow the cell behavior to undergo replicate behavior while being observable. Previous research device designs aim to generate physiologically relevant shear through one of several ways. The most common is through the use of microfluidic channels frequently fabricated of PDMS silicone. Cells are seeded within the channel and fluid is pumped directly across them using a syringe pump. Parallel plate systems also have been used that sandwich cells between a stationary surface and a continuously rotating plate or cone to create a controllable flow. However these designs do not allow the measurement of the underlying traction forces because they lack a mechanism to do so. The device created in this research is flexible in that it can accommodate large arrays of microposts or force sensors and is capable of measuring large monolayers of cells.

1.7 Summary of Shear Mechanotransduction

Previous studies have measured endothelium surface topography using atomic force microscopy to calculate surface shear. Mechanotransduction response surface remodeling to applied shear was found to minimize the peak surface stress and shear gradients. [44] Cell remodeling can be seen as the total mechanotransduction response and examples can be seen in many stages of many cells and is a growing area of interest. [45] When hemodynamic shear is introduced to endothelial cells, there is a mechanical force applied at the luminal surface of the cell. This force is translated through actin and the fibrous cytoskeleton filaments to the focal adhesions holding the cell to the ECM. At the focal adhesion site chemical modification of FAK or other protein allow interactions to take place releasing the ECM holding integrins. Cytoskeletal stress in the strand and focal adhesion displaces the focal adhesion to a new site to relieve the force. Focal adhesion site displacement also pulls and remodels the actin structure with it. At the end of the movement the focal adhesion can rebind to the ECM through

the same integrins that were released when force was applied. The cells actin structure is then changed to align itself with the shear flow. Actin polymerization and its associated regulatory proteins also interact to modify the f-actin strand as appropriate. Since the displaced f-actin is linked to other f-actin through binding proteins the entire cytoskeleton eventually undergoes a shape change resulting in alignment. In a monolayer of cells this results in an organized polarity for the cells. The response is tested in the first hypothesis presented in this dissertation. We investigate the physical focal adhesion forces, or traction forces that cells exert on the abluminal or substrate as well as the organization as related to endothelial permeability in atherosclerosis lesion formation. [30]

1.8 Platelets and Hemostasis

The blood coagulation pathway is a critical component in the body's natural healing response. When a wound develops either externally or internally (as with atherosclerotic plaque rupture) platelets are activated to initiate a clotting cascade to stem bleeding. In severe injury cases, coagulopathy can develop during which intrinsic coagulation pathways become dysfunctional. Genetic abnormalities like Von Willebrand disease, or Bernard-Soulier syndrome also result in prolonged bleeding times which can complicate surgical procedures and recovery. [46] In severe injury cases, hemorrhagic shock can develop and cause intrinsic coagulation pathways to become dysfunctional. Therefore, in both clinical and surgical applications, assessment of platelet coagulation can inform the caregiver about the best course of treatment which may include infusion of clotting factors, whole blood, or additional platelets. Therefore, a method to accurately assess platelet coagulation can inform the caregiver about the best course of treatment or therapeutics.

Platelet binding occurs preferentially at locations of extreme shear microgradients or rapid shear change. [11] This mechanobiological phenomenon has been observed to occur both *in vitro* and *in vivo*. [9] Microgradients arise as a result of differentials in the velocities layers of laminar flow, whether caused by extreme bends, vessel wall damage, or protruding implant structures like stents. Microgradients are also present due to natural morphology of the endothelial wall. Platelets typically become segregated towards the wall of vessels because of a combination of larger cells like erythrocytes pushing them away from the center of the flow and their lower mass. These effects concentrate platelets against the wall, allowing for intermittent contact between the platelet and wall.

Shear has also been found to induce direct activation of resting platelets. [9, 11] Once at a binding site and activated, a positive feedback loop of shear can develop where platelets bind to the vessel wall, narrowing the cross-sectional area, and forcing blood flowing through the stenosed site to accelerate. The increased velocity then further increases the shear microgradients that develop and the cycle continues to attract more and more platelets. Severe stenosis or total occlusion of a vessel may result if no steps are taken to either biochemically reduce platelet coagulation or physically remove the thrombus. Currently, some available therapeutics includes abciximab (ReoPro), clopidogrel (Plavix), and acetylsalicylic acid (aspirin). These antiplatelet drugs generally act as antagonists for platelet receptors like $\alpha_{IIb}\beta_3$, $P2Y_{12}$, or prevent the generation of signal molecules such as T_xA_2 respectively. [46]

Currently, it is thought that capture and formation of a stable thrombus under physiologic shear flow (400-5000 s^{-1}) first starts with contact between the vWF A1 domain and the platelet GPIb receptor. [47] This GPIb-VWF complex has been observed to associate and form very rapidly in order to stop platelets out of quickly moving whole blood. Hemostatic drag on the platelet contributes to a force to the small receptor-ligand bonds extruding membrane tethers and increasing the procoagulant activity of the platelet. [48] However, this interaction also has a rapid disassociation rate, making the engagement transient and mainly results in platelet rolling due to only temporary contacts being established. A secondary receptor-ligand such as $\alpha_{IIb}\beta_3$ with fibrinogen or collagen with GPVI is necessary for firm and stable irreversible surface adhesion. [49-54] Subsequent association of aIIbß3 drives platelet shape change and inwards contraction stabilizing and stiffening the clot structure. The securing of the clot is critical to the formation of a fibrin meshwork that aids in further platelet activation and for long term stability of the clot. [55-57] Therefore, understanding platelet contractile force under shear gives an indication of hemostasis response, however this phenomenon is not well understood nor characterized.

Shear also plays a role in increasing the thrombogenic potential of vWF. At sites of vascular injury sub-endothelial collagen is exposed allowing for plasma solubilized VWF to bind. Normally, circulating VWF has a limited affinity for surface GPIb on passing platelets. But in the presence of exposed collagen type I, high molecular weight VWF chains bind to the surface and unfurl under high shear presenting many more binding sites and increasing the thrombogenicity of the molecule. [58] Additionally, self-association of VWF monomer is enhanced within fluid shear and increases the size of VWF multimers bound to GPIb reinforcing its ability to capture

particles in flow. [59] Experiments utilizing plasma-derived VWF have shown that VWF forms a filamentous meshwork of multimers on collagen that are functionally active. [60]

Upon receptor engagement, contractility develops and is driven through calcium mediated myosin action in the platelet body. VWF A1 and GPIb interactions in the presence of ADP enhance the release of this intercellular calcium leading to sustained activation. Critical VWF binding receptors include GPVI and factor VIII with collagen; these factors also play roles in further biochemical signaling for activation that lead to contractility and force generation. [61] Just as with endothelial and other cells, platelet forces are important for thrombus stability. [62, 63] Platelets pull on fibrin and stiffen it, referred to as strain stiffening. [64] A clot with higher fibrin stiffness will be subject to less deformation by fluid shear stress and can be anchored more strongly to the vessel wall. The compact nature of a contractile versus non-contractile clot may also mean that fibrinolysis occurs slower as interactions between plasma borne plasmin and interior clot fibrin becomes more difficult. Measuring the contractile force for thrombi that form at microgradients should reveal if the platelet-rich structure is stably adhered at the vessel wall.

1.9 Existing Platelet Tools

Existing coagulation tests currently in use generally test the coagulation response at the whole blood level. That is to say, these tests examine either whole blood or blood plasma viscosity as it thickens in response to an agonist or stimuli; typically this is some agent such as calcium, kaolin, or ADP. Clinically, tests such as PT/INR are used for assessing bleeding disorders and response to antiplatelet therapies. In PT/INR, a sample of blood is drawn into a tube containing sodium citrate which serves as an anticoagulant. Platelet poor plasma is separated through centrifugation and a specified amount of calcium and thromboplastin are added to the sample before it is loaded into an analyzing machine. The addition of these factors initiates platelet activation and causes platelets to collect into microthrombi. As these coalesce, the opacity and electro-mechanical properties of the solution changes which is measured through a number of techniques. The clotting is rapid, typically in the range of 8-12 seconds. These types of tests are suitable for evaluating extrinsic coagulation pathways with high sensitivity to changes in clotting factor levels. [65] However, PT/INR is a reporter for aggregation only, and is not able to measure platelet contractile function or the internal intrinsic activation pathway.

Researchers and companies have also developed different systems to test platelet thrombus formation. There are many useful clinical applications for such devices whenever a patient's blood coagulation status needs to be evaluated. An example is during cardiac catherization, where a patient has heparin sulfate applied to allow for tools and medical devices to be inserted into an artery without incident clotting and seizing of the tool. After the procedure, it is important to know the speed at which heparin depletes from their system, in order to withdraw catheters and heal the incision in the artery. To test this, one method is with a thromboelastography machine that operates by gently rotating a sensor surface in a sample of blood. As clotting initiates, a fibrin network develops that places a resistive force on the sensor and is measurable. The speed and strength of the clot in the bulk of the blood determines how healthy the response is. Agonists and agents can be added to probe for the cause of the platelet dysfunction if one is found to be affecting the force measurements.

Researchers have used different methods for observing thrombosis phenomena *in vitro.* These devices require a different approach than endothelial or other cells since they are non-adherent yet extremely sensitive to mechanical stimulation, time-factors, and handling. In this research, a platelet shear device was developed to investigate clot formation and the forces associated with platelet shape-change during shear-activation. The advantage of the device presented here is a more immediate measurement compared to bulk blood measurements which have a delay associated with them before conclusions can be drawn. With microfluidics platelet forces can be captured from the very start of clotting, without needing to wait for a fibrin network to form. This potentially shrinks the measurement time window from 20-30 minutes down to 1-5 minutes, which has clear implications for emergency medicine and trauma care.

2. Device Designs

Primary requirements were transparency for imaging and observance, biocompatibility for cell health and growth, and sterility. The endothelial shear flow device needed to be modular such that flat or micropost arrays could be inserted, and the method of shear generation had to be able to generate both laminar and disturbed conditions of flow. For platelets, different design requirements were used in order to move them in suspension without activating or them and a focus was made on fine control of shear micro-gradients.

2.1 Endothelial Cell Shear Bioreactor

In order to create shear across endothelial cells, a device would need to be created. Since the primary goal is the application of shear flow, the design evolution started with investigating different methods to impart shear forces across the cells.

At its most basic, shear flow can be imparted simply by two parallel plates moving relative to each other. Known as Couette flow, this creates a constant shear force at any height within the flow domain. Actually creating a device that can maintain constant parallel plate motion over extended amounts of time proves to be problematic. Firstly, such a device requires that the distance between the two plates be held constant. Initial concepts included a two-banded concept that used a stationary outer ring and a moving inner ring. Cells would be placed on the stationary ring and the inner ring would spin to impart a constant shear. The problem here is that while this would work for a flat cell substrate, slight bending of the substrate would make the use of posts inaccurate since the substrate would need to be bent to fit within the device. An alternative of this was an established cup-cone configuration with a stationary circular cup and a top conic surface to maintain constant shear across radius from center to edge. [66] This would allow cells to be grown on micropost arrays but the flow would not be unidirectional across samples, since the flow itself would be curved around the axis.

Ultimately the chamber had to be able to accommodate both flat substrates and PDMS microposts under shear, so modularity was kept in mind when forming the initial concept. The most flexible setup brainstormed used a straight channel with a securing mechanism for cell samples and an adjustable height in order to achieve a high aspect ratio, assuring that the flow can be laminar for any given pumping rate. Cells would be first grown outside the device, transferred onto extracellular matrix coated substrates to adhere, and then placed into the device after sufficient time to form monolayers. Flat channel setups like the first concept are

closed loop systems that could remain sterile over many hours. This design concept is shown in Figure 1A.

2.1.1 First Design

Initial 3-d modeling was done in Solidworks in order to map out dimensions and fabrication requirements. The first design created is seen in Figure 1B and shows a trimetric view of the three major parts that form the shear device. The channel block on the bottom features a milled out well for the sample to sit in, as well as fastening holes and an elliptical track on the top surface to fit a Polydimethylsiloxane (PDMS) seal. At each end of the bottom block are ports for fluidic lines to pump in and out of. The middle block is the height control block and has adjustable screw mounting holes that are used to control the height of the microchannel that forms between it and the channel block. The top block forms the seal and has holes to sandwich the height control block against the channel piece.

2.1.2 Challenges

This first design has a limitation however, in that it required the bottom channel block be milled to a set depth, leaving a certain thickness at the bottom. A depth milling operations across the bottom surface would leave an inherent surface roughness translating into an opaqueness, which would prevent imaging or observation. Adding to this, since the most likely material would be either glass or a transparent polymer, tolerances are difficult to maintain. In these materials challenges arise due to brittle surface chipping (glass) or thermal expansion and melting (polymers) during milling. Additionally, the sample chip is only secured by press-fit forces to the bottom surface, and there was concern that under fluid flow the sample piece would detach.

2.1.3 Second Design

These concerns lead to a second redesign of the device. Important changes include the splitting of the bottom plate into two pieces. In this design the bottom block became the imaging block, eliminating the need to do a depth milling operation as well as allowing the device to use an extremely thin bottom plate so that imaging can occur using high magnification lenses; these lenses have a very short focal distance. In the new channel block, a second elliptical track for a PDMS seal seals the channel block to the imaging block. Cell samples on chips are secured now by height control shims which are not shown. The shims would be either inert metal or PDMS fabricated, and act to also control the channel height. Lastly, the height control piece was made smooth and would be pressed by the top block downwards to form the shear channel to

simplify the wetted surface area and eliminate media-exposed crevices that would be hard to wash and sterilize.

2.1.4 Challenges

Again, analysis of this design shows several critical issues. The elliptical channels are still milled seals, so PDMS would need to be molded to the correct shape within the device itself to ensure a proper seating shape creating an error-prone step in fabrication. Media input and output ports on the channel block were still located on the side, and in practice this makes introduction of media into the system extremely difficult from inherent bubble entrapment. In the body, bubbles in the blood stream are a significant threat, both due to vessel blockage and mechanical pressure exerted by the bubble on endothelial cells. In the chamber, bubbles that could be pushed through the cell channel could potentially exert sufficient forces to destroy the cells. Because the cells have to be put in at room temperature, it is detrimental to have a complex assembly procedure that requires the cells sit outside the incubator for prolonged times. With these issues in mind, the second design was revised.

2.1.5 Final Design

The third design, and the design actually fabricated and tested with contains major adjustments designed to address ease-of-sterilization and sterile-assembly procedure time. We decided to remove the elliptical PDMS seal tracks in order to further simplify sterilization. Sealing is then done purely through block to block contact or through a very thin flat PDMS film placed between the block. The channel block's fluid ports were removed to address the bubble entrapment issue and we moved these to the top block changing it from a passive piece to the input block. By slightly elongating the channel pathway but keeping the height spacer block the same, it introduces a natural reservoir or air damper on either end of the channel that can smooth out pump pulsatility. This version also uses physical spacer pieces to hold down the samples and form the gap height of the channel. Because plastic adhesives and cements are often toxic, we wanted to avoid using any of them in construction. This presents a unique problem in creating the channel block. As stated before, milling is largely a highly thermal procedure that can potentially melt plastic and is exceedingly hard to do with glass. To address this we utilized a water jet to blast through the center portion and create a highly straight and uniform cut. To maintain similar tolerances and surfacing for the height control block the water jet cut it as well. Assembled, the four blocks (imaging, channel, height control, and input) form the shear flow device.

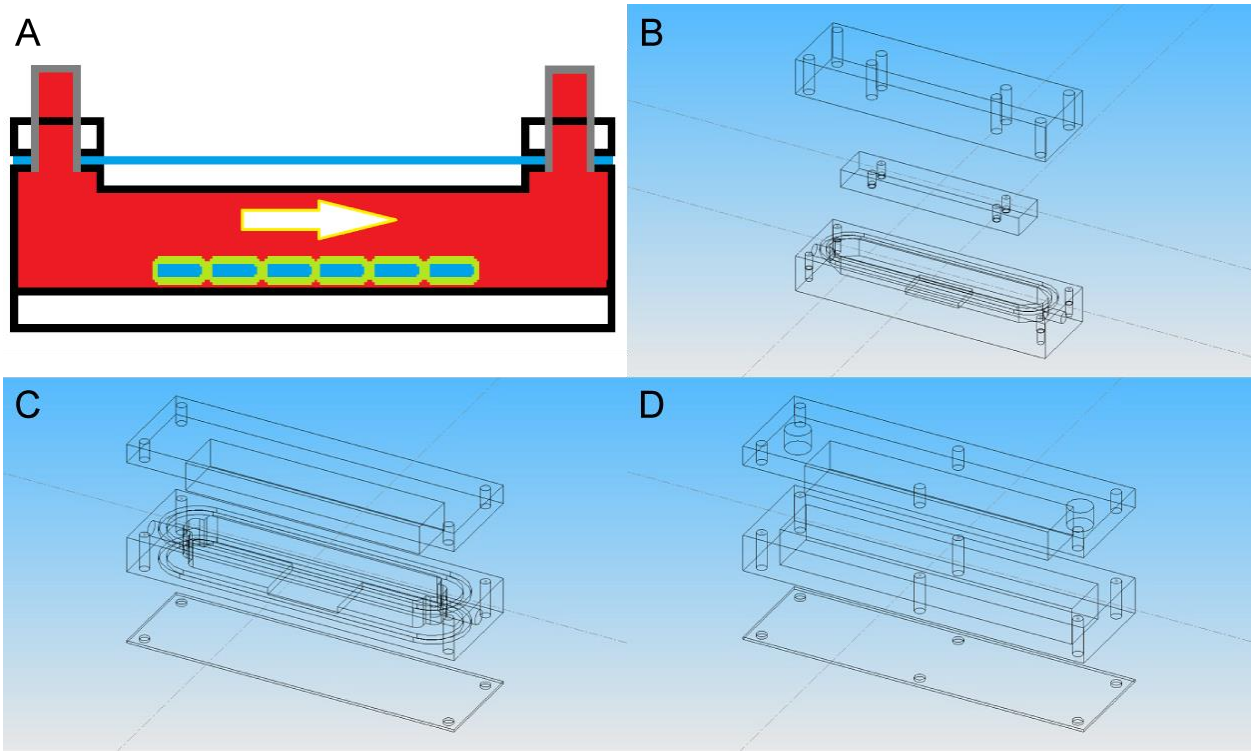

Figure 1 - (A) Shear flow concept (B) First iteration (C) Second iteration (D) Final iteration.

2.1.6 Pumping - Endothelial Cell Device

To drive the fluid through the device several options are considered. First we attempted to apply a pressure driven system. In this configuration, a constant static fluid pressure source such as compressed gas or an elevated reservoir provides a driving pressure. The pressure forces fluid through a fabricated straight channel and into a secondary reservoir where the fluid is then pumped back into the pressure reservoir. Initially this was the goal system, because pressure driven has a constant velocity which makes shear easily adjustable. Swapping the compressed gas is also an advantage since using a 5% CO_2 content compressed air source could internally maintain the pH of the media. This avoids problems with having to diffuse gas through other means.

The first physically built system used a gravity driven primary reservoir made using 250mL Pyrex chemical jars with two holes drilled for the tubing in the cap. The pressure reservoir was raised 5cm above the device and secondary reservoirs. Water was used in place of media for testing, and an immersion impeller-drive pump recycled fluid between the jars. A diagram of the impeller pump setup is shown in the top of Figure 1. Testing was done over the course of 30 minutes in order to test for leakage and proper maintenance of the fluid levels. ¼

inch stainless steel screws hold the device together for resistance to the acidic environment inside an incubator.

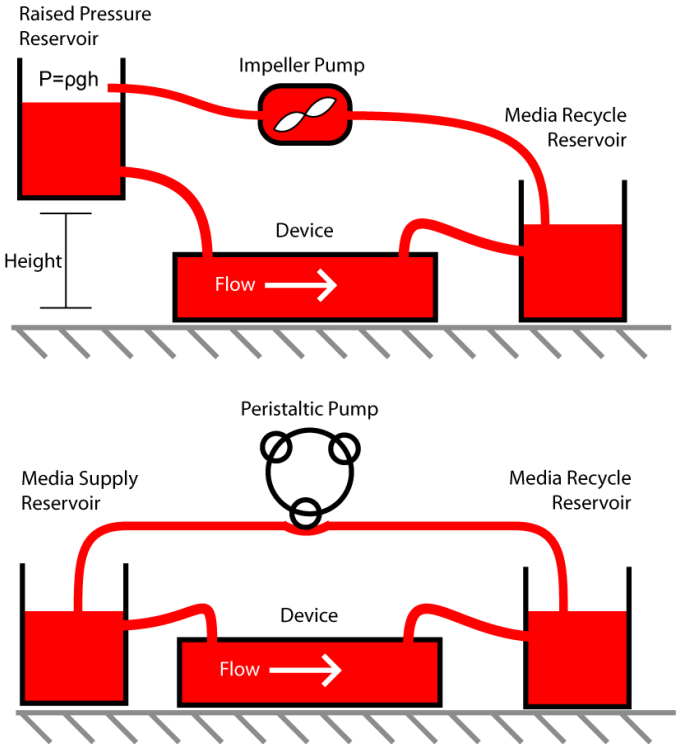

Figure 2 - Shear flow prototypes.

After testing, it was determined that to overcome the pressure reservoir resistance to recycled fluid the system needed a larger and more consistent pump This setup also requires quite a large working volume of cell media due to the internal volume of the long tubing and jars, but the biggest drawback was found that it was absolutely required for the pump to match the flow rate through the device with the recycling rate. Any minor rate offset created a system that would quickly favor one reservoir over the other and interrupt the cycle's fluid path.

The lessons learned from the failure of the first prototype system caused a concept shift towards peristaltic driven flow, or volumetric flow control to generate shear. The bottom setup of Figure 2 shows the peristaltic setup. In this second iteration the reservoirs were placed level with each other and the device. Fluid fills each reservoir partially full and the pump is driven to force the air out of the closed loop system. Shear flow develops within the device as normal and because the volume of fluid removed from the second reservoir is exactly equal to the volume removed from the pressure reservoir it prevents the system from unbalancing liquid levels. It was found eventually that the same effect could be reached by allowing some initial air to exist

in the device automatically trapping it into the well at the end of the channel. A schematic of the final device demonstrating this is shown in

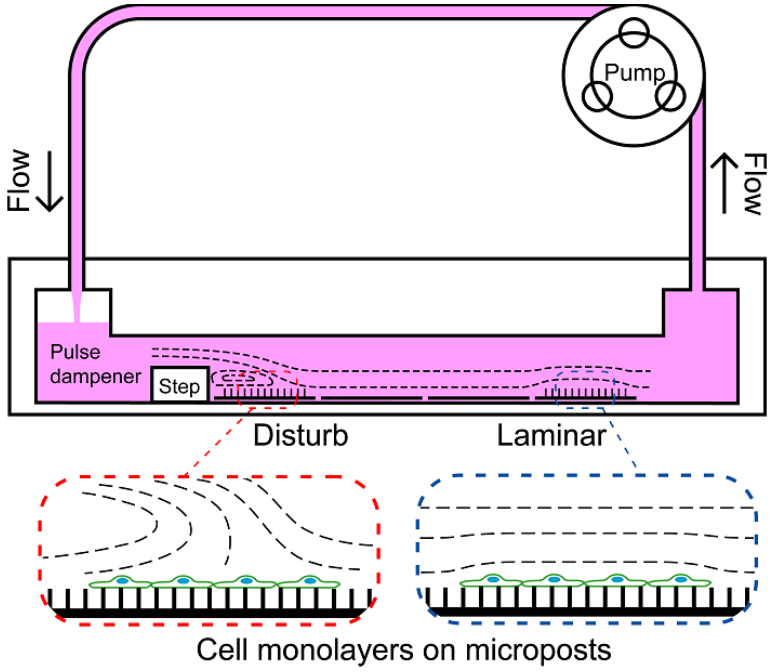

Figure 3 - Shear flow device schematic showing pump, dampener, weir and micropost regions for disturbed and laminar shear generation.

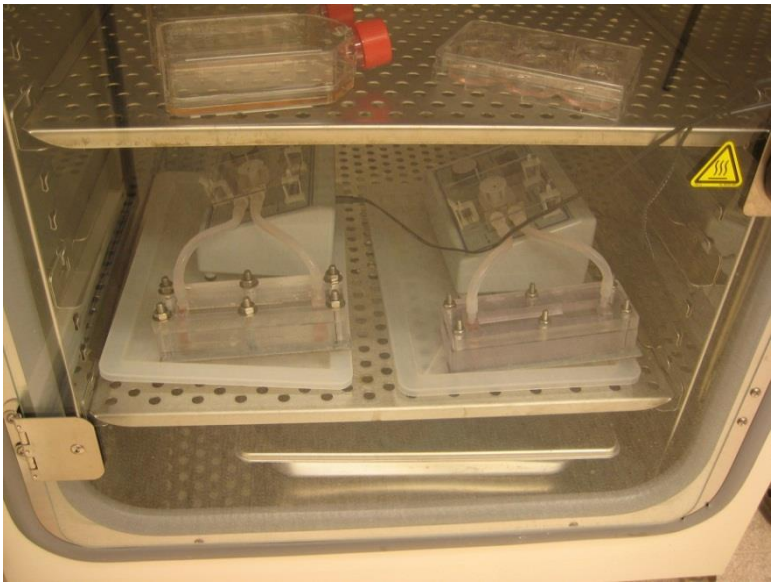

Figure 4 - Microposts in channel in incubator with two pumps each running an experiment.

2.2 Platelet Shear Flow Microfluidic Device

Platelets require a different setup than endothelial cells because they are suspended in the working fluid, and so a peristaltic pump would crush them as they pass through its mechanism. Another challenge is that because they are derived from donated whole blood, the volume of useful platelets extractable is about 20% of the blood volume. This means that the total volume available to perfuse from any single donor is slightly less than 10 mL when the platelets are resuspended in buffer. That restriction means that the reservoirs and channel dimensions have to be scaled down to accommodate tens of minutes of high shear sustained flow without recirculation.

Another consideration for using microfluidics is because it would be desirable to require as little blood as possible during diagnostics, but this is especially critical during hypothetical surgical or trauma settings. During these situations of already high blood loss, it is impractical or unsafe to withdraw 50 mL or more of blood in order to use a larger shear chamber. Ease of operation is another design consideration. The less user intervention that is required the more reliable, repeatable, and dependable the result is. This includes processes such as withdrawing and loading blood into the device, insertion of additional buffers or reagents, manipulation of the valves or switches on the device, or manual interpretation of results. An excellent example of a well refined and user friendly device we would like to approach in usability are electronic diabetic blood sugar testing strips. As an integrated system is only requires the user to load a reagent loaded strip into the reader, and touch the strip to a droplet of blood. All measuring is done automatically and results are presented in an easy to interpret way.

2.2.1 First Generation – Single Channel Assembled Device

The first microfluidic device channels made were fabricated by direct PDMS molding off a bonded glass master. To make these masters, first cleaned and plasma treated glass was cut from cover slips and cover-glass in the right dimensions and a thin layer of PDMS was applied to act as an adhesive. An external channel is made in a similar manner around the perimeter of the flow channel and functions as a vacuum gasket. Bonding and heat treatment at 110 °C sealed the surfaces together. Glass masters were then plasma treated again and silanized for several hours before PDMS was cast against it, forming what is referred to as the top block. Finished example masters are shown in Figure 5.

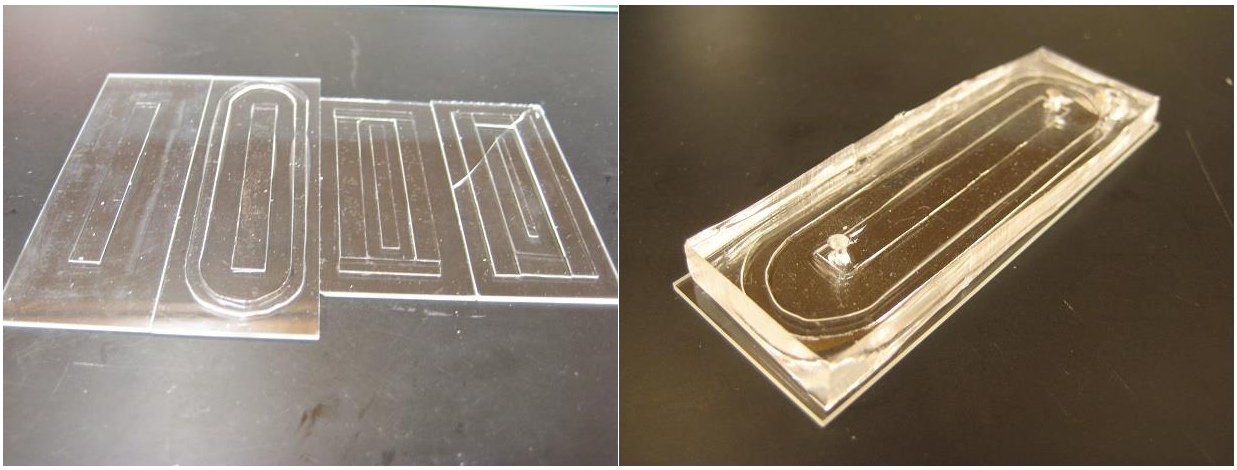

Figure 5 – Left: Bonded glass masters for channel fabrication. Right: An example PDMS channel mold with access ports punched into it. This particular device has a vacuum gasket allowing for disassembly of the top portion from the base after an experiment.

Access ports are punched through the device to coincide with the ends of the central channel and the vacuum gasket. Silicone tubing is inserted and PDMS is used to seal the tubing to the block. An example top block with only the ports punched is shown on the right in Figure 5. Microposts are made separately and functionalized, being left in a wetted state. This is where the vacuum channel is useful, in sealing the device to the microposts despite fluid being present. Experiments could then be performed with stamped and patterned microposts since prior sealing isn't necessary. The device was made with the consideration of mounting it on a 40x oil objective in a live microscope box for real-time imaging. An image of the setup is shown in Figure 6. However, a large disadvantage presented itself over the course of these experiments: only 1 channel could really be fit using an assembled device and residual liquid between the two surfaces meant that an imperfect contact surface or burst in the seal allowed the vacuum gasket to pull the platelet containing fluid out of the channel rapidly and it became extremely difficult to reseal it, ending the experiment.

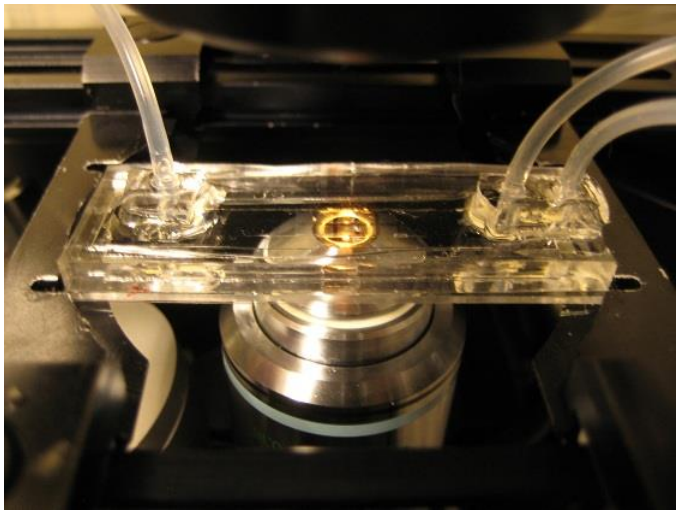

Figure 6 - Assembled first generation platelet device with single channel, microposts, and vacuum gasket.

It was also found that due to the microposts being trimmed there was a step height introduced into the channel upstream of the microposts, making it difficult to gauge the exact speeds and shears flowing over the microposts.

2.2.2 Second Generation – Integrated Microfluidic Device Fabrication

An integrated microfluidic channel that combined the microposts into the fluid path was pursued because then was possible fit run several smaller straight channels onto each device. It also eliminates the minor construction differences that existed between different first generation devices by making every channel identical. Fabrication is done through photolithography processing at the University of Washington nanotech user facility (NTUF) and microfabrication facility (MFF). Parameters were tested and varied from the photoresist manufacturer recommended settings in order to fit our specific needs.

Fabrication follows: silicon wafers are first cleaned of organics with acetone, isopropanol, and DI water before being dehydrated at 200° C. Next, a base layer of SU-8 is applied to enhance adhesion of subsequent layers. This base layer is either SU-8 2005 or SU-8 2007 (Microchem Corp.) and is applied with parameters described in Table 1.

.

Table 1 - Microfabrication Spincoating Settings

Speed, rpm/s (Acceleration, rpm/s^2) [Dwell time at final speed, s]	Base Layer	Micropost Layer	Channel Layer
Photoresist Spreading Cycle	500 (300) [5]	500 (300) [5]	500 (100) [5-10]
Main Spin Cycle	3000 (300) [30]	3000 (300) [30]	3000 (100) [30]
Stopping Cycle	0 (300) [n/a]	0 (300) [n/a]	0 (300) [n/a]

After spin coating, a post-spin thermal bake at 95 °C for 3 minutes hardens the photoresist in preparation for UV exposure. Because the first layer is unpatterned, the wafer is loaded into a contact aligner (ABM) without a mask and an exposure of 10 seconds (~12mW/cm^2) is done. A post-exposure bake at 95 °C for 3 minutes finalizes the photoresist cure.

Next the micropost layer is formed using either SU-8 2007, SU-8 2010, or SU-8 2015 (Microchem Corp.) and another post-spin bake at 95 °C for 3 minutes. For the patterning, a mask with a grid of micropost features is brought into physical contact with the prepared wafer and exposed for 13-17 seconds (~12 mW / cm^2) depending on the thickness of the photoresist. Masks are made by the researcher at the NTUF using 5-inch square chrome blanks and a direct write laser μPG (Heidelberg Instruments. A critical step is contact; if the photoresist spin is uneven or an edge bead exists at the edge of the wafer UV light will overexpose the microposts resulting in malformed sidewalls and diameter dilation. Post-exposure baking at 95 °C is done for 4 minutes. The first two layers are then developed in SU-8 Developer (Microchem) for 5 minutes to remove unexposed SU-8. An optional hardening bake step of 150 °C for 10 minutes is performed to harden the microposts and enhance the bonding between the two layers. Reflective microscopy images of well-formed posts is shown in Figure 7

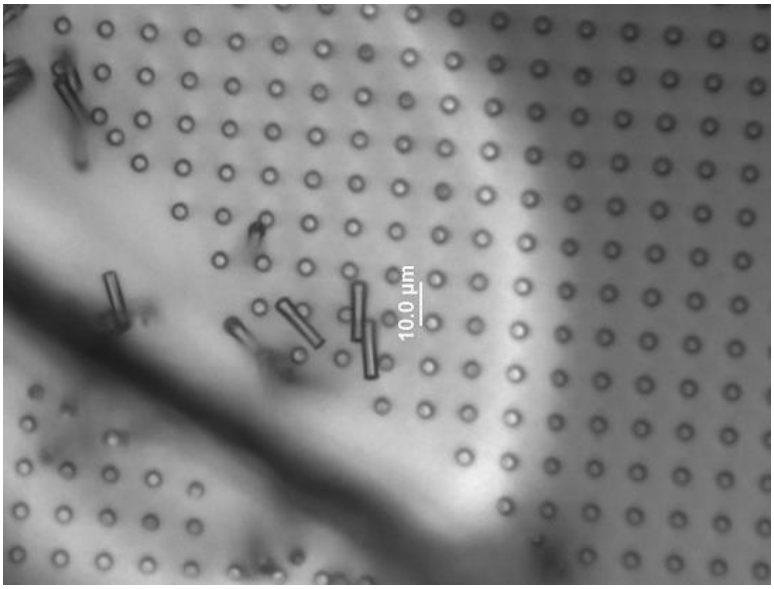

Figure 7 - SU-8 2015 spun onto SU-8 2007. Visible in both horizontal and vertical orientations are 15 micron tall posts in a 9 micron spaced square pattern. A razor blade has been drawn across the surface to purposely knock posts down for sidewall observation.

The microchannel layer is the thickest layer in the device, using SU-8 2100 (Microchem Corp.). An early problem encountered was a tendency for the thick spins to be highly irregular at the surface because of bubbles or strands that were trapped within the resist. To solve this, the photoresist is poured as close to the wafer as possible, and during the entire spin process is covered to prevent strands from re-depositing onto the top surface. An extended post-spin bake in two steps of 65° C for 10 minutes followed by 95° C for 20 minutes is used to reduce thermal stresses in the layer and allows for a controlled evolution of the SU-8 solvent out of the resist. An optional edge bead removal using a nonwoven wipe tip with SU-8 solvent can be done to smooth out the edges for better contact before exposure. Because the resist is so thick, a long exposure time of 60 seconds (~12 mW / cm^2) is needed to fully penetrate the depth of the SU-8 2100 and the wafer undergoes a post-exposure bake of 65° C for 5 minutes then 95° C for 10 minutes. Development through submersion in SU-8 developer for 10 minutes with moderate agitation removes the channel material exposing the microposts at the bottom of the device. Lithography steps are illustrated in steps 1-9 of Figure 8.

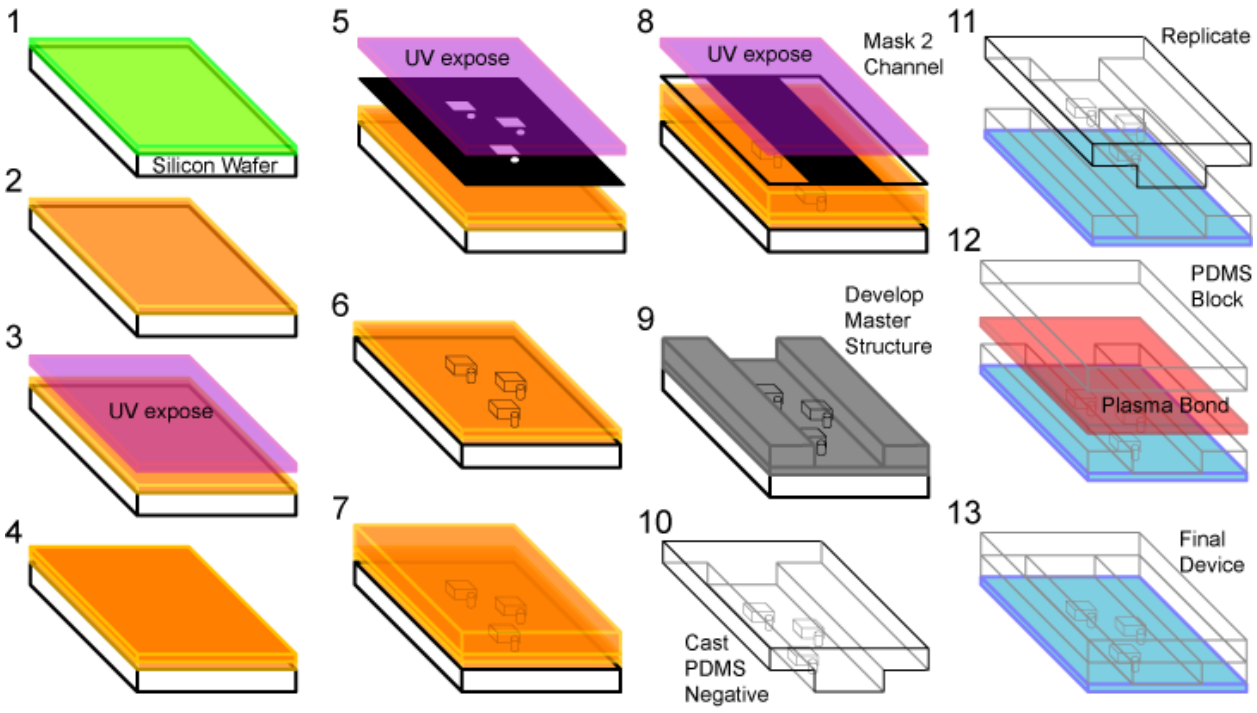

Figure 8 –(1) wafer washing and dehydration is done through organic solvents (2) SU-8 base layer applied (3) maskless exposure cures the base layer (4) a second layer of SU-8 is applied to form microposts and a mask (5) with the appropriate features is used. (6-7) Another layer of thick SU-8 (8) forms the channel and (9) final development reveals the combined structure. (10-13) PDMS replicates and top blocks are bonded through plasma to form the platelet shear flow device.

Final finishing steps include a hardbake cure at 150 °C for >1 hour, plasma treatment and exposure to fluorosilane to passivate the surface. Finally, PDMS can be cast against it to replicate the structure. A top block is secured with plasma forming a permanent watertight covalent bond. Representative images of a final master structure and a functional microfluidic device filled with food coloring is shown

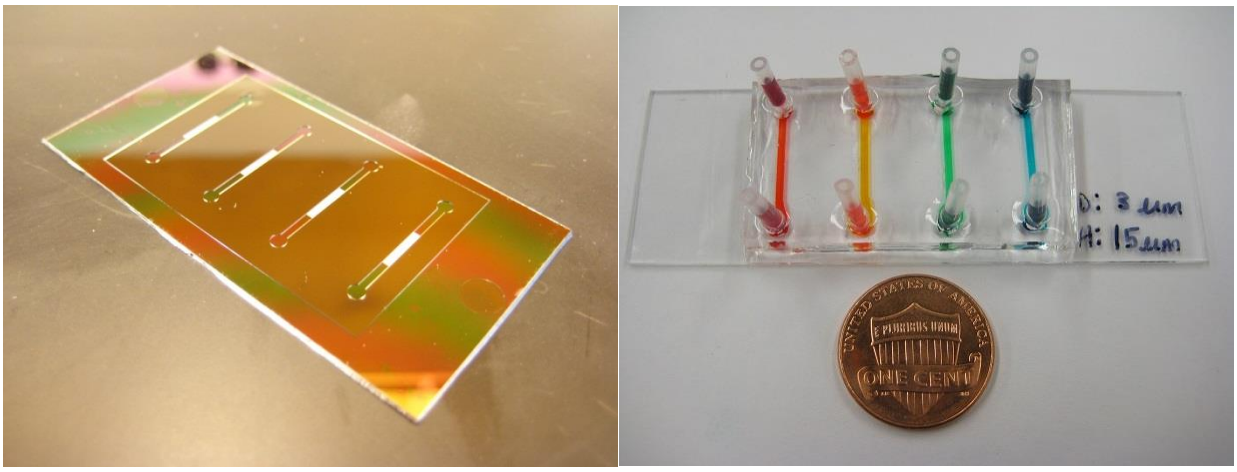

Figure 9 - Silicon and SU-8 photoresist formed microchannel master structure and PDMS replicate with colored channels. A penny is included for scale reference.

2.2.3 Third Generation - Platelet Shear Device with Obstructions

Shear gradients have been seen to have a role in activating platelets, so it is potentially a way of reliably causing thrombus formation independent of protein coatings or agonists which are susceptible to aging and environmental effects. Different shear gradients were created in the fluid by changing the shape of the channel. In initial prototypes, this was done by simply piecing together glass in a fashion that created a narrowed section of microchannel for a master structure. Later designs were again fabricated through photolithography with different geometry incorporated into the channel mask.

Channel masks were created again using the NTUF μPG (Heidelberg) direct writer and micropost masks were made at the NTUF or contracted professionally (Microtronics Inc). Professional masks gave the researchers some slightly smaller design capabilities as well as being more uniform in terms of circularity. Channel dimensions were always 500 μm wide, 100 μm in depth, but varied in length between 10,000 μm to 15,000 μm depending on how closely the channels were packed. Spacing and pitch was decreased as better plasma treating and bonding processes were tested showing less area was needed to get a watertight barrier. A master structure is shown in Figure 10 that has microposts within a large channel with a necking portion that has 20% of the cross sectional area of the main channel and accelerates the fluid to 500% in the narrow region. This concept was created to test the idea of activation purely on bulk shear changes in the fluid. Another design fabricated uses obstacles and places different shapes into the flow path in order to create more localized shear gradients. Figure 11 displays reflection microscope images of these shapes; the channel width is still 500 μm.

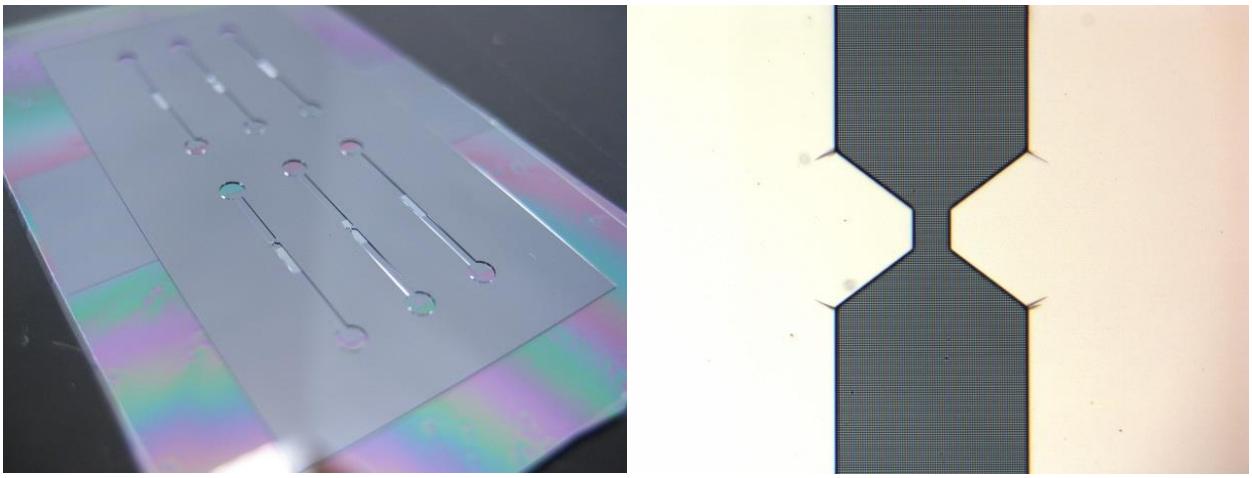

Figure 10 - Third generation microfabricated device in silicon and SU-8 photoresist, showing posts with an incoporated narrowing in the channel.

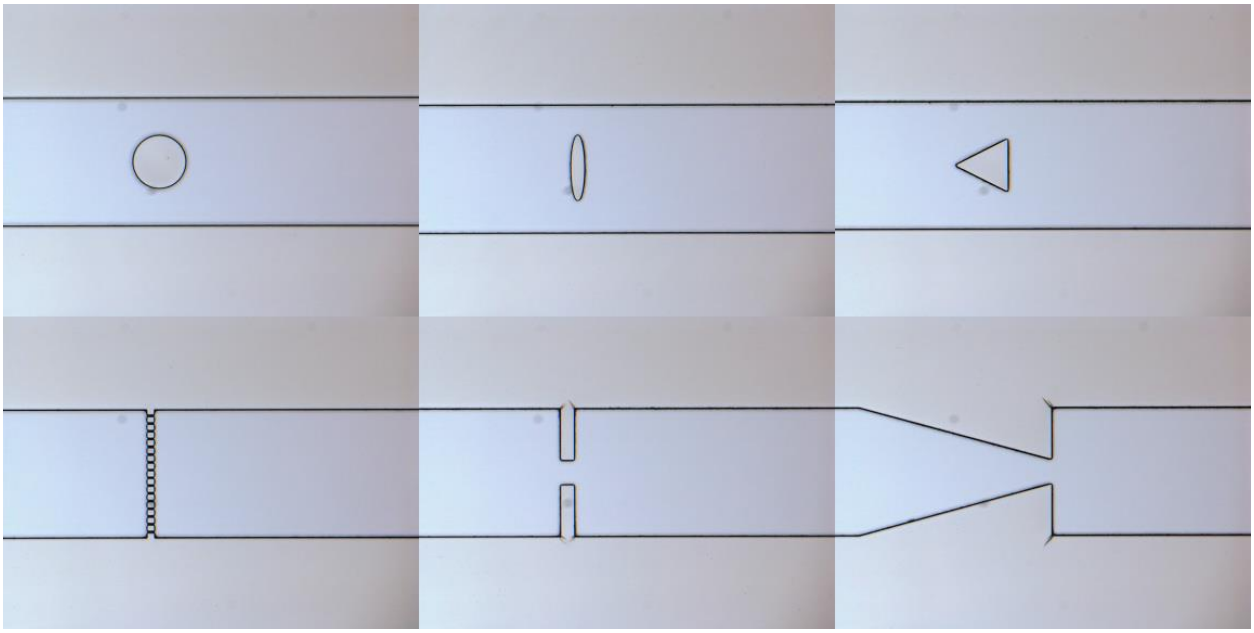

Figure 11 - Different geometries in fluid flow path for generating shear gradients.

It was observed in experiments that the presence of microgradients in a microchannel increased the speed of thrombus nucleation at that location. Using our initial experimental observations, it was thought that the core of activated platelets begins contracting whilst the outermost layers of the aggregate are capturing resting platelets from the flow. This capture leads to a steady growth of the thrombus. Conversely, micro channels fabricated with microgradients less than 10,000 s^{-1} do not show a rapid nucleation and growth of a local thrombus but rather requires several minutes for one to form. These clots are very rarely seen to undergo retraction.

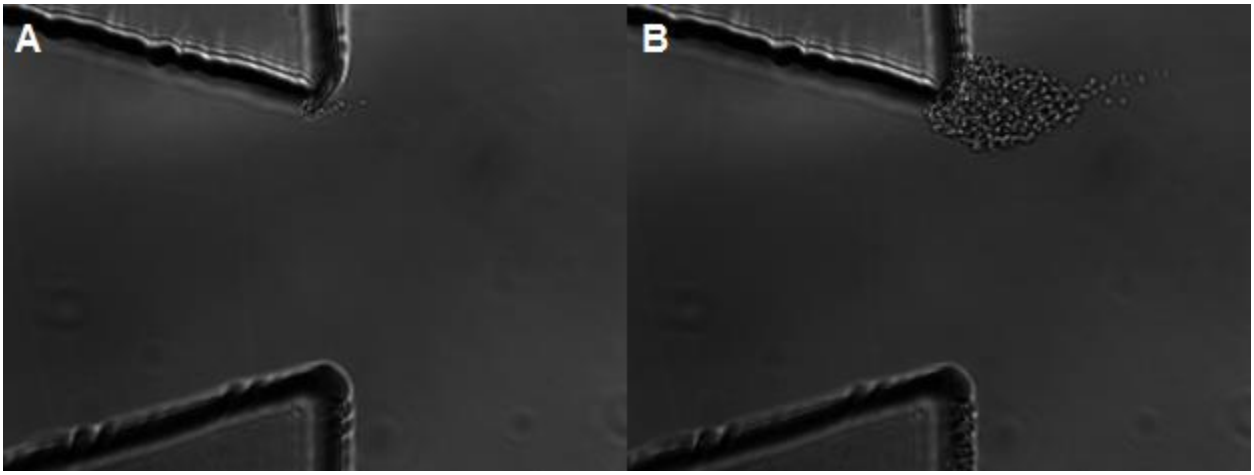

Figure 12 - Platelets sheared at 2000 s-1 through a nozzle geometry at 00'45" and at 03'35" shows that thrombus adhesion is localized to the spike-like structure along the top wall surface. Microchannel width and depth is 100 µm at the narrow. For functionalization, matrix protein coating is done by plasma treating the surfaces and then binding von-willebrand factor in DI at 10 µg/mL for 1 hour.

Simulations run in COMSOL multiphysics (Figure 13) using the laminar fluid module demonstrates that the presence of a small obstacle extending into the high flow zone creates shear gradients that can rapidly increase from the wall shear (400-10,000 s^{-1}) to a peak shear (>40,000 s^{-1}) and back down to the wall shear rate within several platelet body lengths. Further microfluidic channels developed with these shear gradients in mind have been fabricated so that they contain similar size features in high speed and high shear regions.

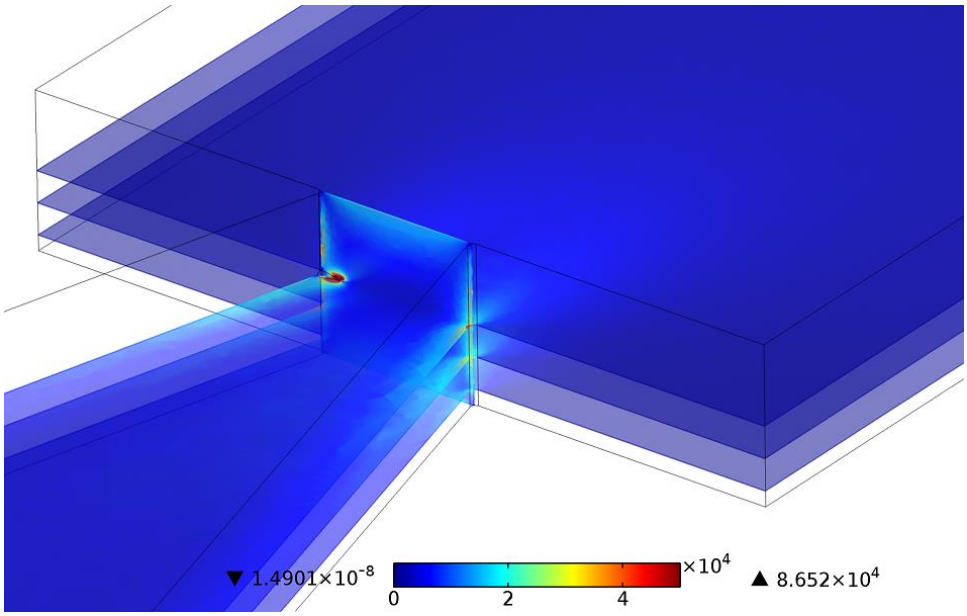

Figure 13 - Fluid shear (1/s) simulated at experimental velocities show a high presence of shear at the location of a spike-like structure but also exhibits a large dropoff from peak to the bulk fluid shear directly behind the spike. Horizontal shear slices are placed at 10, 30, and 50 µm while the vertical shear plane is centered on the spike.

With the use of the microfluidic channels we have also measured the projected area of the thrombus as it grows in size. The rates used were from low physiologic (400 s^{-1}) seen in large arteries to high physiologic or low pathologic (4000 s^{-1}) that are observed in arterioles or places where a constriction or stenosis is present.

2.2.4 Fourth Generation – Block with Microposts

Once it was established that small shear gradients could aggregate platelets in the microchannel, a new approach was adopted to place small obstructions in the microchannel with micropost(s) behind them. This places a high shear gradient that rises and drops rapidly and on the length scale of the platelet. The reduction in the size of the feature as well as the desire to capture the maximum shear gradient meant that the channel was re-dimensioned so that the micropost would extend further into the region of highest flow (centerline flow). Because of this, fourth generation channels had ducts that were 500 μm wide, 55 μm deep, and 10000 μm long. The block features were 20 μm by 10 μm by 15 μm tall into the microchannel, while the microposts were designed to be 3 μm but ended up varying from 4 μm to 4.5 μm due to mask limitations.

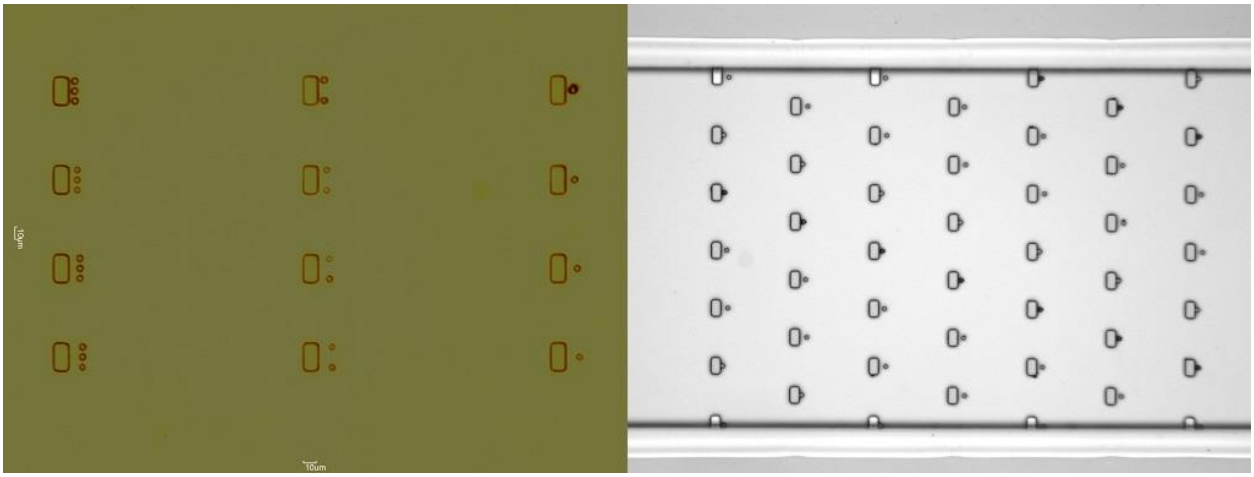

Figure 14 - Various iterations of block-post sensors show evolution of design. A design featuring several microposts was reworked into a single micropost behind each block. The image of the right displays signs of poor mask contact due to larger than designed feature dimensions.

Experiments using this device proved promising, so several revised versions were fabricated to focus in on which arrangement of block and micropost served best in aggregating platelets. The final result was a single micropost behind a rectangular block of the aforementioned dimensions. A set of masters was fabricated with microposts ranging from 6 μm to 15 μm

surface to surface from the block to optimize available volume for platelets between the rigid block and the flexible micropost, with it being found that 9 μm was ideal. A last set of masters was then fabricated with 9 μm spacing only, with the same block and micropost dimensions, again spaced in a hexagonal packing to avoid immediate downstream effects from row to row. We confirmed feature dimensions by fabricating several empty microchannels onto clean silicon wafers to enhance substrate conductivity, then imaged them using SEM. A 45° view is shown in Figure 15.

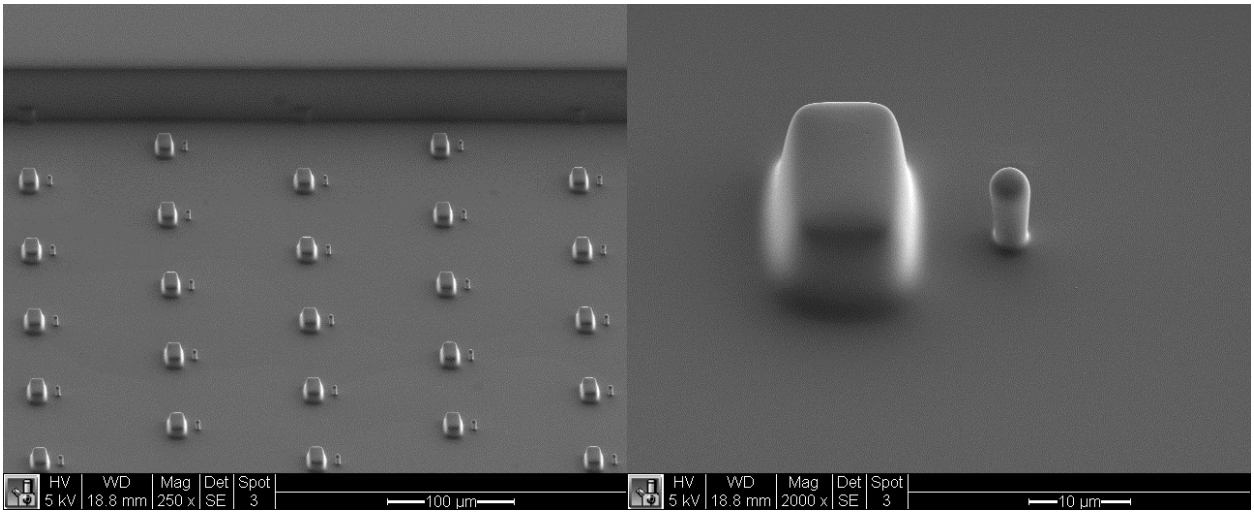

Figure 15 – Left: A SEM micrograph of PDMS block and posts design. Each block generates a localized shear gradient. The microchannel wall is seen in the top of the image. Right: A closer view of the block and post shows an inherent chamfer in the edges of the block.

We observed that there was some feature rounding evident in the corners and base of the block. The micropost also had a slightly larger cross-section at its top than its bottom but bending stiffness is not significantly affected by these imperfections. This device was the final iteration completed within this phase of the research, and produced consistently usable substrates.

2.2.5 Pumping – Platelet Shear Device

While the peristaltic pumping scheme used in the endothelial device was stable and fast, it was desirable to have a pump solution that didn't physically have two surfaces come into contact. Hand-pumping with syringes was done initially, with the eventual conversion to a set of linked master/slave syringe pumps (New Era Pump Systems Inc.) set to pump in opposing directions (Figure 16). This means that there is a minimal increase or drop in pressure as a unit of fluid entering the platelet device means a unit of fluid leaves simultaneously. Using a T-

junction with luer fitting, additional buffer syringes can be connected at the ends of the fluid path to act as flushing and air-purging reservoirs.

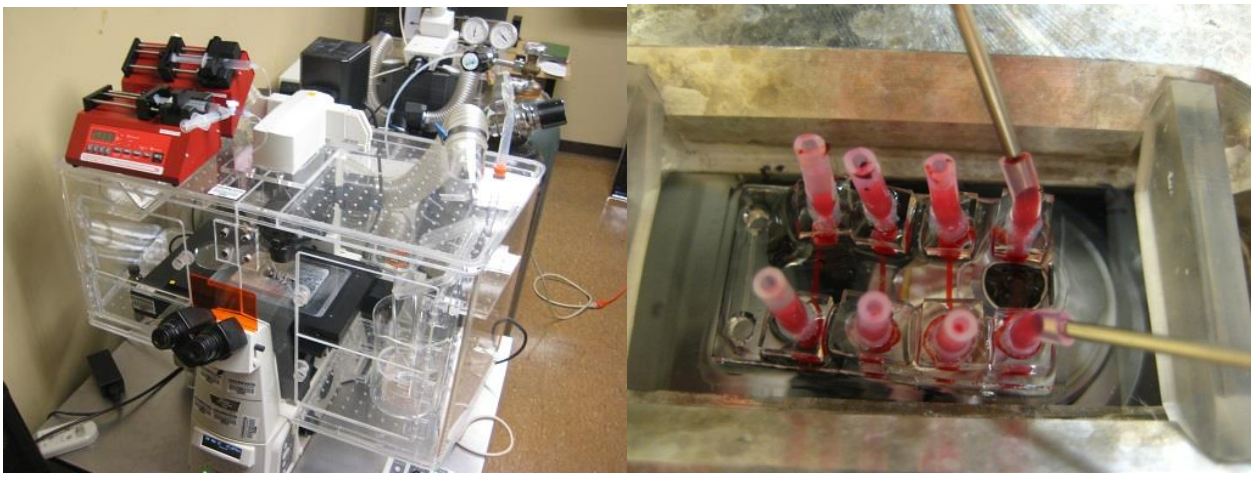

Figure 16 – Left: Live cell experimental setup demonstrating the use of two pumps to contain blood. Right: Integrated fourth generation platelet device sitting within a specifically fabricated holder on the microscope. Each of the 4 filled channels contains whole blood that has been pumped through the device at different shear rates. Stainless steel needle inlet and outlet connectors are used.

Further development lead to the use of both pumps as inlet pumps in order to infuse two separate solutions into the microfluidic device without stopping flow. This was advantageous for to capture platelet clots characteristics without allowing the clot to settle in the fluid. Previous generation platelet devices would require the researcher to stop the fluid flow, disconnect fittings, and manually swap syringes or inject fluid using a pipette. By linking both syringe pumps together with a simple Y-connector the pumps could be run sequentially to first infuse a set volume of blood through the device followed by a set volume of buffer to rinse non-attached cells then followed by a set volume of fixative solution. This method is capable of capturing suspended platelet clots in fix without dropping shear force for the purpose of confocal of SEM imaging, which is presented in later sections.

2.3 Fluid Modeling

2.3.1 Micropost

Laminar flow models were built to investigate and predict how shear gradients present in the device would develop as it passed over and through the microchannels. Concerns were raised that fluid drag forces or viscous shear would deform the microposts in a manner that would give inaccurate force measurements. With both the endothelial cells and the platelets, if there was too much post deflection, then stoppage of the flow pumping might also introduce a recovery force or displacement as the microposts spring back to their neutral state. Fluid

modeling also enables the researchers to investigate geometries before the much longer process of fabrication and testing is done. Models were created in COMSOL 4.0, 4.2, and 4.2a. The advantage of COMSOL over similar computational fluid dynamic programs such as FLUENT is its modularity. Combining the laminar fluid module with linear solid mechanics and allowing for fluid-solid interactions means that shear can deform the microposts, while the microposts can then themselves affect the developing flow of fluid.

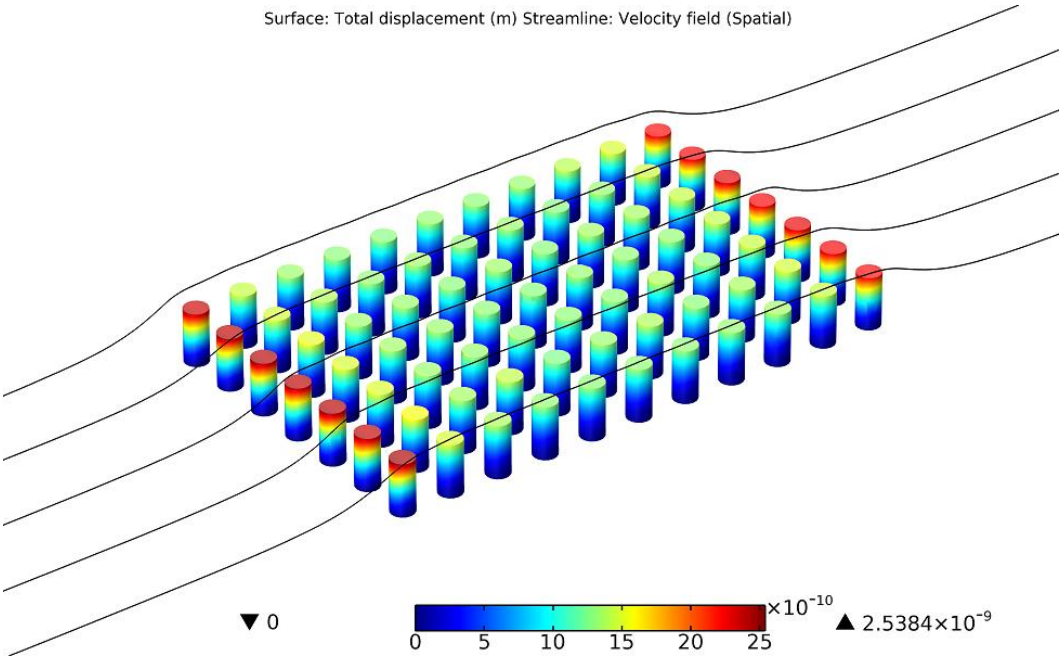

Figure 17 - COMSOL fluid-structure interactive model showing negligible deflection under high drag loading. Streamlines are shown that indicate fluid starting near the bottom of the micropost ends up passing directly over. The first row and the law row are most prone to deflections, but it is still significantly lower than measureable values.

Using this tool we confirmed that there was insignificant micropost deflection. Maximal deflections were noted at the leading and trailing edges, so endothelial monolayer data was not gathered from these zones.

2.3.2 Platelet Shear Modeling

Shear within the microchannel was modeled through COMSOL 4.3. The bulk fluid was matched to viscosity of plasma at body temperature, and platelets and other cells were considered to act independently of neighboring cells. Essentially, a platelet was considered to act as a flow tracer and experience shears appropriate to that streamline. At a pathological wall shear stress rate of 8000 s^{-1} we found that platelets encounter a rapid rise to 30000 s^{-1} or more at the upper leading edges portions of the block. Shear rate then decreases momentarily in the zone between the two microstructures before rising again at the micropost tip.

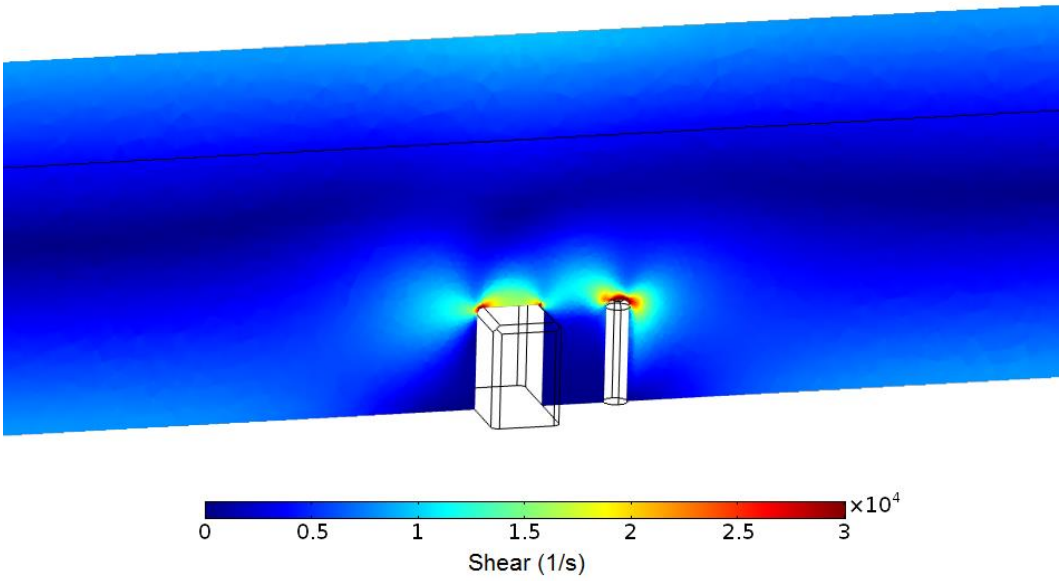

Figure 18 – COMSOL fluid shear model for pathological wall shear stress rate of 8000 s^{-1}. The microchannel is shows the full range of maximal wall shear that drops towards 0 at the centerline of the flow. Maximum flow shear occurs at the top edges of the block and micropost.

These results show parallels with previous research groups that have created structures for shear rate gradient generation. [11] In whole blood experiments we observe that platelets collect at these points first. These initiator platelets then encourage the capture of additional discoid platelets growing the clot.

Understanding the actual shear experienced by platelets during flow is critical to understanding how shear activation is initiated. Therefore, additional simulations focusing on the surface shear at the microstructures were performed. We also mapped simulated trajectories for platelets starting in front of the blocks and microposts. These results are shown in Figure 19 and demonstrate that platelets flowing across the top edge or corners encounter the highest shear stresses as well as the largest shear gradient.

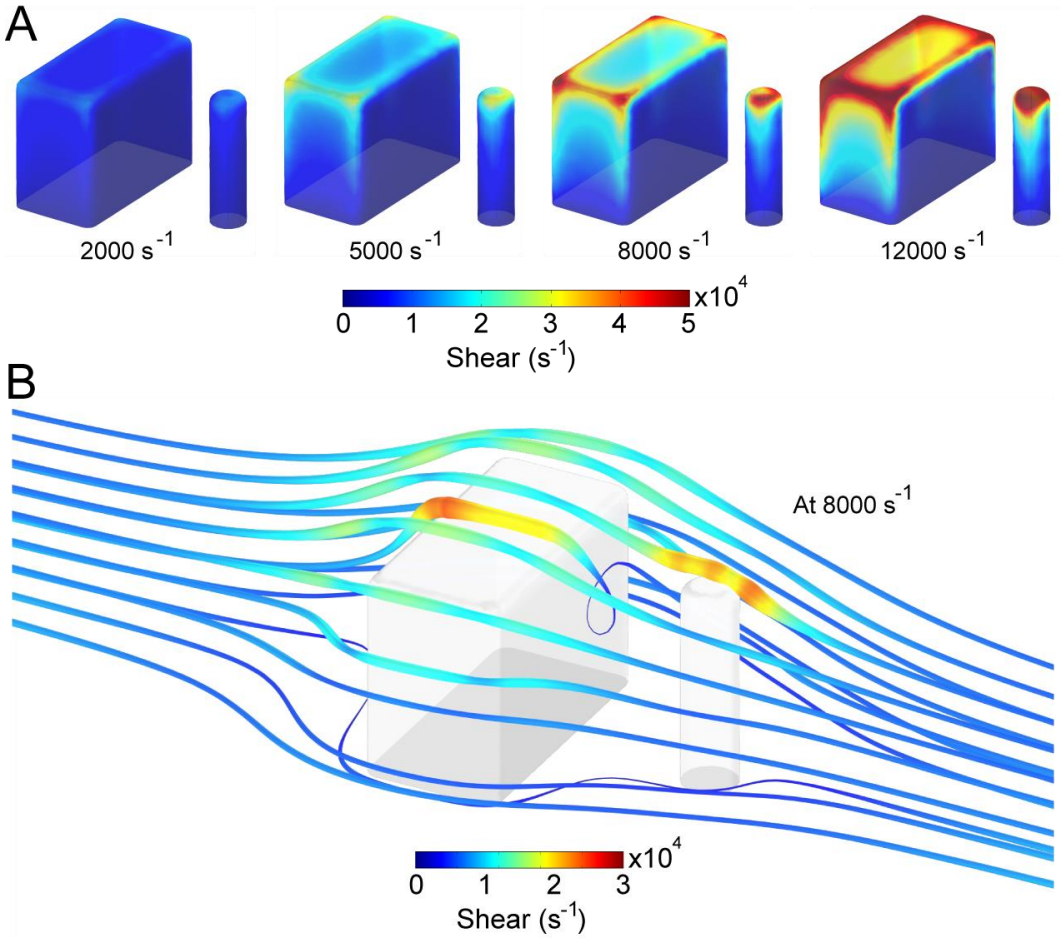

Figure 19 - COMSOL simulations of (A) microstructure surface shear at specified bulk wall shear rate. (B) Platelet flow trajectories are indicated by streamlines with line thickness and color indicating shear. Platelets at flowing across the top and corners of the block experience maximum shear stress magnitude and gradient.

2.4 Materials

The first proposed material for the endothelial shear device was glass, which is bio-inert and nonporous. However, this presented several problems. Firstly, glass is extremely hard to machine accurately without damage or surface chipping. The various incarnations of the device design all required at least some machining be done, and glass casting is prohibitively expensive and cannot be easily modified should changes need to be made. Secondly, the nonporous nature of glass could be detrimental if the device was not able to exchange carbon dioxide with the surrounding incubator to maintain proper pH levels in the cell media. In this case, the pH would need to be manually controlled by injecting buffer or acidifying agents into the media for maintenance. This added complexity of using glass led the experimenter to search for an alternate material for device fabrication.

2.4.1 Material Selection

Glass alternatives examined included Polystyrene (PS), Acrylonitrile butadiene styrene (ABS), Polypropylene (PP), Polycarbonate (PC), Polymethylmethacrylate (PMMA, Acrylic), Polyamide (Nylon), and Polyaryletherketone (PAEK). These are all easily machined thermoplastics that are stable at cell culture temperatures (37° C, 5% CO_2, 90% humidity). In particular, several of these materials were already used for biocompatible applications such as PAEK, which is not damaged during sterilization processes such as autoclaving and is already used in surgical implants. Polystyrene was an initial favorite since tissue culture dishes and flasks used (BD Falcon) make frequent use of it, but thick sheets of polystyrene can only be obtained up to ¼ inch, and are ten times as expensive as PC and PMMA for any given thickness.

2.4.2 Compatibility with Sterilization Process

Sterilization compatibility also impacts choice, since it was not practical to create a new device for every experiment, each device must be reused many times. If there was residual cell matter or media after each use and wash, then bacterial or other contamination will out-compete the cells for media and cause nutrient starvation and cellular death. To address this, the material used in the device must be able to withstand heat and pressure sterilization such as autoclaving, or chemically sterilized such as with a 70% ethanol solution. Glass would be able to withstand all of these treatments but was again impractical to machine. Some of the thermo-polymers are stable at the elevated temperatures and pressures the autoclave runs at (121° C for 30+ minutes), but a concern was cyclic breakdown as the device was reused. That is, after many heating and cooling cycles the tolerances and surface properties of the polymer can distort from the design specification. For this reason, it was decided by the experimenter that chemical sterilization using a 70% ethanol solution was the most appropriate method. All of the plastics proposed resist mildly diluted ethanol solutions without breakdown.

2.4.3 Compatibility with Microscopy

An important consideration for device material choice was also transparency. For live imaging, there had to be sufficient light passage to illuminate the cells through a fairly thick section of the material. This means the material itself had to be near glass-like so that light distortion or diffusion would not be an issue as the microscope to be used illuminates from the top (under phase light) to the camera, situated below the sample. This eliminates many of the materials that are partially transparent such as Nylon, PP, ABS, and PEAK. The remaining

materials, Polycarbonate, and Acrylic all have very good light transmission across all ranges of light and are all easily machined.

2.4.4 Tubing Selection

The second major component of the proposed setup was the tubing that would be used to connect the components together. Trial tubing materials were polypropylene, natural latex, natural rubber, low density polyethylene (LDPE), high density polyethylene (HDPE), and platinum treated silicone. This time, transparency and sterilization compatibility was less important, since imaging would not be done through the tubing and each experiment could use fresh new tubing. Concern had to be made towards the wear resistance of the tubing, since if a peristaltic pump was used; the tubing becomes subject to hundreds of thousands of cycles over the course of a single experiment. Attaching segments of tubing to the pump and running it with deionized (DI) water over 12 hours showed that the natural latex and rubber tubing would become sufficiently damaged to break visible fragments of the tubing into the flow. Any sort of physical structure flowing across the cells can cause cell crushing and detachment, so these were unsuitable. LDPE tubing was the most compliant, so it along with platinum treated silicone were selected as possibilities. Silicone is known to be very biocompatible and inert, so it was not tested.

2.5 Cell Handling

2.5.1 Cell Expansion

Four main cell types were used in the research. The first, were 3T3 fibroblast cells. The other three were all vascular endothelial cells: Bovine Aortic Endothelial Cells (BAEC), Bovine Pulmonary Artery Endothelial Cells (BPAEC), and Human Pulmonary Artery Endothelial Cells (HPAEC). All cells were low pass cells from pooled sources and received from Lonza in frozen 1 mL bullets. All procedures were done under a sterile BSL-2 biosafety cabinet (Nuaire, NU-407-600) and 70% ethanol was used to sterilize surfaces, while flame sterilization was done to clean glass pipettes and direct cell contact instruments. The researchers referenced many previous protocols for growing and maintaining human endothelial cells and used them as a guide. [67]

To increase the cell stock and have an available inventory for experiments, cell count was increased by an expansion protocol. Frozen bullets were thawed at room temperature, and 5 mL of prepared media is placed in a T25 (25 cm^2 area) polystyrene cell culture flask. Thawed cells are placed into the culture flask and placed into a 37°C incubator (Thermo, Forma Steri-Cycle) with 5% CO_2 environment. Media was replaced after 1 hour to remove unattached or

nonviable cells. Afterwards, media was replaced every 48 hours to maintain nutrient and waste levels. When the cells are confluent, or formed a solid monolayer along the bottom, they were moved to a larger T75 (75 cm^2 area) tissue culture flask. The cells in the T25 flask had their media removed using a sterile glass pipette through vacuum. 10 mL of 1X PBS was added to the T25 to dilute the residual media in the flask and removed after 30 seconds of rinsing. 500 µL of Trypsin EDTA (Mediatech) was added to the flask and incubated for 30 seconds. Trypsin and EDTA act as chelating agents, attracting the calcium and other ions responsible for integrin activation on the cell's membrane. Without these activators, integrins release and the cells separate away from their attachments. After the initial 30 seconds, every 15 seconds following, the cells were checked to see if they have detached from the bottom surface of the flask. When they have they appear as floating spheres loosely grouped or floating individually. At this point 5 mL of the cell media was added to the flask to stop the Trypsin and EDTA reaction as prolonged exposure can harm the cells. With a sterile polystyrene pipette, the media was drawn vertically into the tube and pushed across the bottom surface of the flask to loosen any cells still attached through shear forces. This is repeated 10 times total and the media is drawn vertically into the tube and pushed into the gathered media at the bottom of the flask 10 times. Aggregated cells still attached to each other were forced through the nozzle into the stationary fluid imparting a mixing action and separating cells. Using Trypan blue (Sigma) and a coulter counter the cell density was counted and cells were diluted to 5000 to 15,000 viable cells per cm^2 of area in the new container. In a majority of cases, moving a confluent cell layer from a T25 to a T75 was acceptable to the cells.

The cells suspended in media were moved into the T75 tissue culture flask and an additional 9.5 mL of media was added to bring the total volume to 15 mL and placed into an incubator. After 1 hour the media was replaced to remove the remaining Trypsin, EDTA, nonattached, and nonviable cells. Every 48 hours after the media was replaced to maintain nutrients and remove waste. Total time to reach confluence from thaw to a full T75 monolayer varies, with 3T3 cells reaching confluence within 5 days, BAECS and BPAECs taking up to 8 days, and HPAECs taking up to 10 days. Transferring cells from container to container was referred as a pass and each successive pass means older and older generations of cells as they divide and proliferate. Cells from low passes will inherently be more close to the original cells and so while expansion of the cells may increase their passage number, a large count of cells can be cryo-preserved to use an equal generation of cells in experiments. Cell media is listed in Table 2.

Table 2 - Media used in cell expansion

Cell Type	Base media	Serum	Factors	Antibiotic/fungal
BAEC (Lonza)	EBM-2 (Lonza)	10% FBS	EGM-2 SingleQuot Kit (Lonza)	-
BPAEC (Lonza)	EBM-2 (Lonza)	10% FBS	EGM-SmBM SingleQuot Kit (Lonza)	1% P/S/G
HPAEC (Lonza)	Ham's F12-K (Thermo)	10% FBS	EGM-MV SingleQuot Kit (Lonza)	1% P/S/G

2.5.2 Cell Cryopreservation

Cells to be frozen were counted using Trypan Blue and a coulter counter. They were detached from their expansion container using Trypsin EDTA and re-suspended into media as described in the Cell Expansion section. This media was placed into a sterile 15 mL centrifuge tube and spun at 1000 rpm for 5 minutes with a counter mass in a CL-2 Centrifuge (Thermo Scientific). The cells were forced to the bottom of the tube and a sterile glass pipette with vacuum was used to remove the media above leaving the cell pellet. A solution of 90% Fetal Bovine Serum (FBS) (Gibco) and 10% of the cryo-protectant Dimethyl Sulfoxide (DMSO) was added to re-suspend the cells to a 10,000 cell per cm^2 density for tissue culture. The pellet was broken up using shear action from a pipette and 1 mL of the cell solution was dispensed into sterile 1.8 mL CryoTubes (Nalge Nunc International).

Freezing cells was done by placing the CryoTubes in a room temperature isopropyl alcohol cooling container and placed into a -80°C freezer. Dropping the temperature needs to be controlled to prevent rapid ice crystal formation which can puncture the cell walls and reduce viable cell count. By using this container, the temperature was lowered at a rate of approximately 1°C/min. Once they have reached -80°C the CryoTubes are moved to liquid nitrogen (LN2) for storage. Through the research, cells were found to have no significant drop in viability when revived from the LN2 container using this method of cryopreservation.

2.6 Biocompatibility Testing

Biocompatibility experiments were done to ensure that the materials to use for the proposed device were not harmful to cells and would not affect intercellular or intracellular signaling. Plasticizers used in both high density and low density plastics can leach out of the material and into the surrounding media over time. Primary goals of these experiments were to

check if cellular shape and behavior was altered when exposed to media in contact with the materials.

The three materials for the device were obtained from a common source (TAP Plastics, Seattle) and fragments of the material were made to maximize exposed surface area. Tubing materials were obtained from the University of Washington and McMaster-Carr, and diced to also maximize exposed surface area.

2.6.1 Procedure: Biocompatibility

Bovine Pulmonary Aortic Endothelial Cells (BPAECs) and Bovine Aortic Endothelial Cells (BAECs) were grown in Lonza Bovine cell media with 10% fetal bovine serum. Cells were thawed from frozen, and seeded at 33% confluence into a T25 flask with 5mL of media. Cells were allowed to grow for 5 days prior to the experiment to confluence with media switched after 2 days. The purpose of the initial time was to allow cells to acclimate to thaw and resume normal biochemical operation. At the start of the experiments, the T25 flasks had the media suctioned away. 1X phosphate buffer solution (PBS) (MP Biomedicals) solution was added to the flask to dilute and wash the remaining media off the cells and removed. 0.5mL of Trypsin solution was added to the flask to digest the external integrin bonds of the cell to the flask surface and detach the cells. The flask was placed into the incubator for 30 seconds to promote Trypsin activity. After this time was up, 5mL of media was added to the flask to stop the Trypsin reaction and shear mixing and washing was done manually to separate cells from one another in solution. Suspended cells can then be transferred into the experimental wells.

6-well (30mm diameter per well) polystyrene cell culture plates were used for biocompatibility experiments. Fragments of each tested material were placed into each well before each experiment. Cells were seeded into each well at 33% confluence density and the well was placed into the incubator for one hour. After one hour, the media was suctioned away to remove unattached cells. After this, we replaced media every 2 days to ensure proper supplies of nutrients and pH of the media. Phase light images were taken every 24 hours at 10x magnification from initial seeding time to observe cell morphology and general growth behavior.

2.6.2 Results: Biocompatibility

Results are shown in Figure 20. The control samples of both BAEC and BPAEC cells grew normally over 72 hours and display normal morphology. These images were used to compare for each material. BAECs were sensitive to Polycarbonate at the 72 hour mark, showing a low density of growth, the BPAECs were insensitive to Polycarbonate and matched

the control densities. Interestingly, the opposite held true for Polyethylene. BAECs grew, albeit at a slower rate compared to control, when in contact with polyethylene. BPAECs were severely harmed by the polyethylene and showed no viable cells after 72 hours. For PMMA, BAECs again showed stunted growth rates, but BPAECs had no issue growing with PMMA.

The results of this experiment indicated that the hardiest and least affected cells were BPAEC, since they had no stunted growth rates with either Polycarbonate or PMMA. BAEC cells did not grow as fast as control in any of the 3 materials. It was also theorized that the BAEC cells were irregular at the start due to their fibrous and elongated nature, indicating a higher fibroblast population.

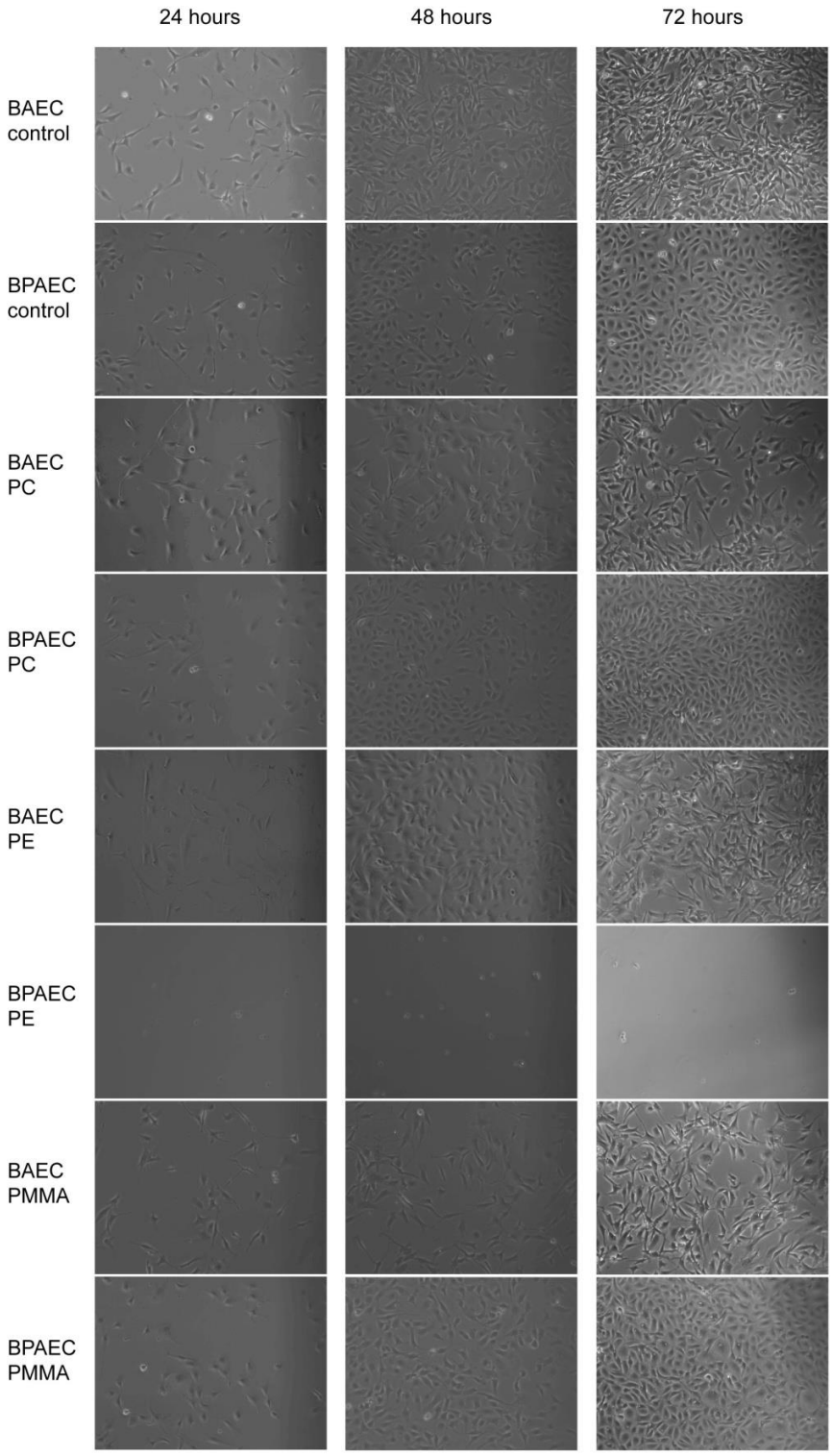

Figure 20 – BAEC, BPAEC biocompatibility. Images taken under phase light to examine morphology and density while in media contact with tested materials.

2.7 Cell Culture Media

Cell media provides cells with the necessary nutrients including sugars, salts, and growth promotion signalers. In the incubator, the cells were cultured in an environment that was maintained at 37 degrees Celsius, with a 5% carbon dioxide content, and 90% humidity. This creates a slightly acidic environment for the cells as the carbon dioxide is diffused into the cell media, forming carbonic acid over time. Rates of nutrient consumption and the rate of waste generation additionally impact the health and the general growth rate of the cells over time. In order to find the most effective media for growing our cell types after selecting through to BPAECs, a series of media experiments was performed. It was necessary to determine what effect different nutrient mixes would have on our chosen cells.

2.7.1 Procedure: Cell Culture Media

Testing for cell effect across media led to testing between different basal media and serum combinations. The first media combination (EGM) was Lonza sourced bovine endothelial cell growth medium base with a 10% Fetal Bovine Serum (Hyclone, Thermo) concentration and 1% Penicillin (Cellgro, Mediatech), streptomycin (Cellgro, Mediatech), L-glutamine (Gibco), which came with the BAECs and BPAECs. The second media combination (DMEM-FBS) was high glucose DMEM (Hyclone, Thermo) base with 10% Fetal Bovine Serum and 1% penicillin, streptomycin, L-glutamine. The third media combination (DMEM-BS) was high glucose DMEM base with 10% Bovine Serum (Gibco) and 1% penicillin, streptomycin, and L-glutamine. The fourth media combination (EBM) was plain endothelial basal media, which did not have the added fetal bovine serum, growth factors or antibacterial/antifungal agents to serve as a negative control. The fifth and sixth media combinations were 50% each of the EGM and DMEM-FBS, and EGM and DMEM-BS respectively. EGM/DMEM-FBS and EGM/DMEM-BS combination media was tested as a cost saving possibility.

Low passage HPAEC cells were grown to confluence prior to the testing. Trypsin was again used to detach cells from the substrate. EBM media was used to neutralize the Trypsin in order to avoid introducing any growth factors into the suspension. This was then diluted with 1X PBS and the cells were suspended in the 1X PBS solution. HPAEC Cells were seeded at 33% confluence into each well on a polystyrene 6-well (30mm diameter) plate. 2 mL of media combinations (one through six) were each added to separate wells and the plate was incubated. Media was removed after one hour to wash unattached cells off and replaced. After this, media was replaced every 24 hours and the cells were allowed to grow in the incubator. Images were captured every 24 hours to record growth rate and morphology.

2.7.2 Results: Cell Culture Media

All images for the experiment are shown in Figure 21. The results of the experiment show that the standard EGM media had the best cell morphology and growth maintenance characteristics. As was expected, without the growth factors and in a zero serum (serum starved) condition as seen with EBM media, the cells were not able to propagate. The two mixes of media, EGM with both DMEM-FBS and DMEM-BS showed similar results, with the general morphology of the DMEM-FBS being generally better looking with fewer irregularly large cells. Both samples of the pure DMEM-FBS and DMEM-BS media samples showed slower growth compared to the pure EGM or the EGM mixes. The lack the growth factor supplement additions means the cells must rely entirely on signal contributions from the fetal bovine serum or the bovine serum. It can be presumed that this significantly lower growth signaling contributed to the slower growth rate. The DMEM-BS sample in particular had the largest number of irregularly large cells, suggesting that a non-optimal blend of nutrients or starvation was causing cells to switch behavioral states or become fibroblast like. This suggests that in order to maintain the proper behavior under shear regimes, cells must be grown and exposed to rich media and adding dilution mixtures could potentially cause problems. It was determined that media used would be least 50% EGM with fetal bovine serum.

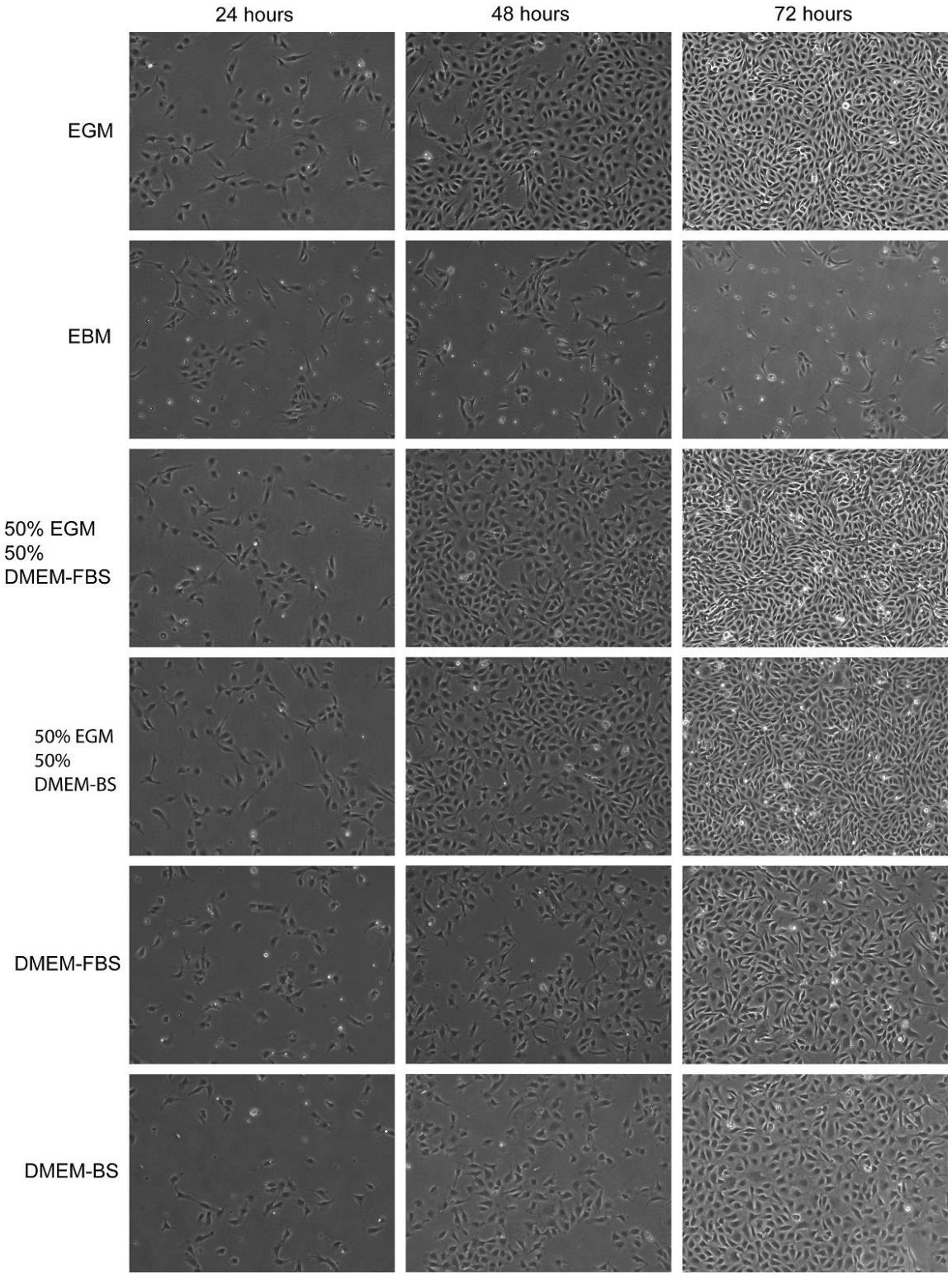

Figure 21 - cell culture media growth over 72 hours. Images were taken under phase light to examine morphology and density in various media.

2.8 Platelet and Whole Blood Preparation

2.8.1 Whole Blood Collection

Whole blood for platelet shear experiments running whole blood was collected in lithium heparin tubes (10mL 158USP BD) from consenting donors under University of Washington donor regulation compliance. Lithium heparin was used over other anticoagulants such as ACD for the reason that it does not diminish effective calcium levels within platelets. [68] Samples were stored in the collection tubes on an orbital rocker to prevent blood cell separation that would cause contact activation in platelets as well as to equally distribute heparin within the collection tubes. Because platelet behavior time sensitive, blood was put through the microchannel within 1 hour of collection.

2.8.2 Platelet isolation in buffer

Platelet isolation was done using the following solutions:

CGS Buffer: 120 mM NaCl, 13mM sodium citrate, 30 mM glucose in DI water.

Tyrode Buffer: 10mM HEPES, 138 mM NaCl, 5.5 mM glucose, 12 mM $NaHCO_3$, 0.36 mM Na_2HPO_4, 2.9 mM KCl, 0.4 mM $MgCl_2$, 0.8 mM $CaCl_2$ in DI water.

Platelets are obtained from fresh human blood samples collected in ACD following consent and compliance with University of Washington donor regulations. Fresh whole blood is first centrifuged at 120 g's to separate out platelet rich plasma from the volume. This plasma is then separated and diluted 1:1 with CGS buffer before centrifuging again at 1200 g's. This pellets the platelets to the bottom, allowing for the plasma and CGS to be removed and the platelets to be resuspended in Tyrode buffer.

2.8.3 Platelet Inhibition using Blebbistatin, Inhibitors, and Antibodies

For blebbistatin inhibition of myosin-II, whole blood was incubated with 5 μM blebbistatin for 10 minutes at room temperature prior to being introduced into the device. Controls were incubated at the same temperature and time to compensate for delay effects.

For experiments that utilized AK2 (Abcam) and c7E3, also known as 'ReoPro' (Eli Lily), whole blood was incubated with 5 μM and 20 μM of each antibody respectively, for 25 minutes at room temperature as well. Control was again incubated for 25 minutes at identical conditions to act as reliable control blood.

Due to the extremely low volumes that were used for blebbistatin and antibody treatment (<1.5 mL), incubated whole blood was drawn into their disposable pumping syringes as slowly as possible through a 18 gauge stainless steel fill needle to avoid shear activation.

For experiments using 2-methylthioadenosine 5' -monophosphate triethylammonium salt, also known as '2-MeSAMP' (Sigma-Aldrich), whole blood was incubated with 10 μM of the inhibitor for 25 minutes at room temperature before being drawn into a syringe directly, without a needle. Control was incubated with an identical amount of carrier solution (DI) for 25 minutes.

2.8.4 Platelet Experimental Protocols

Two networked syringe pumps are used to provide a steady push of Tyrode suspended platelets through the microchannel. The shear rate is set by the combination of the dimensions of the microchannel and the volumetric flow rate of the syringe pumps. Microchannels are placed on top of a 40x oil objective in a heated (37°C) live cell chamber on the microscope. Silicone connecting tubing along with a T-junction valve and a syringe of Tyrode buffer is used to pre-wet the lines and to remove as many air bubbles as possible. Platelets flowed through the device are imaged either under phase-light, or in the case of a dyed micropost, the 594 nm fluorescence channel.

3. Blood Shear Dynamics and Mechanotransduction

Human vasculature is a complex network of irregular channels, variable diameters and bifurcations. During the cardiovascular cycle the heart muscles contract as a pulse and drive a volume of blood through this system. Arteries are compliant and largely hold their cross-sectional shape through this cycle with an elastic expansion resistance to the pressure pulse. Expansion of up to 10% is normal and comes from the blood transferring internal pressure on the artery walls. Veins are far more flexible, hold ~2/3 of a body's blood volume, and are thin walled (compared to arteries). As such, they can collapse completely during the cardiovascular cycle and in response to the pulsatility.[69] *In vivo*, there exists a wide range of vascular diameters and configurations. Within these, two main types of hemodynamic flow develop. The first is laminar flow which forms when the blood flows through the smoother, straighter, or narrower paths of the vasculature. Disturbed flow is the other, developing in veins and arteries at bifurcations, or in the regions downstream of a blood clot or stent. An important assumption we make is that blood is Newtonian. However, we know that blood at the tissue length scale level is a non-Newtonian shear thinning fluid. The heart too, pumps in an extremely pulsatile manner, this pressure wave becomes translated throughout the vasculature and the pulsatility is felt by the endothelial cells. Movement of the body also creates these pressure pulses as muscle squeezes on the artery networks throughout them. Additionally, curvature, bifurcations and other natural geometry cause complex vortexes to form. [70]These are all very complex interactions that are outside of the scope of this research and these factors are not considered in the wall shear stress analysis. The researcher assumes that the blood has constant viscosity at different velocities.

Previous literature has looked at the mechanical realignment of the endothelial cells under shear showing alignment to directional flow starting in as little as 6 hours. [6, 71] This remodeling process occurs as a mechanotransductive response, that is, the endothelial cells sense a mechanical force (shear) and initiate biochemical signal cascades. Signaling pathways such as the RhoA/Rock Pathway start activating actin polymerization and focal adhesions first stiffening their cytoskeleton to resist detachment and then becoming transient for remodeling. [71, 72] This sliding of the cells supports to new locations resolves into the cell becoming physically deformed. [73] Relevant shear levels are those seen in the vessels prone to atherosclerotic lesion formation throughout the vasculature system: carotid artery bifurcation, coronary, infrarenal, to the femoral artery vasculature. [74] Shear stress of interest is in between

10 and 20 dynes, or 1.0 to 2.0 Pascal based on the vessel dimensions, and this range has been used for many previous studies.

We wanted to model the physical characteristics of the shear flow experienced at the surface by the endothelium. The approach taken was to assume that the cell monolayer was smooth enough to treat as a smooth boundary, so that individual cell height did not affect shear from cell to cell. This allowed us to calculate shear at the wall as shear on the cell. Classic no slip conditions dictate that at the surface, the molecules of fluid have zero movement and that as you approach the center of the flow the molecules speed up in what is known as a shear gradient. To calculate shear stress at boundary walls we have to decide if the device channel is either an infinitely wide plane and can be approximated as such, or if the wall effects of the vertical sides affect the flat bottom and top and choose duct flow. Because the aspect ratio of the width to the height of the channel was so large (>20:1) we can use the assumption of an infinitely wide duct. Previous research has applied shear stress with a channel and makes this assumption for wall shear calculations. [75] Wall shear stress (τ) is calculated using:

$$\tau = \frac{6\mu Q}{wh^2}$$

With media viscosity (μ) equal to 0.7E-3 N/(sm^2) at 37°C), Q is the volumetric flow rate (m^3/s); w is the channel width (m), h is the channel height (m). This equation was used to calculate shear stress in this research and for making adjustments to the height of the device. A graphical representation of the range of shears that can be generated is shown in Figure 22.

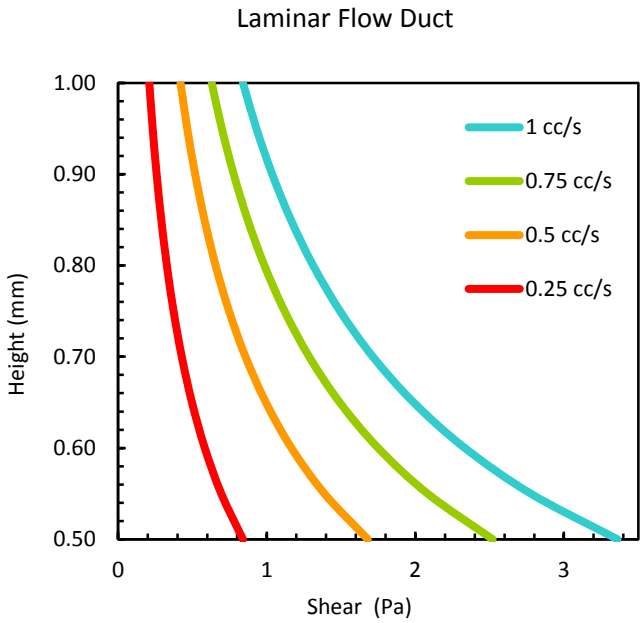

Figure 22 - Shear range of endothelial device channel.

One early concern the researchers had was if the micropost array could become deformed from shear flow alone. If they did, this would effectively create two different 'neutral states' of the microposts. What this means is they would have an under-shear state that would be globally shifted in the downstream direction under shear forces and this is the surface that cells would sense and remodel on. If removed from the shear forces they would spring back to their static form potentially shifting relative distance between posts, and deforming cells that had grown on them. To confirm that this did not happen under flow, microposts were placed into the device and run with the highest pump settings (3 mL/s) and narrowest configurable channel height (500 microns). This induces the maximum possible shear stress gradient on the microposts. Images were taken at the top and bottom of the microposts and their relative positions were analyzed. No discernible forces were seen from this analysis. Since these were done at maximum shear, we were confident that at the hemodynamically relevant shears (30% of maximum) the microposts would not deform.

4. Experimental Setup

Experiments done in the shear device were the core of the research done because they accurately replicate *in-vivo* shear forces across the cellular monolayers. Endothelial cells are from Lonza Corporation from a pooled set of bovine and human sources. Data was all collected from low pass cells such that proliferation mutation and fibroblast differentiation does not impact the data gathered.

4.1 Substrates

Substrates used to grow cells were either glass or PDMS silicone coated glass. VWR brand square 18mm no. 2 glass coverslips formed the physical base in either case. The coverslips were washed with a 70% ethanol solution if there was dirt of oil on them, and then air dried for at least 1 hour. Initial tests started with smooth glass substrates with the extracellular protein fibronectin bonded to promote cell adhesion and growth. Afterwards, the researches shifted to a PDMS coated glass layer to act as a softer surface; this layer also had fibronectin bonded. Lastly, when measuring forces, microposts acted as the substrate within the shear device. All versions of the glass coverslips or “chips” are prepared in a sterile environment.

4.1.1 Flat Substrate: Glass

Cleaned glass coverslips were plasma treated in a plasma etcher (Structure Probes Inc., Plasma Prep II) for 90 seconds. Plasma treatment attacks the surface of the glass and changes its surface from hydrophobic to hydrophilic. The glass coverslips are moved into a sterile biological hood. Fibronectin (BD Biosciences) in DI water at a concentration of 50 µg/mL is applied to coat the top of the glass. The fibronectin is allowed to absorb onto the glass surface for 1 hour. The substrates are washed in DI water (Millipore, Direct-Q 3) for 15 seconds to remove unabsorbed fibronectin then washed again in a 70% solution for 15 seconds to ensure that any aerial contaminants that may have bonded are sterilized. Another 15 second DI water submersion follows to remove remaining ethanol and they are air-dried. The glass chips are then ready to have cells seeded onto them.

4.1.2 Flat Substrate: PDMS coated Glass

PDMS silicone is prepared by mixing a 10:1 ratio of PDMS silicone base with its hardener catalyst. This mixture has many bubbles trapped in it so degassing is done by placing the mixture into a vacuum chamber that is pumped to 0.25 Atmospheres and left for 1 hour. This forces the bubbles out of the mixture and effectively removes microbubbles that can expand during heat curing. Cleaned glass substrates are plasma treated for 90 seconds in order to

activate their surface. The glass is placed onto a larger silane treated glass platform and 100 mL of PDMS silicone is dispensed into the center of each piece. When the PDMS has spread sufficiently outward, another large silane treated glass platform is placed on top forcing the PDMS into a thin film on top of the glass substrates. This triple layer of glass is placed into a 110°C oven (Fischer Scientific) for 2 hours to cure. Afterwards the PDMS is removed from the oven and allowed to cool; separating the layers results in the chips having an even thickness of hardened PDMS in a thin film on one side. The edges of the chips are trimmed of excess PDMS. Several options exist at this stage.

To create whole chip monolayers the chips were placed in a UV-Ozone Cleaner (Jelight, Model 342) and ozone exposed for 7 minutes to promote fibronectin adhesion. They are then moved to a sterile biosafety hood where fibronectin at 50 µg/mL is applied to the surface and allowed it to absorb for 1 hour. Afterwards, chips are washed in DI water for 15 seconds, 70% ethanol for 15 seconds to sterilize them, and DI water for 15 seconds. Air-drying is done and the chips are ready for cell seeding.

The second option is to create a controlled area for the cells to grow on. Microcontact stamping is our process of doing this and can be thought of as a stamp and ink technique. Features for the stamp are created in negative profile and developed in SU-8 through photolithography on a silicon wafer. This wafer is silane treated, and PDMS at a 30:1 ratio of silicone base to elastomer catalyst is poured on top and cured. This process forms a positive stamp. When microcontact stamping is desired, the stamps are ozone treated for 7 minutes and placed feature side up in a deep dish. Fibronectin at 50 µg/mL is applied to the surface by using small drops to coat the surface then joining the droplets together. Since PDMS is highly hydrophobic, this drop-join procedure was necessary to fully coat the area using a reasonable volume. Otherwise, adding one large drop will roll off before it spread. After 1 hour of fibronectin absorption we add DI water to flood the dish. At this point the fibronectin has formed a surface film. Flooding the dish from the bottom up lifts the film away from the stamps to avoid depositing it. Stamps are submerged into a dish of DI water for 15 seconds and into a second dish of DI water for 15 more seconds. Nitrogen is used to dry the stamps in a sterile environment. Glass backed PDMS films are ozone treated for 7 minutes and placed onto a flat surface. The stamps are gently lowered to come into contact with the chips and a clean layer of fibronectin is transferred from the raised features of the stamp to the PDMS surface of the chip. Now that there is a pattern of fibronectin on the chips, the stamp is removed and a 0.2% solution of Pluronic F127 in 1X PBS is applied which forms a monolayer of water saturated particles on the

non-stamped surface area, blocking off the ability of cells to attach there. Washing steps of 15 seconds in 100% ethanol, then 15 seconds in 70% ethanol, then 15 seconds in 1X PBS, and lastly another 15 seconds in 1X PBS solution sterilize and remove excess Pluronic. The chips are stored in 1X PBS until ready to use in order to maintain the Pluronic layer. This whole process results in a chip with highly adhesive areas and highly slippery areas with the combination of the two working to create a patterned controllable growth area for seeded cells.

4.1.3 Micropost Substrate: Flat Stamped

To perform basic functions like locomotion or proliferation, cells exert traction forces at their focal adhesion sites and we have an interest in how these forces become modified under different shear regimes. Previous methods of measuring traction forces include the use of surface particle tracking or polyacrylamide gel substrate deformations. A previously established method using PDMS micropost arrays has been shown to be able to measure traction forces reliably, and was used in this research. [76] On a silicon wafer coated with SU-8 photopolymer, a grid of vertically oriented circular pillars is designed and etched. This hardened wafer acts as the master for soft lithography casting. The wafer is diced and the pieces are coated with silane to act as a non-stick layer. PDMS silicone in a 10:1 ratio is poured over the wafer and heated to 110°C degrees for 10 minutes. Despite the short time at heat, the PDMS negative casting cures and is then removed from the SU-8 master. It is trimmed to form a smooth surface along its feature side. Next, the wafer undergoes a plasma treatment and becomes exposed to silane gas for 24 hours to form PDMS release surface. After treatment, the mold is ready for soft lithography contact.

Cleaned glass coverslips are plasma treated for 90 seconds to increase the adhesion between the glass and silicone. These coverslips are then laid on a larger glass panel to ensure even heating. 100 mL of degassed 10:1 ratio PDMS is added to the center of each cover piece. When the PDMS has spread sufficiently, the feature sides of the negative molds are placed in contact with the uncured PDMS droplet. Heating to 110°C for 2 hours cures the microposts. After removal, the microposts can be separated from the negative mold. However, removal of the microposts without post collapse was a tricky process that required several iterations. In the end, it was determined that using a razor blade to remove the over-flow of PDMS first greatly aided in removal. Microposts will stick in the negative hole and resist removal. When they do disengage they can spring outwards and contact other microposts permanently sticking the two together and preventing proper cell detection. Peeling from one corner to the opposing corner

maximizes the distance between posts as they come out of their wells and can minimize post to post sticking.

To bio-functionalize the microposts, an extracellular protein matrix must be applied to encourage seeded cells to attach and spread on the posts. Microcontact printing allows this to be done even on microposts. A 30:1 ratio of PDMS is applied to the top surface of a cleaned flat silicon wafer. The resulting stamp has a flat surface and is cut into the appropriate size for the microposts. The stamps are ozone treated for 7 minutes and 50 µg/mL fibronectin is applied to the top surface to absorb. After one hour of absorption, the stamps are gently lowered protein side down to contact the tops of the micropost arrays. After a short contact time of around 10 seconds, the stamps are gently removed and the micropost chips are placed into 95% ethanol solution for 15 seconds, 70% ethanol solution for 15 seconds, washed with a sequence of DI water for 15 seconds each and then into a dish with 1 µg/mL DiI (Life Technologies) solution in 1X PBS for 1 hour. DiI is a hydrophobic and lipophilic fluorescent dye that readily binds to PDMS silicone and excites at 594 nm for imaging the tops and the bottoms of the microposts. After the DiI staining, the chips are washed with a sequence of DI water for 15 seconds each and placed into 0.2% Pluronic F127 solution in 1X PBS for 1 hour. The Pluronic layer acts to block off the non-stamped areas of the microposts including the sides of the pillars and the base surface. Without proper blocking, the cell could first attach to the fibronectin tips and migrate downwards on the microposts preventing accurate force measurements. After the 1 hour of Pluronic blocking the cells are washed in 1X PBS for 15 seconds two times and stored in 1X PBS at 4°C for up to 1 week prior to use.

4.1.4 Micropost Substrate: Patterned Stamped

Controlling the area that cells have available to grow became important in later experiments and the process is similar to flat stamped micropost substrates. In this case, the stamp is fabricated with the same method, but has patterned features that match the desired area for cells to grow on. Stamping is done in an identical fashion except with the new featured stamp. Because of the decreased contact area between the stamp and the microposts, there is a magnified incidence rate of the microposts collapsing from contact. Care must be taken to exert as little additional force beyond the weight of the stamp being placed on the microposts as possible. Peeling of the stamp must also be done to carefully as shifting of the stamp relative to the glass substrate can collapse the microposts. Peeling is ideally a smooth fluid motion that minimizes transverse movement and results in a vertical liftoff at the surface. Blocking with Pluronic is done once again to stop non-desired posts from allowing cell contact.

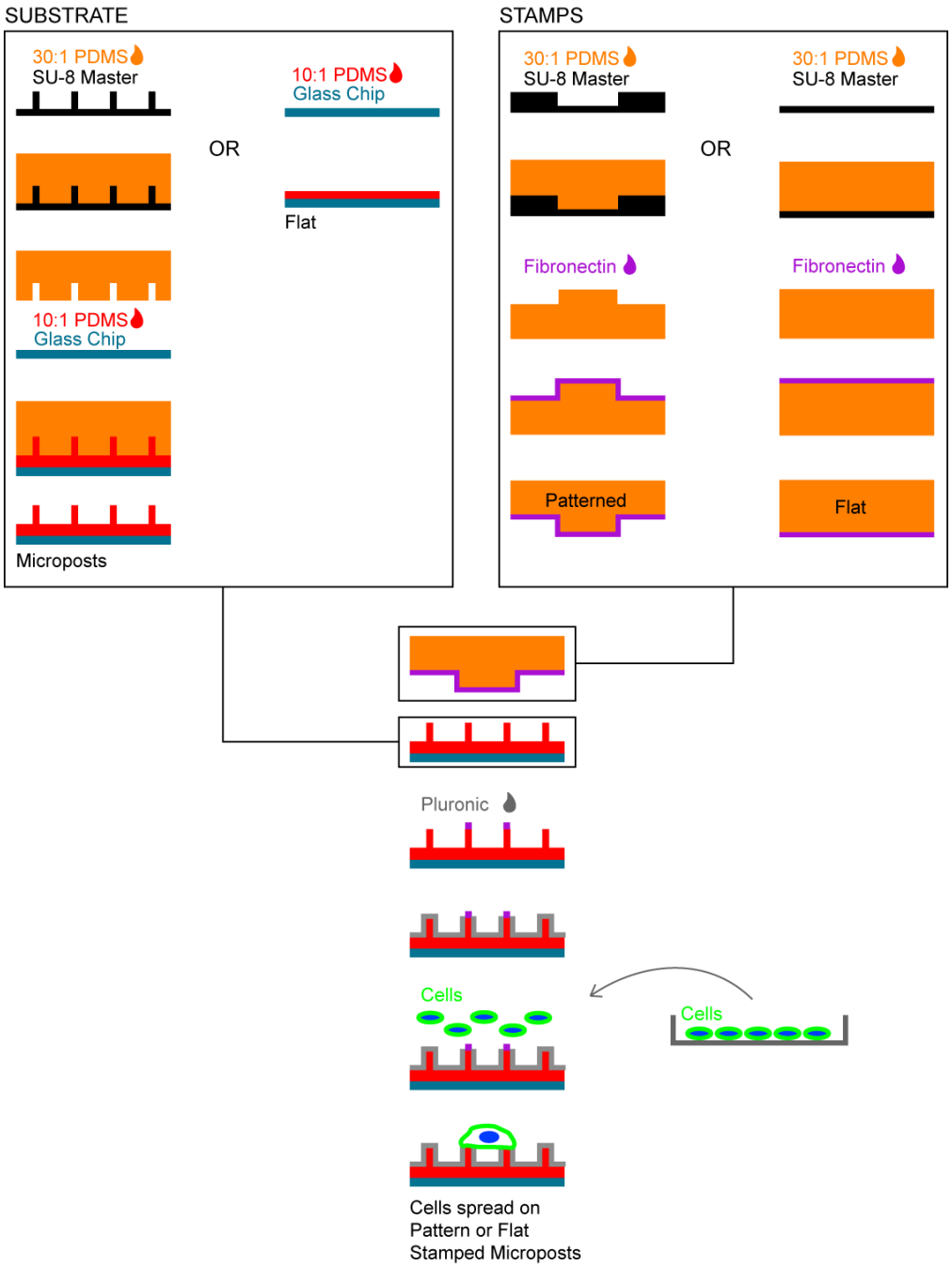

Figure 23 - Substrate Fabrication. Base substrates are in the left column. Stamp choices are in the right column. The bottom column shows stamping for biofunctionalization and blocking of the remaining area and cell seeding.

4.1.5 Platelet Devices – Assembled First Generation

Platelet devices used microposts fabricated directly onto no.0 glass coverslips (Electron Microscopy Services) which have a thickness of ~125 μm. Coverslips were first cleaned, then a droplet of PDMS was placed into the center. A pre-silanized mold of the desired micropost

structure is brought into contact with the coverslip and this sandwich is put into a vacuum degasser for 10 minutes. This draws PDMS into the mold cavity and assists in forcing bubbles out of the system. Afterwards, a bake at 110 °C overnight is done and the microposts can be removed. Depending on the aspect ratio, collapse may be present if they are of the softer variety. Channels used in the device are generally much thinner than the width of the total micropost mold so this can be worked around by choosing the best row of posts to use.

Microfluidic channels are made by aforementioned PDMS replicate casting off a silanized master structure and silanized glass plate. When these are ready, both the micropost substrate and the PDMS microfluidic channel cap are plasma treated for 90 seconds. Immediately afterwards, they are brought into alignment and contact with light pressure to form a permanent bond. Hygiene of each individual surface is critical as dust or PDMS fragments will prevent large areas from touching.

4.1.6 Platelet Devices – Integrated Second, Third Generation

Integrated platelet devices were constructed using a slightly more complex triple SU-8 layering technique. The functioning microfluidic devices are made by PDMS replication casting of the master onto a no. 0 glass coverslip. The top block is cast against a silanized glass cover slide and inlets and outlets are punched with a 2.5 mm biopsy punch. Both the micropost coverslip and the top block pieces are plasma treated for 90 seconds and pressed together to form an irreversible water tight seal. In some cases, a thin ring of PDMS is applied against the outer contact edges then quickly cured at 110° C for 2 minutes to form a more permanent seal. This was typically done for samples using whole blood to ensure no microchannel bursting would occur.

4.1.7 Platelet Device Biofunctionalization

Proteins in solution are prepared in Tyrode's buffer or 0.1 molar acetic acid (for collagen) with the optimized concentrations shown in Table 3. These concentrations have been used previously for investigations into platelet adhesion on single or mixed extracellular matrices.

Table 3 - Platelet protein concentrations

Protein	Concentration, Diluent
Collagen	200 µg/mL, 0.1 M Acetic Acid
Fibronectin	50 µg/mL, Tyrode's Buffer
Fibrinogen	50 µg/mL, Tyrode's Buffer
von Willebrand Factor	10 µg/mL, Tyrode's Buffer

In experiments using whole blood, the 50 µL protein solution was first flowed through the microchannel at the inlet and incubated for 1 hour at room temperature. This is typically done within 10 minutes of plasma treatment. Next, the protein solution is washed out by using a syringe pump (rate: 0.3 mL / min) to flow 200 µL of Tyrode buffer through the microchannel in both inlet-to-outlet and outlet-to-inlet directions. In cases where a secondary protein such as VWF on collagen is used, 50 µL of the second protein solution is flowed through the channel and incubated overnight (14 hours) at room temperature as shown in Figure 24.

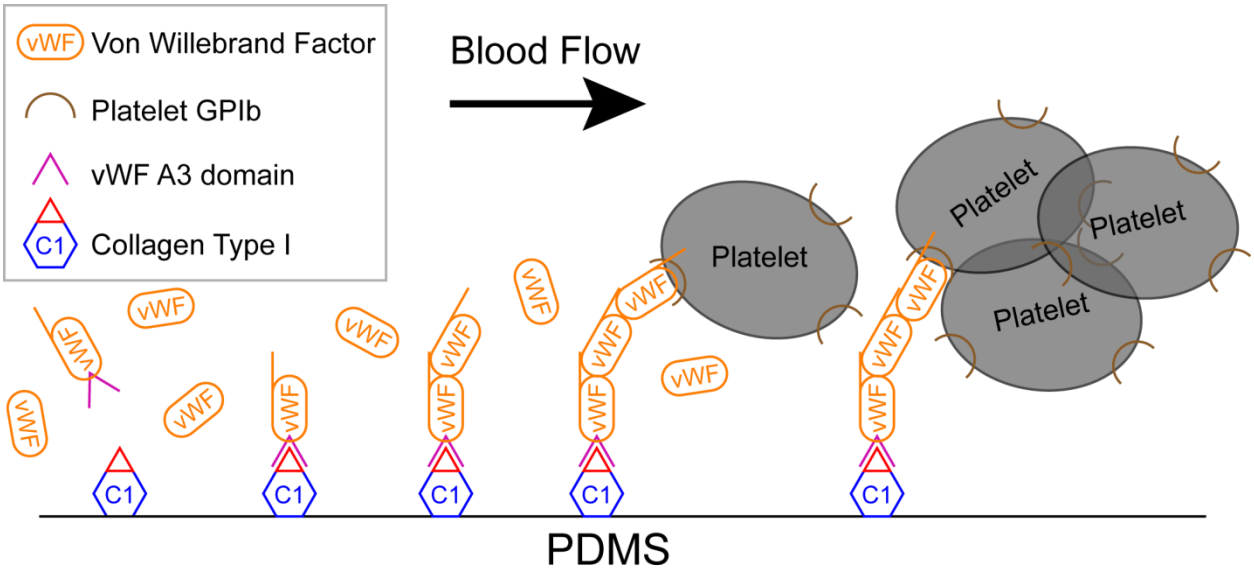

Figure 24 - Biofunctionalization of platelet microfluidic devices.

To prevent evaporation of the solution, incubation steps were performed in a capped petri dish with a container of water for humidity. After the final protein solution incubates another series of 200 µL washes of Tyrode buffer in both directions is done. Finally, 50 µL of DiI solution (1 µg/mL) prepared in DI is inserted into the channel to label the blocks and microposts and binds for 1 hour. A final wash of 200 µL of Tyrode buffer in each direction removes the unbound DiI molecules and buffer remains in the channel prior to the experiment.

4.1.8 Micropost Forces of Endothelial Cells

After cell experiments are performed, the cells exert forces on the tips of the individual microposts in the array. These are the traction forces and are calculated by considering the micropost as a simple beam in bending. The dimensions of the micropost such as height (h) and diameter (w) are determined by the dimensions of the SU-8 master. The elastic Young's modulus (E) is a function of the mixing ratio of PDMS and elastomer catalyst during fabrication.

Horizontal or planar force (F) was calculated by comparing the displacement (δ) of the tip of the micropost with the base, and follows the equation:

$$F = \left(\frac{3}{64}\pi E \frac{D^4}{L^3}\right)\delta$$

The deflection of the post was considered to be entirely in plane with the starting position. A normal force to the micropost may exist, but as the deflection distance compared to the length scale of the micropost height was very small, the vertical shift of the micropost tip was ignored in calculations.

An early issue was the aforementioned drag effect by the fluid on microposts. For the velocities of fluid we utilized in the endothelial shear device, the Reynolds number was between 50 and 100. For the platelet microfluidic device, due to the much smaller scale the Reynolds number drops to under 1. This means for infinitely long cylinders of diameter D, the drag coefficient (C_d) has experimentally been shown to be between 1.2 and 2 for the endothelial cells and up to 90 for the platelet device depending on the specific Reynolds number. We made the assumption that the length scale of the micropost compared to the device height (6 microns to 100-1000 microns respectively) allows us to ignore the shear gradient between the bottom of the post and the top of the post. The drag force generated on the posts is then:

$$F_D = \frac{1}{2} C_D \rho v^2 A$$

The area (A) was calculated by the width of the microposts used of 2.81 microns (scanning electron microscope measurement) multiplied by the height of 6.34 microns (scanning electron microscope measurement) to give 1.78E-11 m^2. Media used was similar in density (ρ) to water again, so 993 kg/m^3 and velocity (v) was calculated through the height at the tip of the micropost by using the mean velocity, which was a drastic overestimation of the velocity at the post tip, but was done for illustrative purposes; this estimate of velocity gives ~0.05 m/s. The total force experienced at the post by drag with maximum numbers and a gross velocity estimate was 0.04 nanonewtons, which was 2-3 orders of magnitudes smaller than the forces exerted by the cells, as well as being far smaller than the detectable forces for the camera and image analysis. We could then ignore the force in the final force per post calculations. Confirmation of these results was done through COMSOL and showed similar scales for drag forces and net deflections.

4.1.9 Intercellular Force

Traction forces not show how the cell interacts with the ECM, but with multiple cell systems, indeed they can show how cells affect the whole monolayer tension. With a single cell system, we can make the assumption that the traction forces would be in static equilibrium and sum to zero (Figure 25 A):

$$\sum_{i}^{n} \vec{F}_i = 0$$

For a binary cell system, each cell pulls against both the microposts they attach to and, through adherens junctions, each other. This force is equivalent to the imbalance seen when summing the traction forces underneath each cell individually:

$$\sum_{i}^{n} \vec{F}_i + \vec{T}_{ij} = 0$$

The researchers term this force a ‘tugging force’, and then an ‘intercellular force’, or sum of all external forces on any cell is defined as such:

$$\vec{I}_i = -\vec{T}_{ij}$$

This idea can be extended to multiple cell monolayers with the consideration that past the binary system it’s only possible to determine the net tugging force on a cell from all others, and not individual tugging force from another cell:

$$\sum_{i}^{n} \vec{F}_i + \vec{T}_{12} + \vec{T}_{13} = 0$$

Again, a vector sum of all tugging forces is termed ‘intercellular force’:

$$\vec{I}_i = -\sum_{i}^{n} \vec{T}_{ij} = -\left(\vec{T}_{12} + \vec{T}_{13}\right)$$

The intercellular force is relateable to traction forces directly because of the tugging force relationship:

$$\vec{I}_i = \sum_{i}^{n} \vec{F}_i$$

Finally, an average intercellular force is representative of what external force individual cells sense within a larger monolayer. Higher intercellular force means higher monolayer tension, and what this regulation of intercellular force means is explored:

$$\text{Avg I} = \frac{1}{N}\sum_{j}^{N}\left|\vec{I}_j\right| = \frac{1}{N}\sum_{j}^{N}\left|\sum_{i}^{n}\vec{F}_i\right|$$

A graphical representation of this calculation is included in Figure 25.

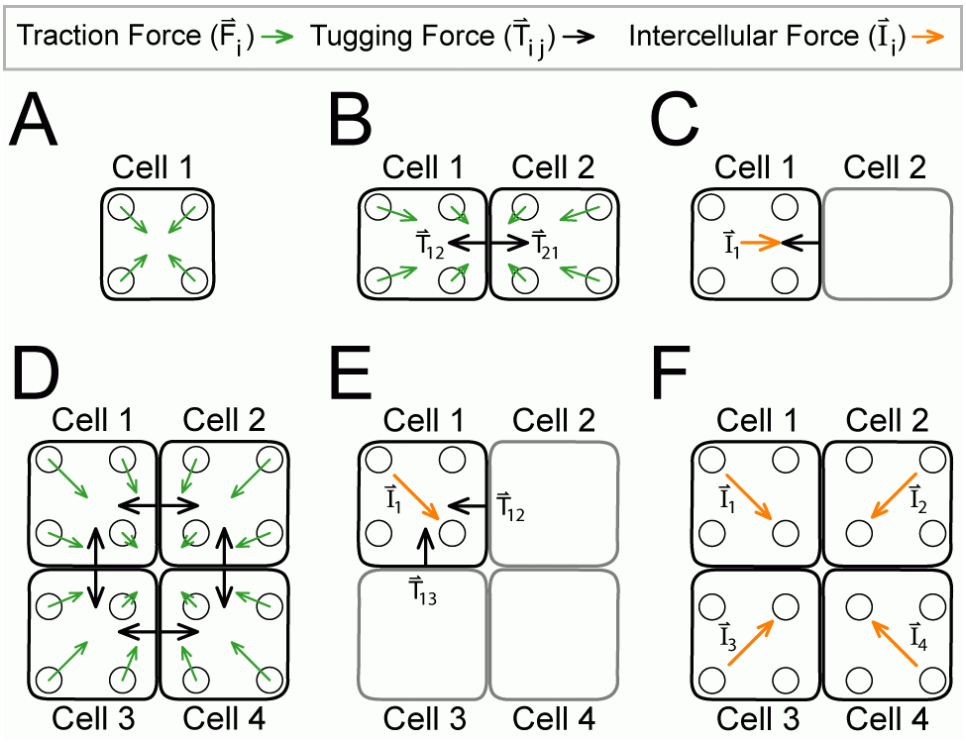

Figure 25 - Calculation of intercellular force. (A) Single cell equillibrium assumption. (B-C) Binary cell system shows that imbalance from equilibrium relates directly to tugging forces between cells. (D-F) The same extraction can be done with multi-cell systems.

4.1.10 Micropost Forces of Platelets

The platelet clots present their own challenge for force analysis because the platelet clots were observed to be along the lengths of the micropost versus endothelial cell measurements which are point loads at the post tips.

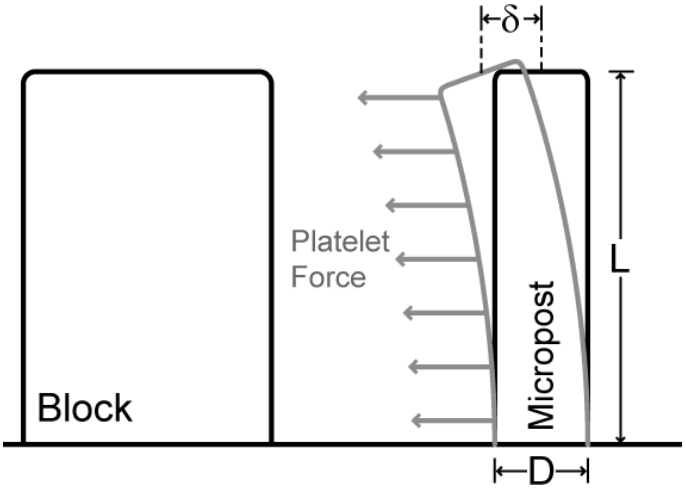

Figure 26 - Diagram relating block and micropost deflection to forces.

A calculation for the distributed load can be simplified by making the assumption that the force is evenly distributed throughout the height of the micropost. Applying elastic beam bending theory once again results in an expression to relate tip-deflection with total platelet force:

$$F = \left(\frac{D^4 \pi E}{8L^3}\right)\delta$$

Several complications potentially arise when we investigated the clot position on the post. Firstly, does a platelet clot adhere to the bottom surface of the channel between the block and post? If so, this means some of the force is exerted in a downward manner which may then inaccurately reflect the magnitude of contractility. Secondly, does the platelet clot 'tail' adhere in the downstream region? In this case, contractile platelets would place an opposing force on the micropost causing it to pull backwards away from the block and inducing a negative contractility component to the observation. To address these concerns, experiments were performed by fixing the platelet clots on the microposts while under flow to prevent clot sedimentation or settling. These are detailed in a separate section, but revealed that the forming clots appeared to be floating above the bottom surface, which gave us confidence that measured forces could be compared.

4.2 Imaging

Each experiment results in a group of live cells on either flat or micropost substrates. Phase light imaging can capture morphology or cell density but does not reveal the cell cytoskeleton or locations of specific proteins. To do so requires the use of immunofluorescent

imaging. Samples from all conditions are prepared at the same time using the same solutions to equalize reagent absorption rates. The process used is presented in this section.

4.2.1 Microscope Equipment

Images were taken on a Nikon Eclipse Ti (TI-E) inverted microscope with a 40x (platelet) or 60x (endothelial cell) oil immersion objective using Nikon fluorescent microscope oil. The light source for phase light images was a Nikon TI-100 source and for fluorescent images was a Nikon Intensilight C-HGFIE mercury lamp. The light sources were allowed to idle for 15 minutes prior to taking images so that elements within the source would stabilize in temperature and reach steady state intensity. Surrounding environmental light to the microscope was minimized by taking images in a dark room. The camera used for endothelial cell work was a Nikon Coolpix. The camera used for platelet imaging was an Andor Clara. NIS-Elements was used to control the microscope, light sources, and the camera. This allowed computer control of the focus, light intensities, filters, and camera settings and can automatically cycle through fluorescent channels. Additionally NIS-Elements gives the researcher z-distance which was critical when capturing images of the micropost tops and bottoms. The DiI top image was taken on the same focus plane as the actin and then the z-distance was used to scroll vertically to the bottom of the micropost based upon its fabricated height and a second DiI image representing the bottom of the microposts was captured.

4.2.2 Endothelial Sample Preparation

Samples of live cells on substrates are fixed in order to preserve them as accurately as possible and allow for chemical labeling and analysis. The fixing solution is made by combining 30 mL of DI water, 10 mL of 16% paraformaldehyde (Electron Microscopy Supplies), and 4.5 mL of 10X PBS. The paraformaldehyde solution forms aqueous formaldehyde which creates covalent bonds between proteins in the cell, stabilizing it both chemically and mechanically (fixed cells become more rigid). If the cells are on a deformable substrate such as the PDMS microposts the fixative process also preserves the deflections. This process kills the cells but also protects the cell from structural damage during the rest of the sample preparation process.

Samples are placed on a layer of parafilm and 1 mL of the fixative solution is dispensed on top and fixed for 20 minutes. Then they are washed by submersion in three dishes of 1X PBS for 15 seconds each. Next the cell membranes must be made permeable using 0.1% Triton X-100 (Sigma) in 1X PBS. Samples are fully submerged in this solution for 10 minutes and washed twice with 1X PBS for 15 seconds. They are then placed into a 1X PBS dish for 10

minutes to dilute and move the residual fixative and Triton. To block nonspecific ligands, samples are submerged in 10% goat serum (GS) for 1 hour.

Primary and secondary immunofluorescence solutions can then be applied depending on the protein and imaging wavelengths that are desired. Primary solutions contain an antibody that targets the antigen of interest. The secondary dye-coupled antibody is added that recognizes the primary antibody. This system gives us flexibility in choosing what we want to label and in what wavelength it will excite at. A primary solution and a secondary solution are made by combining a volume of 10% GS (150 µL for every sample) and adding in a ratio of primary antibodies or secondary antibodies respectively. The secondary solution also has direct stains added that labels Nuclear DNA (via DAPI) or Actin (via Phalloidin). All reagents are shown in Table 4.

Table 4 - Immunofluorescent reagents

Primary Solution (10% GS base)	Secondary Solution (10% GS base)
1:200 Mouse IgG Anti-Vinculin	1:200 AF647 Goat Anti-Mouse IgG
1:400 Mouse IgG Anti-β-Catenin	1:200 AF647 Goat Anti-Rabbit IgG
1:500 Rabbit IgG Anti-Fibronectin	1:200 AF594 Goat Anti-Mouse IgG
1:400 Rabbit IgG Anti-Myosin	1:200 AF594 Goat Anti-Rabbit IgG
1:200 Rabbit IgG Anti-Von Willebrand	1:200 AF488 Goat Anti-Mouse IgG
1:200 Mouse IgG Anti-ZO-1	1:200 AF488 Goat Anti-Rabbit IgG
Direct Stains	**Micropost Stains**
1:500 Phalloidin-AF488	1:1000 DiI
1:500 Phalloidin-AF594	1:200 BSA 594
1:1000 DAPI	

150 µL of the primary solution is added to the sample and absorbs for 1 hour. The sample is washed twice in 1X PBS for 15 seconds to remove residual primary antibodies. Samples are placed into 10% GS for 1 hour to wash further. Next 150 µL of secondary solution is added to the sample and absorbs for 1 hour. Again they are washed in 1X PBS for 15 seconds and placed into 10% GS for 1 hour. Lastly they are washed in 1X PBS for 15 seconds, then DI for 15 seconds.

At this point the samples have been fixed and stained and are ready to be mounted using Fluoromount-G (Electron Microscopy Supplies). Initially we sandwiched the sample between a traditional glass microscope slide on the bottom and a cover-slip on top but this resulted in the cover-slip sitting non-parallel to the slide because of tilt introduced during the substrate fabrication. When imaged through the cover-slip – the glass slide is too thick, and the tilt becomes apparent. To remedy this we swapped to using a large thin cover-slip as the base layer and mounting the sample upside down with another cover-slip as the top. This modification is shown in Figure 27.

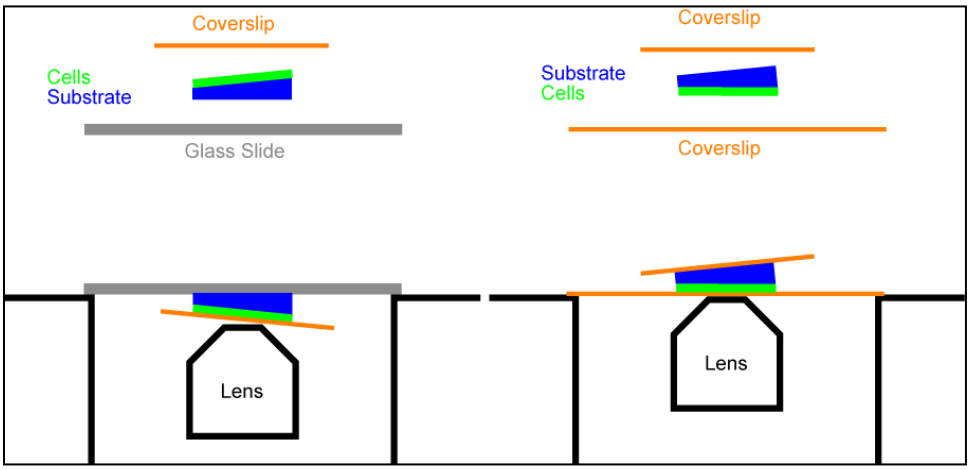

Figure 27 - Sample mounting for fluorescent imaging of micropost substrates.

4.2.3 Platelet Device Shear Live Imaging

Platelet binding occurs rapidly and has a lot of transient behavior that was of interest. Because of this, we decided to move from seeding platelets onto micro or nanoposts statically and instead using syringe pumps to perfuse platelets across microposts in an effort to observe attachment and force development. An acrylic live cell chamber (Nikon) was mounted on top of the microscope with hoses providing circulating warm air. Several days prior to experiments this system was turned on to keep the enclosure at 37 °C and thermally equilibrate the microscope. A specially designed holder fitted to platelet microchannels is used to minimize x-y-z drift as much as possible. Samples are mounted in the holder 30 minutes before the experiment to allow for the device to rise to the enclosure temperature. A Nikon 40x oil immersion lens is used to capture a wide field of view encompassing 5 block-post pairs.

In order to focus to the top of the micropost, an initially focus was made to the bottom plane where the micropost is largest then the stage is translated in the z-reiction 13-15 μm to arrive at the micropost tips. Micropost imaging was automatically set to occur every 1 second

while phase light imaging occurs every 20 seconds. Neither channel is binned to preserve as much data as possible. It was unnecessary to image the bottom of the microposts because a comparison is made to the starting position of the micropost tip rather than to the base.

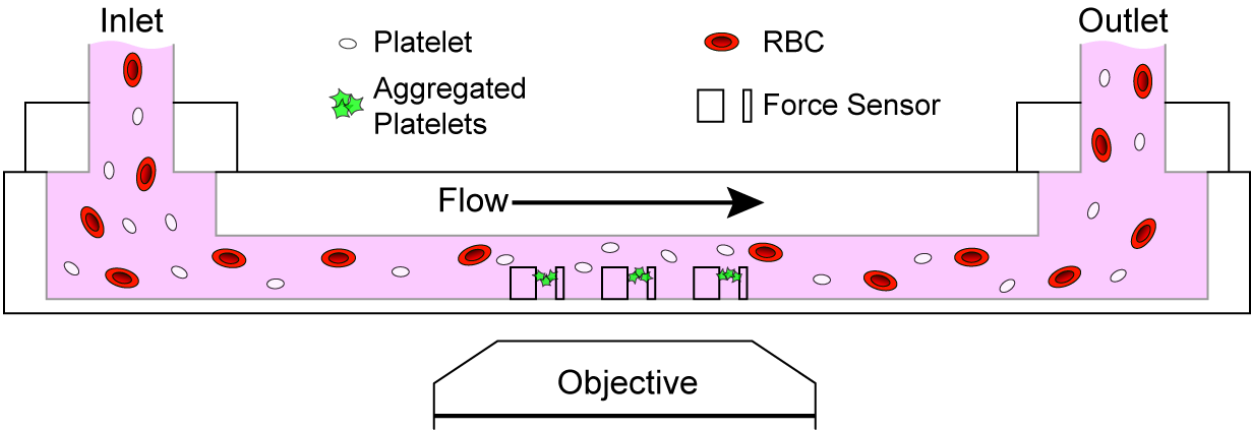

Figure 28 - Platelet device mounting for live shear experiment imaging.

Close packing of multiple channels into one master means rapid changeovers from one experimental condition to the next. In general, each condition takes between 5 and 15 minutes to run to completion including time associated with loading the next blood sample.

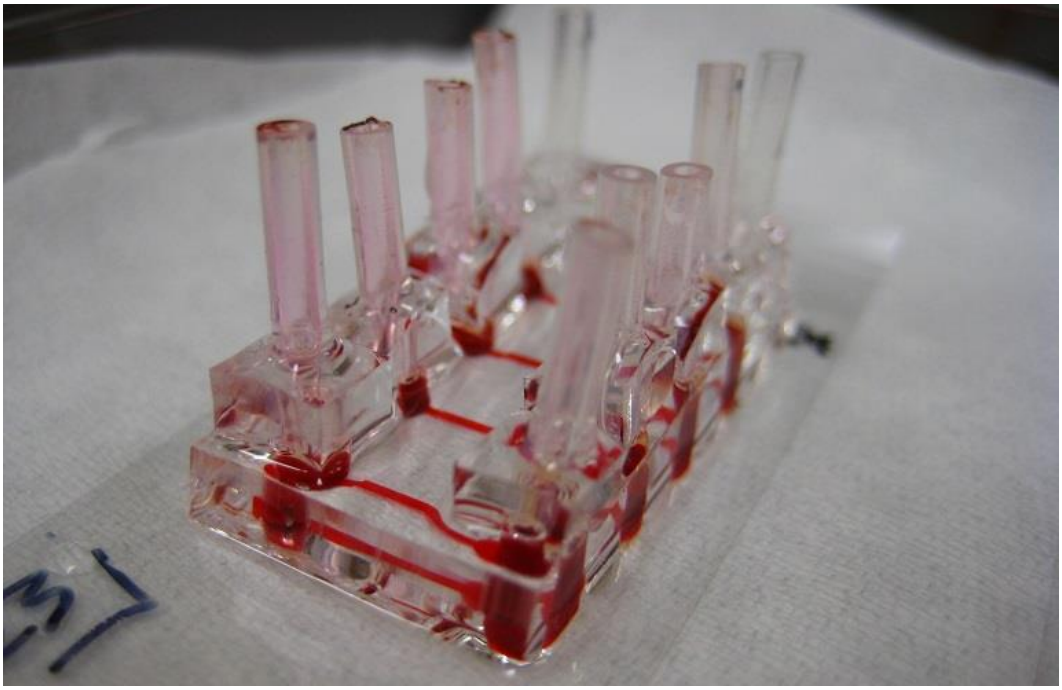

Figure 29 - Microfluidic device after an experiment showing whole blood in 4 of the 5 available channels.

4.2.4 Platelet Sample Imaging Preparation

A similar technique was used to fix and stain platelets within the microfluidic device. However, to better capture the clot structure, we fix while under shear. After an experiment, a 50/50 mix of 16% paraformaldehyde and 0.2% Triton solution in 1X PBS was perfused through the channel to both stabilize and permeabilized the cells and cell membranes. The appropriate sequences of primary and secondary antibodies were then injected in sequence to image the desired protein as previously described. Final fixation was achieved by mixing Fluoromount-G with distilled water in a 50/50 mix to thin the solution then injecting this into the microchannels. When confocal imaging was done, this was done within several days of the final mount.

For SEM imaging of clots, a solution of 16% paraformaldehyde was injected directly into the channel and allowed to fix the platelets for 30 minutes. Then the glass in the microfluidic device is carefully broken along inscribed lines to remove the section containing the sensors. At this point, the platelets are fixed well in place, and the glass is rinsed with PBS before being mounted onto a silicon wafer for critical point drying (CPD) and SEM imaging. Briefly, CPD is a process of dehydrating samples without destruction of structures associated with conventional drying techniques. This enables the imaging of cell structures in as close to a native state as possible. An example SEM micrograph of platelet clots (45 seconds, 8000 s^{-1}) before fixing and CPD is shown in Figure 30 to demonstrate image quality. There is some noticeable shrinking associated with CPD due to the dehydration of proteins within each sample, which may cause the microposts and blocks to be deflected more than they are prior to the process.

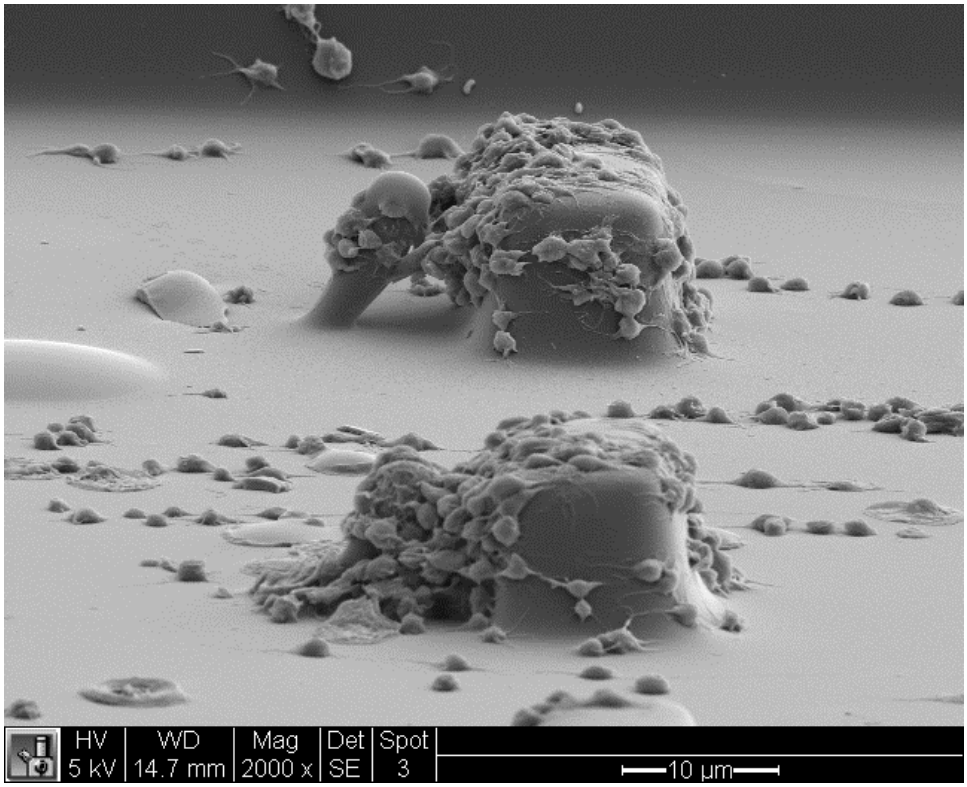

Figure 30 – Platelet clots formed on a set of sensors. Imaging was done by first applying CPD to the sample. Sample shrinkage due to dehydration is expected and exaggerates the bending of the micropost. Flow is from right to left for 45 seconds.

4.2.5 Immunofluorescent Imaging Bleaching

With immunofluorescence imaging, prolonged exposure of the sample to the excitation source can cause fluorescent bleaching of the region observed. This effect is exacerbated by higher intensities of the light source. Because one of the metrics developed in this research was β-Catenin intensity correlating to cell permeability, it was necessary for the researchers to minimize this effect as it introduces error into relative intensity measurements for experimental conditions. To gather images and minimize bleaching the researchers chose a region of the sample to be used for focusing and initial adjustment of the microscope. Once the proper focal plane was achieved the researcher moved the sample stage to the region of interest and began taking images. All images within all conditions in individual experiments for β-Catenin were taken at the same settings for source intensity and exposure time in order to acquire relatable images. Different channels such as DAPI (Invitrogen), phalloidin-AF488 (Alexa Fluor® 488, Invitrogen), and AF594 (Alexa Fluor® 594, Invitrogen) were taken for each sample without pixel binning and layered in NIS-Elements.

5. Image Analysis

Cell morphology is a visually very quantifiable but quantification is necessary to develop a metric for cross-condition comparison. Previous literature has taken various approaches to quantifying cell alignment or cell monolayer permeability including hand tracing and calculating angular direction manually. [77] An automatic protocol for analysis provides a non-biased way to calculate orientation such as seeding particles onto the surfaces of cells and tracking the particle movement [78], 3-D image segmentation and analysis of the shift [79], genetic protein level expression like IL-8 or VACM-1 that become expressed with remodeling [3], gene expression patterns responding to shear regimes [80], and cytoskeletal fiber orientation [81]. Our approach uses fiber orientation because we are interested in f-actin stress-fiber alignment and cytoskeleton tension driven focal adhesion remodeling. Image analysis processes were created in MATLAB 2007a and the researchers developed the metrics from no starting code.

5.1 Actin and Cell Orientation

Our cell orientation analysis program determines direction by examining actin stress fiber direction and is loosely based off Yoshigi *et al* fiber orientation. The immunofluorescent staining procedure gives us bright actin filament images. F-actin is a mostly a linear strand with few branches but length of the actin filament can differ greatly between cells and across experiments. Complicating this is that f-actin forms a network, so one strand intercepts many other f-actin stress fibers so a program that looks for isolated strands may work on specific sections of the cell, but does not give us reasonable functionality across one entire cell and monolayers of cells. Our solution to this was to analyze every pixel in an image looking for the direction of the greatest brightness in the surrounding 8 pixels (except on edge pixels). Essentially we find the direction of greatest brightness gradient. Once the direction is determined, we generate a vector. The magnitude of this vector is calculated by taking the ratio of the analyzed pixel brightness over the image's brightest pixel. We analyze every pixel in the image and the result is a vector for every pixel in the image with a direction and a magnitude proportional to its relative brightness. Analysis of an actin stress fiber creates a series of vectors pointing towards the center of the fiber core as shown in blue in Figure 31. The vectors are rotated orthogonally so that they become in line with the actin strand as seen in green in the figure. All vectors above an actin strand will thus point to the right of the image and all vectors below a strand will point to the left. We take all of the left pointing vectors and do a 180° rotation on those to bring them around.

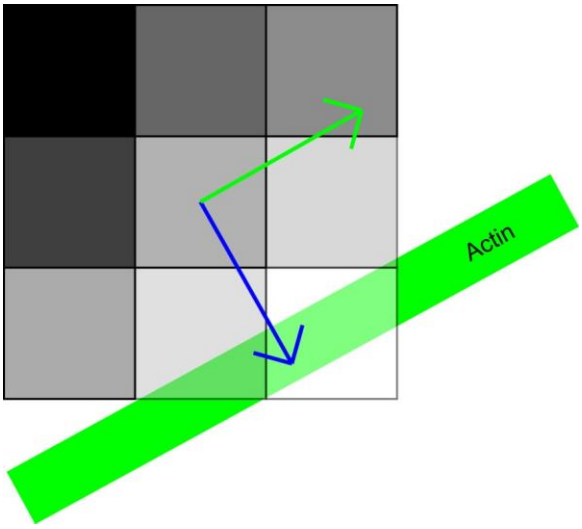

Figure 31 - Actin fiber vector generation. Blue is initial vector with magnitude based on relative brightness. Green vector shows rotation to become parallel with actin strand.

Once the vectors are generated a noise reduction step is done to drop the bottom 40% magnitude vectors. This threshold was experimented with and 40% gave us the most consistent vector set from images taken on the microscope. After thresholding the data is binned, rotationally reflected to form the second half of the rose plot, and data is graphically represented in rose plot form as seen in the results.

5.2 β-Catenin, ZO-1 Intensity and Quantifying Permeability

Adherens junctions that bind cell cytoskeletons to each other are not evenly distributed nor are they continuous bands around the perimeter. Tight junctions form after adherens junctions and can form multiple bands when viewed from the vertical direction. These structures therefore present a problem when trying to form a continuous path for quantification. Fluorescent staining of β-catenin or ZO-1 can reveal the locations, and optical blurring can naturally join up some of the junctions but this also does not give us an easily traceable path. However, though some creative MATLAB image processing tricks we can connect the fragments together and get an intensity measurement that can be cross-compared between shear conditions.

The first step is to dilate all of the pixels in a junctional image based upon their brightness. Brighter regions will be higher concentrations of the protein and are dilated more than regions without the protein. When dilated ideally, discontinuous pixels are now touching which is shown in the center panel in Figure 32. A path can be drawn through the centers of using the watershed function which can be thought of as connecting the ‘peaks’ of the highest,

or most intense pixels together. Then a band of region is generated using the path and the total pixel intensity within this path is summed. Dividing by the path length gives a number that means ‘total junctional protein intensity per length’ for each image.

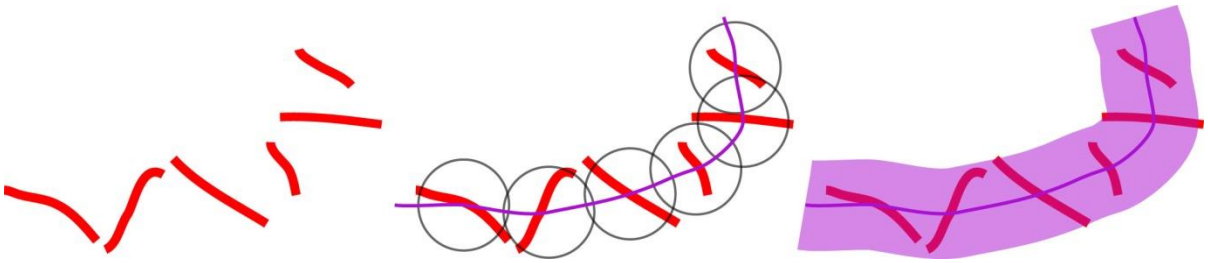

Figure 32 - MATLAB process to join discontinuous fragments and count intensity (L) Fragments, (C) pixel dilation and joining, (R) a band of interest is drawn and intensity per length calculated.

Setting different degrees of dilation and the minimum area necessary to form a complete enclosed area is done per image to try and best match the pathway seen in the fluorescent image. The MATLAB program is also able to calculate how many enclosed pathways are formed by the image processing. We can consider this as supplemental data in calculating how many cells are in the image. A denser image has more cells, but also consequently more β-catenin, so we normalize across images by taking the intensity per length and divide by the number of cells – calculated either through enclosed path count or by manually counting DAPI stained nucleuses of cells. This ‘total junctional protein intensity per length per cell’ number is then cross-compared between shear samples and control to determine relative permeability.

5.3 Analysis of Platelet Forces

To make rapid and accurate measurements of clot forces, we needed a methodology that would be resistant to common microscope artifacts such as x-y-z drift, shake, and luminescence fall-off that is commonly associated with fluorescence imaging. Adding to this, during platelet aggregation, the individual platelets become highly entangled, and become more dense when they contract as a clot, making a phase light image through this mass to the microposts difficult. To get around this, microposts were again fluorescently stained with DiI. During experiments, images are taken of both the microposts at the 594 nm wavelength every second and in phase-light of the platelet clot every 20 seconds. This is outputted as an uncompressed video that lasts the duration of each experimental run for accurate analysis in MATLAB.

A custom script was written to analyze each frame of the 594nm video and does so by tracking the relative position of the block with the micropost. First, each frame is taken out as a

.tiff image, and numbered sequentially then stored temporarily. Then, thresholding is used to eliminate background fluorescence by manual selection of the threshold point. It does so by presenting the user with images of images taken at 0%, 25%, 50%, and 100% of the video length with the selected threshold applied. The user can then choose whether to increase or decrease the threshold to maintain appropriate shape selection throughout the length. This was done to ensure that fluorescence spikes and drop-off could be compensated for. Typically, the block and micropost DiI signal is significantly brighter than the background plane because they have much more surface area for DiI to absorb into the volume when compared to the flat regions of the microchannel. Because of this, simple thresholding is sufficient to eliminate the bulk of DiI background noise. Next, the script takes each thresholded image and applies a series of erosive filters to eliminate small objects like noisy points or speckles of dust that appear during fabrication. Then the edges of the block and the micropost are identified by the program by looking for large remaining objects. This typically results in only the rectangular block and the circular top of the micropost remaining. Object analysis is then performed to find the relative distance between their centroids. The result is a pixel distance that is then compared to the average distance of the first 20 frames which is a range in which the micropost is not considered to be moving. Knowledge of the pixel distance to real distance conversion along with the micropost and clot properties means a force can be computed. A starting and final image is shown in Figure 33.

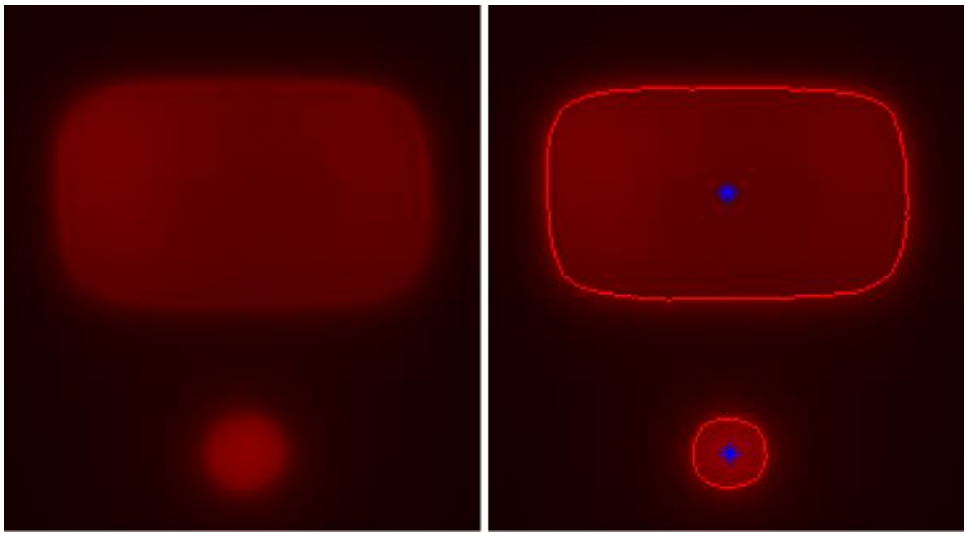

Figure 33 – MATLAB analysis of each frame of the raw frame on the left and after thresholding and filters are applied. The red outline denotes the identified boundaries of each object while the centroid is marked blue.

5.4 Analysis of Platelet Clot Area

In this study we are interested in the clot size as it reflects the propensity for platelet to platelet adhesion under shear stress. To quantify this, we investigate projected clot area as an indirect means of comparing clot volume across conditions. Phase light images taken during shear experiments have advantages in that they reveal a great deal of the geometry of the forming clot. However, a drawback is that phase light imaging is difficult to perform automatic area analysis on because each growing clot is formed out of many smaller objects, which can be identified individually, but attempts to group them together logically into one object is a technical challenge. For area analysis, manual assessment of the platelet area was then performed using Nikon NIS-Elements software. Parameters for identification of clot area were setup so that analysis was consistent across users, and that data could be considered reliable. During experiments, care was also taken so that a maximum of each clot would be visible, meaning that images were captured with 2 leading edge sensors and 3 second row sensors in frame, which was kept consistent whenever possible.

To gauge potentially how many platelets are occupying the space between the block and post, an estimate was made based on mean platelet volume, which is an established metric that has been used in the past to study platelet size distribution. The volume between the block and the micropost in the sensor geometry, shown in Figure 34, is 1620 fL.

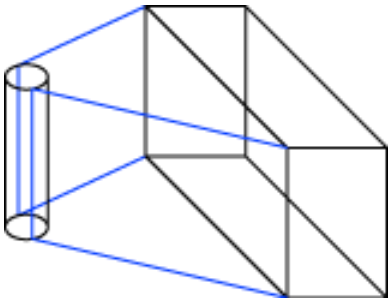

Figure 34 - Platelets in the blue volume affect the force measurements to the highest degree

Each platelet was considered to be spherical with a mean volume of 8.84 fL. [82] Close packing of spheres results in a maximal occupied volume fraction of 0.74078. Taken together, this implies that up to 135 inactive platelets can aggregate into this volume. Additionally, considering the area and volume to be proportional, we can determine that for every 100 μm^2 of projected area, this translates to 125 platelets.

5.5 Statistical Analysis

For calculations for significance of actin alignment, a parametric two-sample second-order analysis of angles was performed. A nonparametric second-order analysis Watson's U^2 test was used for cells on microposts. [83]. For comparisons of different values of junctional proteins, an ANOVA analysis with a Bonferroni's post hoc adjustment was used. Analysis of platelet force and area significance at ending time points was done using a two-tailed Student's t-test with unequal variance. Significance was considered for *P* values <0.05 (indicated with asterisk *). Software packages used were Microsoft Excel 2007, Microsoft Excel 2010, and Minitab.

6. Results & Discussion

6.1 Shear Alignment of Endothelial Cells on Flat Substrates

BPAECs and HPAECs cells on PDMS glass exposed to shear flow behaved as expected realigning actin cytoskeleton and cell shape to the direction of flow. A set of 3 experiments were run each including static, laminar, and disturbed conditions. 5 random areas were sampled within the monolayers with immunofluorescence marking of nuclear DNA, actin, and the transmembrane cadherins binding protein β-catenin. Combined results of actin images with the analysis process detailed in 6.1 are shown in Figure 35.

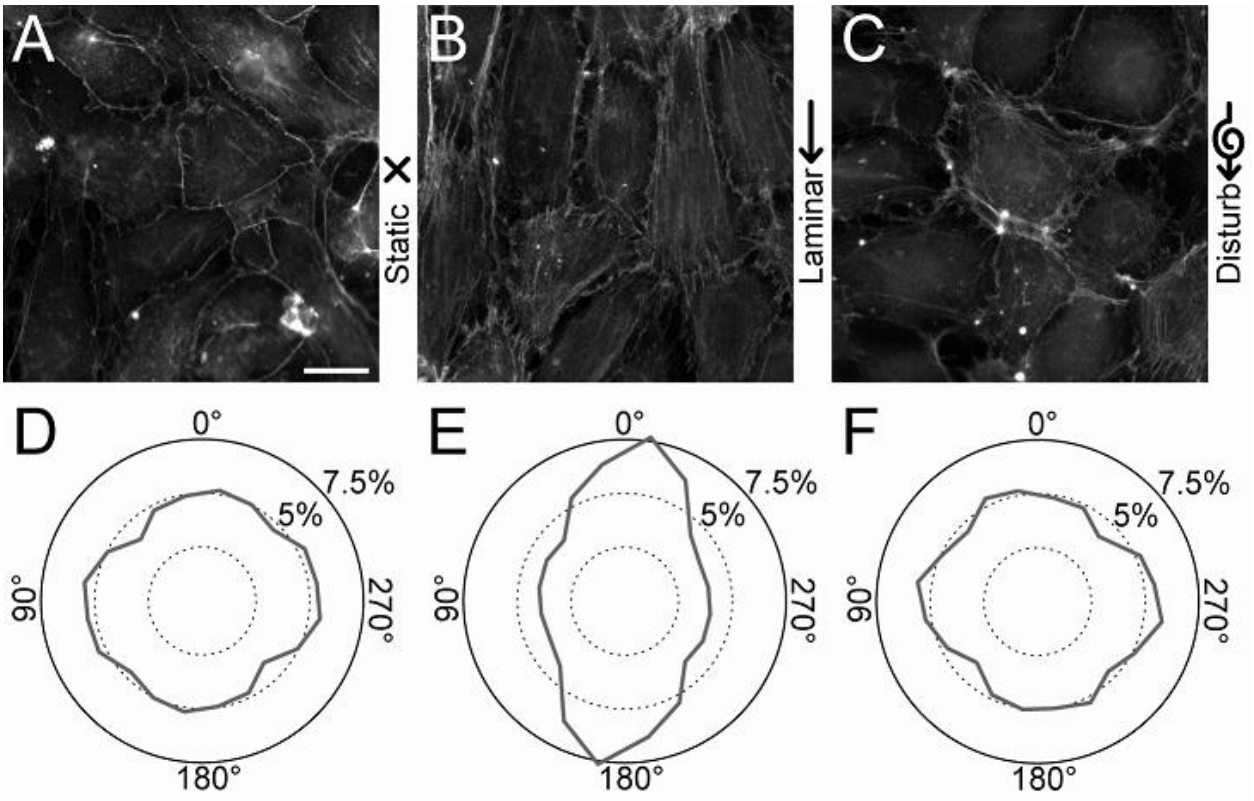

Figure 35 – HPAEC (A) static (B) vertical laminar shear (C) vertical disturbed shear (D) static rose (E) laminar rose (F) disturbed rose. n=15 per condition, 5 images each for 3 experiments, 14 hour runtime. Scale bar 20 μm.

The static flow in (A) and disturbed flow in (C) show no polarization of actin fibers to the flow direction; (D) and (F) respectively. Constant laminar shear in (B) and its corresponding rose plot (E) demonstrate that the shear generated is causing mechanotransduction realignment that matches previous studies and introduces a novel metric for analyzing orientation.

6.2 Cytoskeletal Tension Driven Remodeling with Inhibition

With a proven system capable of creating constant shear verified in 7.1, the next important step was to investigate the driving force behind remodeling. Previous research described in chapter 1 suggested that surface shear on a cell is transduced through the fibrous cytoskeleton to focal adhesions and activates the rho pathway. Through rho, the ROCK signal chain causes MLC to become phosphorylated and inhibits MLCK; these two effects increase myosin contractility. Example images and compiled rose plot results from HPAEC ROCK inhibitor Y-27632 experiments are shown in Figure 36.

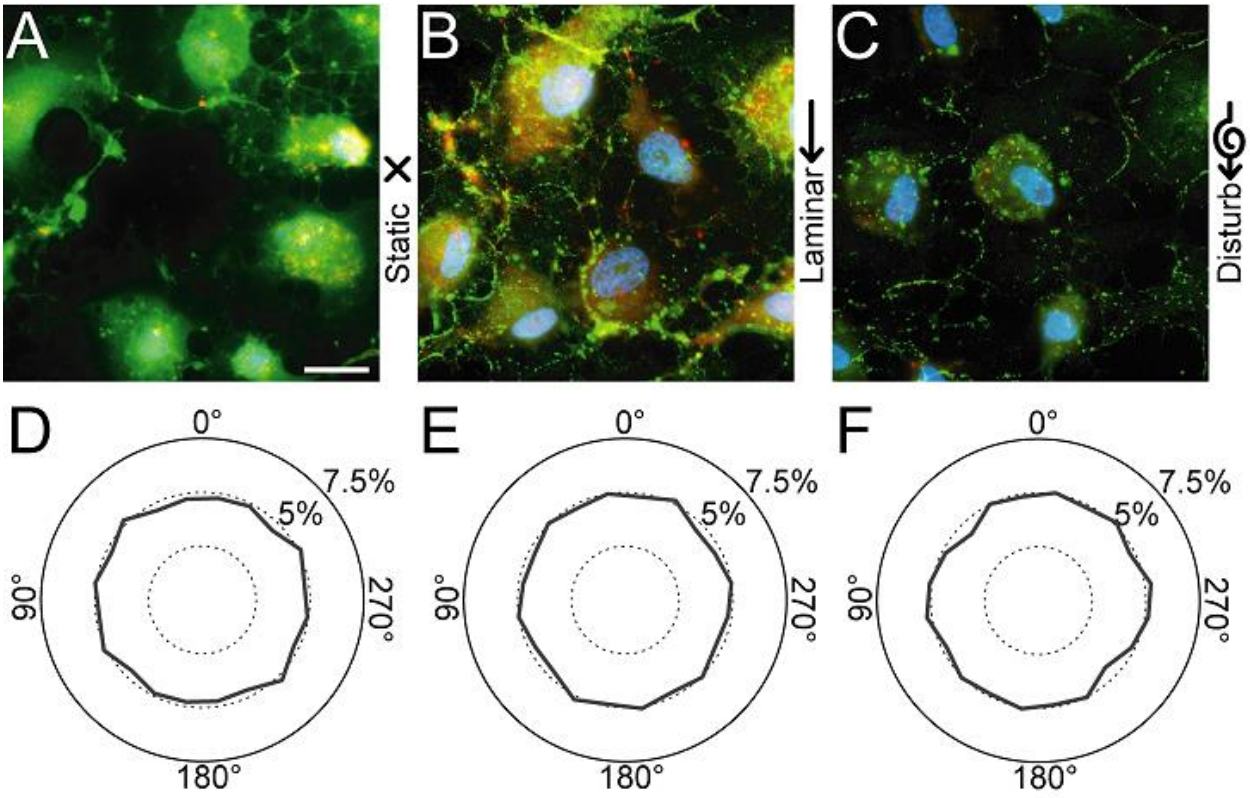

Figure 36 - HPAEC (A) static with Y-27 (B) vertical laminar shear with Y-27 (C) vertical disturbed shear with Y-27 (D) static rose (E) laminar rose (F) disturbed rose. n=15 per condition, 5 images each for 3 experiments, 14 hour runtime. Blue: nucleus, Green: Actin. Scale bar 20 μm.

Neither of the 3 conditions of static (A), laminar (B), or disturbed (C) had noticeable alignment in their rose plots; (D), (E), (F) respectively. F-actin stress fibers polymerize in response to stress, and it is demonstrated that global deactivation of myosin driven contraction leads to a breakdown of f-actin strands within the cell. [25] Indeed in the images actin tends to congregate near the nucleus of each cell without forming distinct strands. The catenin marked boundaries between cells is similarly disrupted as adherens junctions require actin filaments to form.

6.3 Shear Alignment of Endothelial Cells on Patterned Microposts

Establishing that cells on flat substrates have a mechanotransduction response is useful for checking that the device is functional and that it created accurate behavior response but does not enable the direct measurement of traction forces because of its rigidity. Using square 160 μm square patterned stamps we microcontact printed fibronectin to PDMS post tips, cultured HPAECs, and placed them under shear forces. Afterwards, immunofluorescent imaging and analysis through MATLAB was done. Example images and compiled rose plots are shown in Figure 37.

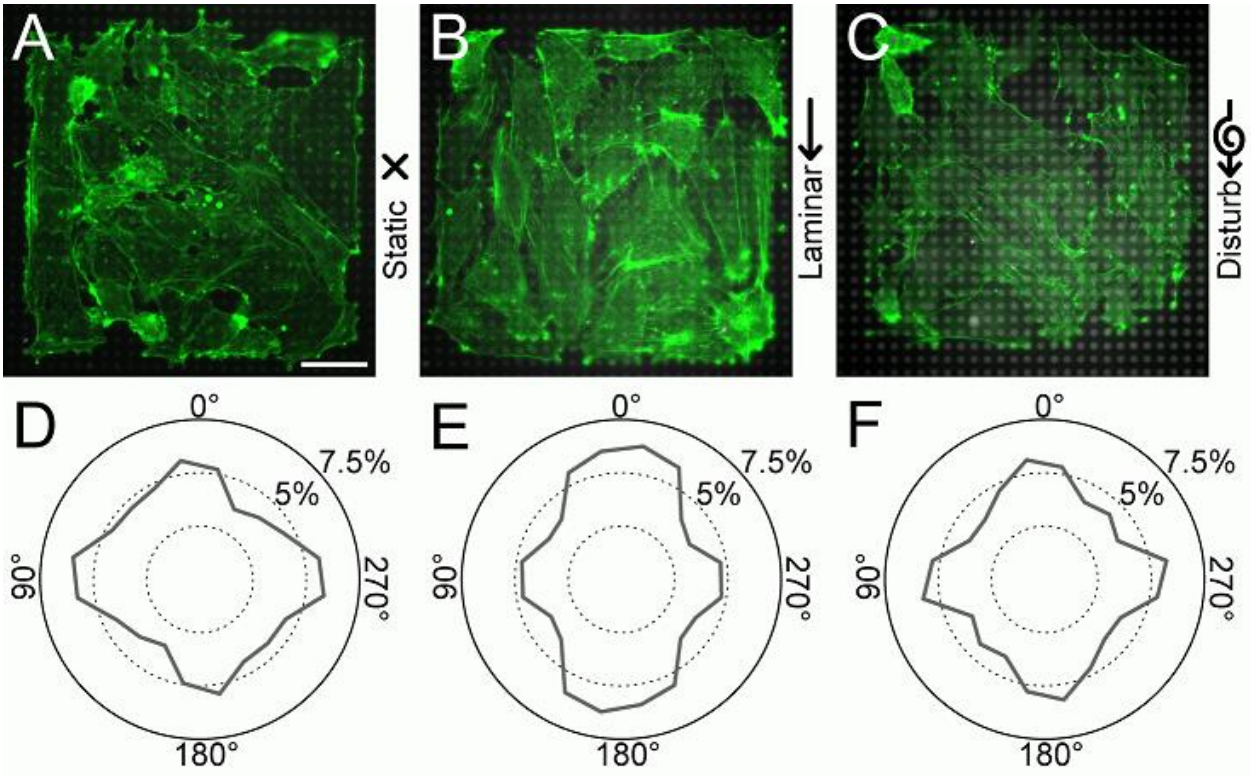

Figure 37 – HPAECs (A) static on microposts (B) vertical laminar shear on microposts (C) vertical disturbed shear on microposts (D) static rose (E) laminar rose (F) disturbed rose. n=15+ per condition, images compiled over 5 experiments . 14 hour runtime; Green: Actin, Grey: microposts. Scale bar 40 μm.

We see that a majority of the realignment behavior seen in HPAECs on flat substrates is preserved.

6.4 Traction Force Mapping of Monolayers

HPAECs were patterned onto microposts to find the force distribution for each shear condition. Following a similar procedure for flats, micropost substrates with square monolayers were first cultured in an incubator for 48 hours before being placed into the shear device. An example traction force map for each type of monolayer is shown in Figure 38 (A-C). What we

found was that forces per post were higher for the laminar condition, and lower for disturbed flow. When each vector is binned with respect to direction, it was higher forces are seen in the direction of flow for laminar shear, while disturbed and static had more unidirectional distributions. This means that the laminar monolayer had higher tension within its cytoskeleton with shear, which coincides with its realignment.

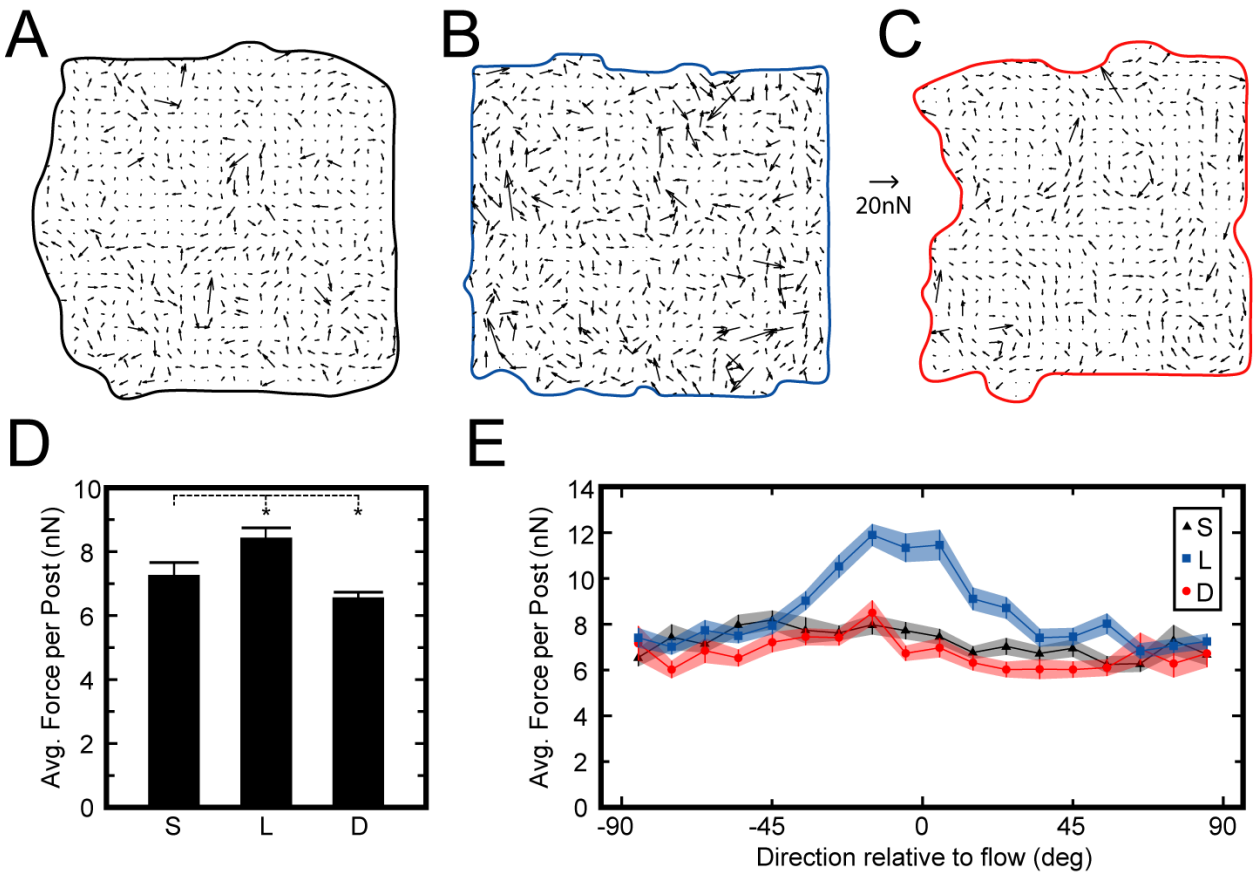

Figure 38 - (A) Static, (B) Laminar, and (C) Disturbed traction force maps for 160 μm square monolayers. (D) Increased average force per post for laminar and decreased for disturbed compared to static reference levels. (E) Force alignment indicates higher traction forces in the direction of shear flow.

6.5 Adherens Junctions Remodel in Shear Alone

Quantification of boundary adherens junction density was also performed. The presence of more junctions means better cross-cell cytoskeletal interaction, and since adherens junctions are generally thought to be a precursor and companion to both tight and gap junction formation [84], it gives a good indication as to the permeability. HPAECs cultured as full monolayers on flat substrates were again exposed to the three different shear regimes and edge identification and protein quantification was done as previously described in image analysis and shown in Figure 39. Distinct adherens plaques form observable structures at edge contacts and have

been seen to undergo turnover and remodeling with different laminar shear rates [85].Here its seen that they also varied in structural density with shear type (A-C). Significant increases were noted with laminar and significant decreases with disturbed parallel the observations seen with measured traction forces. To rule out the effects of laminar shear creating a pro-proliferative environment [86], nuclear counting through DAPI staining was done for each shear condition to confirm that the overall cell density per field of view was similar (F).

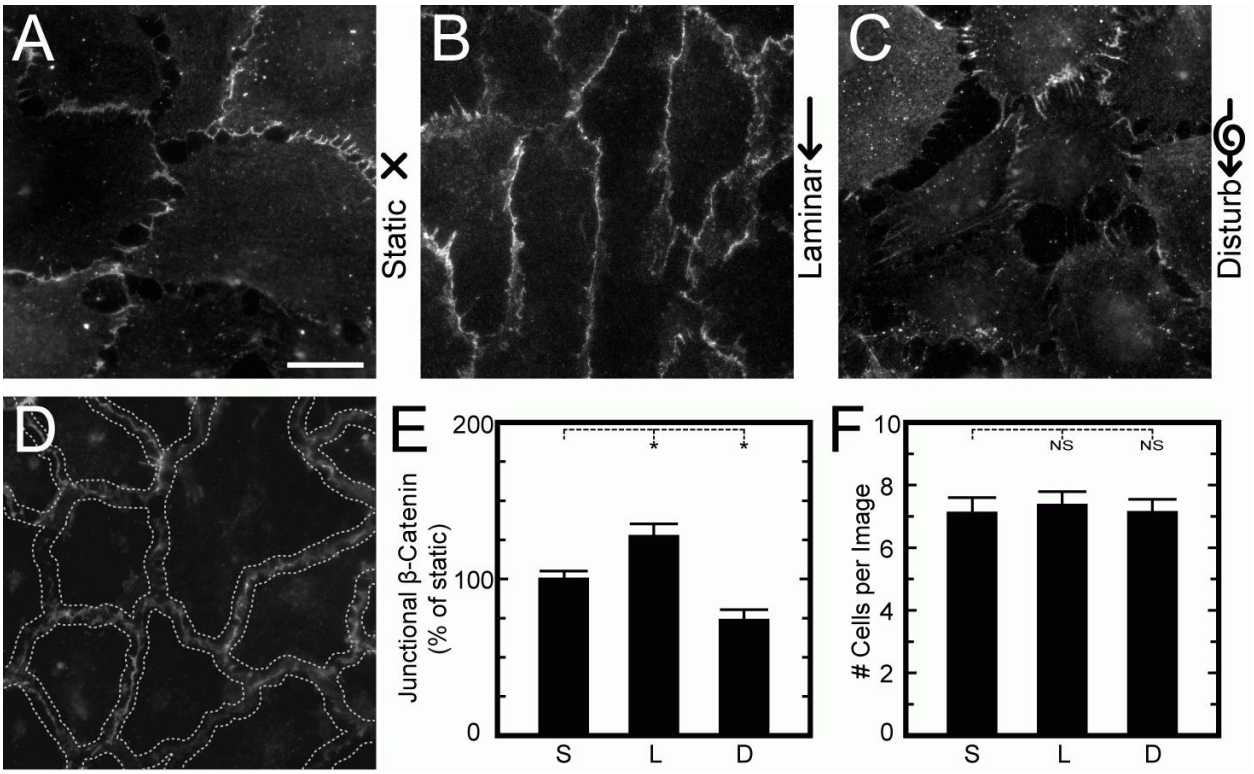

Figure 39 – Immunofluorescent stains for β-catenin, a structural protein in adherens junctions. (A) Static (B) Laminar shear (C) Disturbed shear (D) Example region of interest shown for measurements (E) Protein intensity per length per cell for each shear condition (F) Cell count per condition shows no bias due to proliferative effects.

6.6 Molecular Modification of Cell Contractility

The hypothesis of endothelial mechanotransduction relies on the ability of cells to sense and then alter their own contractility in a way that results in a restructuring of the cytoskeleton and related protein junctions. To independently test how necessary force regulation is to this process, molecular inhibitors were used that either inhibited contractility or boosted it by interfering with the Rho-Rock-Myosin chain. Y-27 and Calyculin-A added to the culture media creates an interference with ROCK signaling or inhibits myosin phosphatase directly.

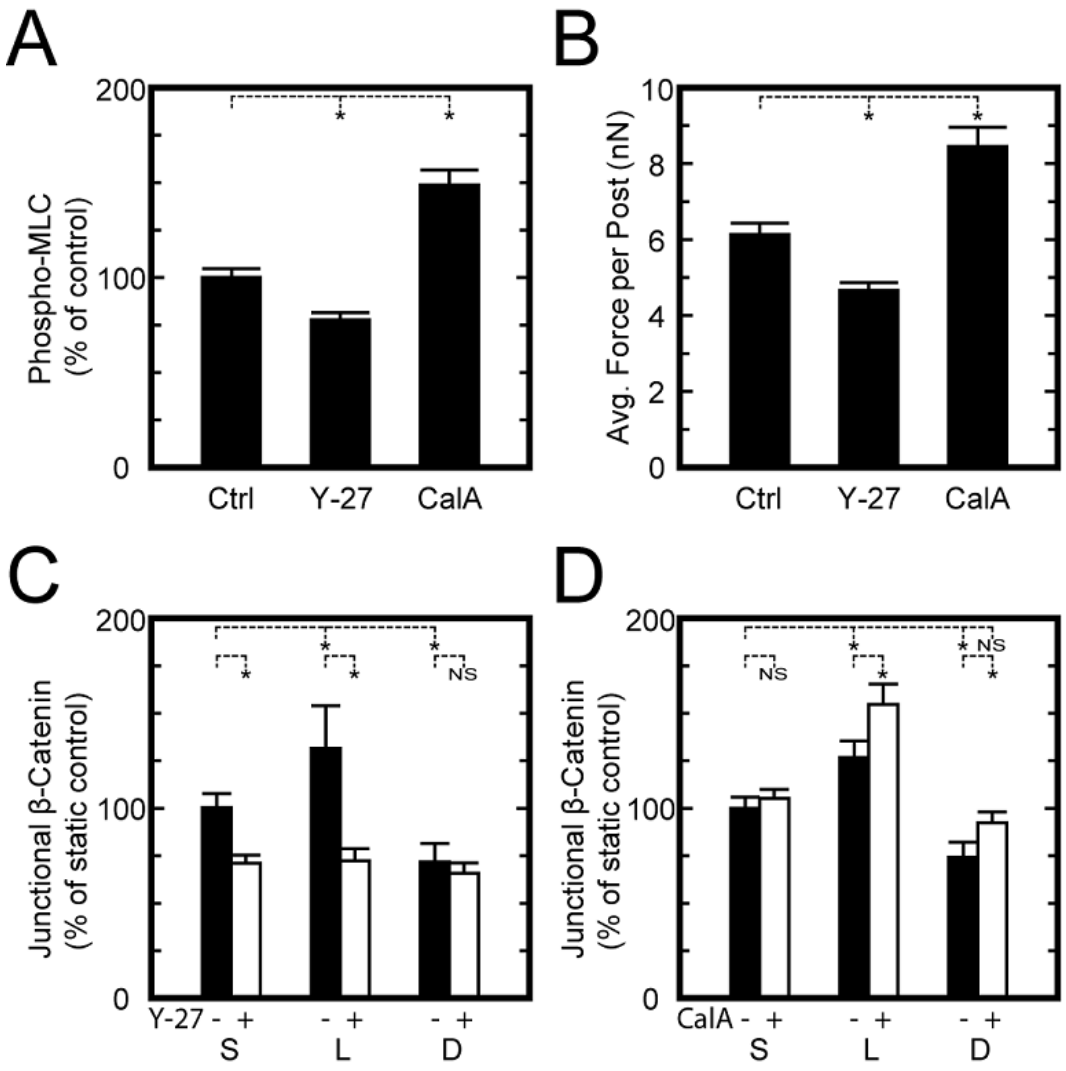

Figure 40 - Molecular inhibitors to control contractility (A) Y-27 and Calyculin-A affected myosin phosphorylation in distinct ways. (B) Forces reacted directly to changes in myosin phosphorylation activity (C) Measurements of Y-27 exposed adherens junction protein β-catenin show a significant decrease in adherens junction presence while (D) Calyculin-A boosted cell adherens junctions.

Verifying the effect of the molecules was done through quantification of myosin phosphorylation by comparing average image intensity for each condition to a control group. Cells with Y-27 exposure had lower phosphorylated myosin, while Calyculin-A was responsible for a large boost seen in Figure 40 (A). Higher phosphorylation levels imply more myosin-actin engagement and hence higher tension potential. In (B), cells cultured on microposts also react predictably with lower force per post for Y-27 and higher force per post for Calyculin-A confirming that phosphorylation levels are representative of traction force generation. Analyzing for adherens junctions after shear exposure demonstrates how contractility-inhibited (C, Y-27+) and contractility-boosted (D, CalA +) cells are able to form less and more junctions respectively.

Its notable that with Y-27, levels were reduced to equivalence to as if the cells had been exposed to disturbed shear, meaning a significant loss in monolayer integrity, while when the cells were contractility-enhanced sheared cells were able to exceed their non-inhibited controls. With no shear, adherens junctions did not significantly increase.

6.7 Intercellular Force Reflected in Adherens and Tight Junction Presence

Remodeling of traction forces mean that measurable intercellular forces change as well. By identifying the boundary of each cell, and comparing that to the traction force field, a summation of traction forces under each cell was done. The imbalance from a zero vector is the intercellular force, with an example seen in Figure 41 (A). An average for several monolayers under each condition was measured to understand the level of tension present. Laminar shear increased not just the traction force but also this intercellular force (B). Example images and measurements of (C-D) adherens and (E-F) tight junctions show that even on microposts, this restructuring involves both cell-to-cell forces and cell-to-cell junctions. A distinction seen in cells on microposts is that even though average traction forces fall, the tension remained similar between static and disturb sheared cells. The adherens junctions, which can be regulated through tugging forces reflect this while tight junctions depleted significantly.

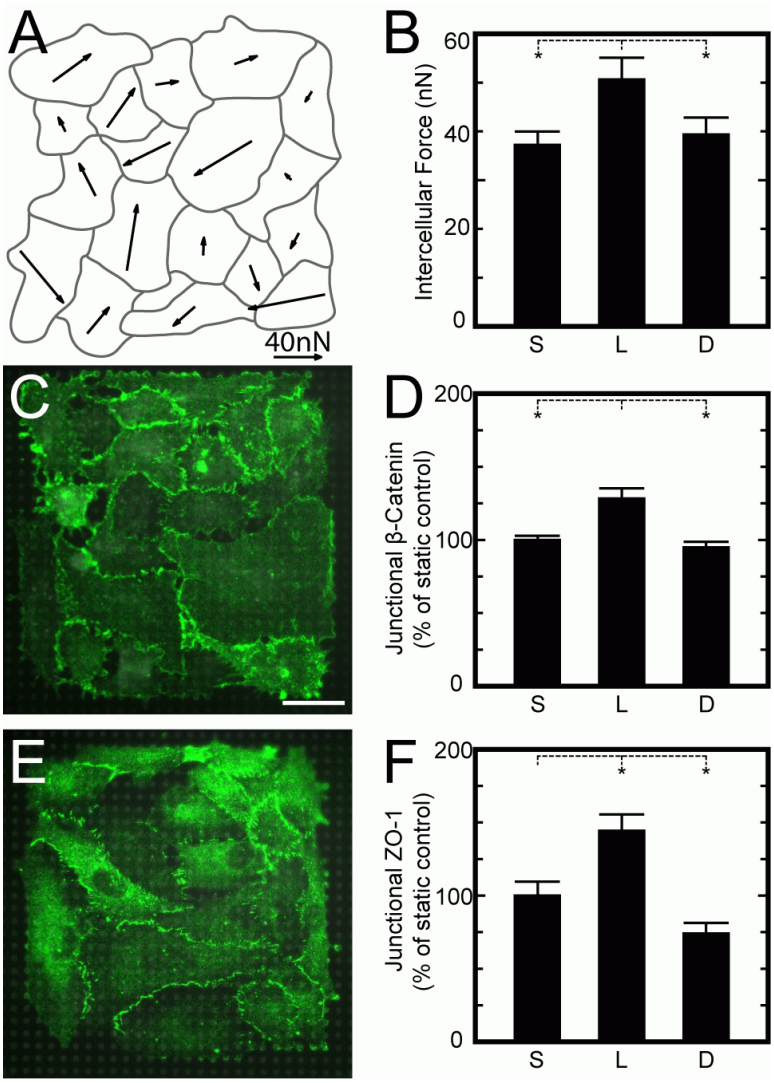

Figure 41 - Intercellular force changes for monolayers under laminar shear, and (A-B) relates with adherens (C-D) and tight junctions (E-F).

6.8 Live Platelet Experiments - Changes in Shear

Different fluid shear rates have been seen to activate platelets and cause thrombus formation [10, 87-89], so testing of how different shear rates in the fabricated microfluidic system was done to observe if aggregates could be formed against the microposts. Several trials from between 500 s^{-1} to over 10,000 s^{-1} were performed. Channel dimensions were identical between trials, so shear was controlled purely by altering the fluid velocity. Representatives at 1500 s^{-1} and 9000 s^{-1} are displayed in Figure 42.

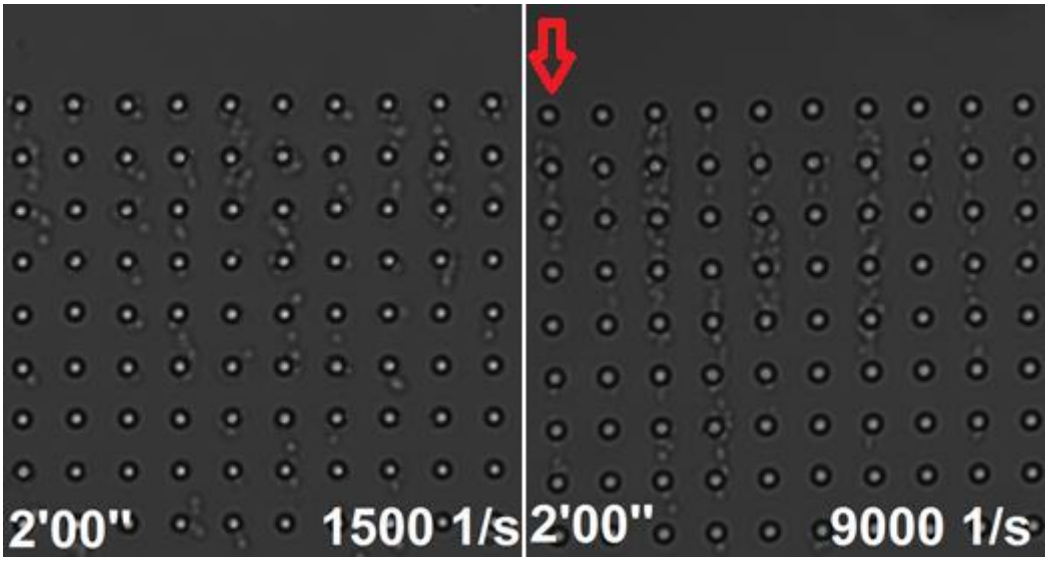

Figure 42 - Platelets flowed across 9 um spaced microposts. Higher shear gradients correspond to faster platelet capture between posts; red arrow indicates direction of flow.

Greater capture was seen at higher shear rates, although with higher flow velocity this means greater numbers of platelets pass by at any time point. Additional experiments may be planned to isolate the platelet count per volume buffer so that platelets pass at the same rate.

6.9 Live Platelet Experiments - Changes in ECM

Different extracellular matrix proteins offer different integrin-receptor binding to platelets. To test how well platelets bound to each matrix under shear, and possibly determine which one allowed for the greatest or quickest capture of passing platelets, identical devices were fabricated and absorbed with one of four different proteins: Fibronectin, Fibrinogen, Collagen, and von Willebrand Factor (Factor VIII present). Tyrode buffer suspended platelets sheared at 1500 s^{-1} are applied with images recorded over time. Representative images for each matrix midway through each experiment are shown in Figure 43.

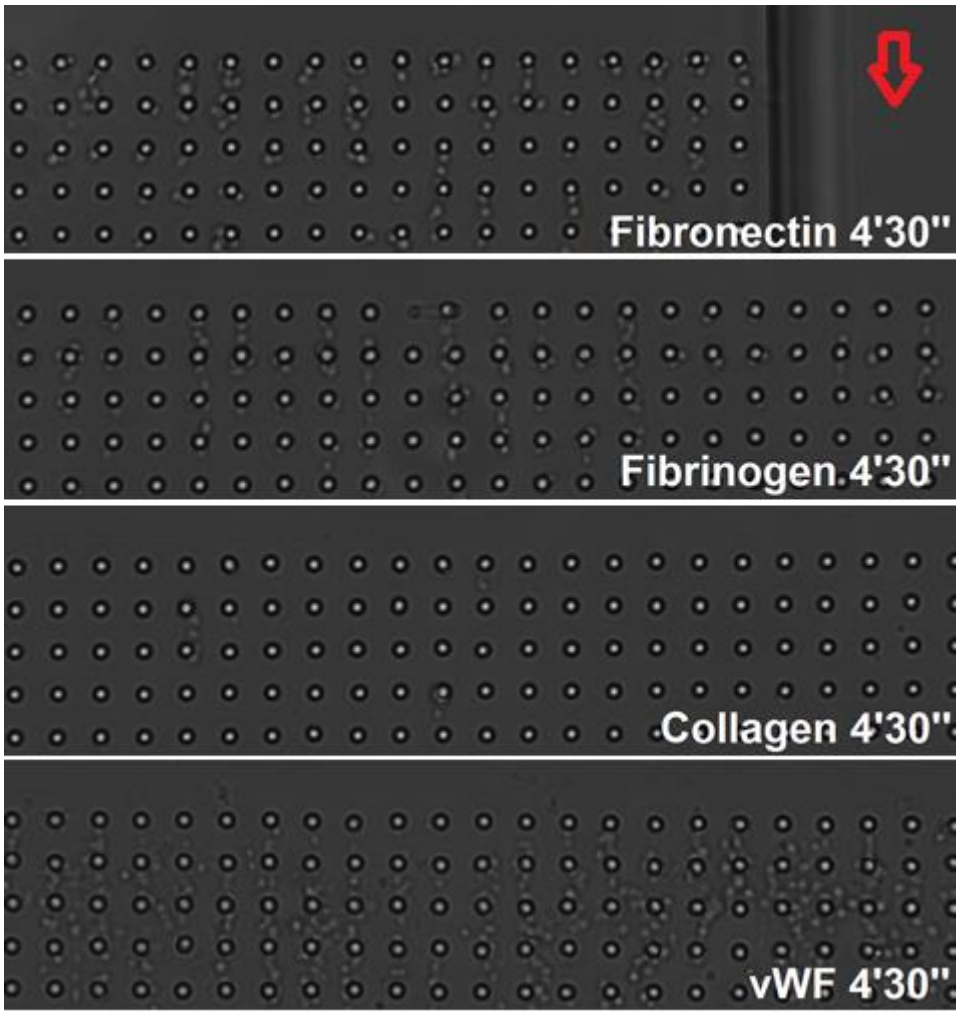

Figure 43 - Matrix proteins with platelets flowed across at 1500s-1. Images taken at 4 minutes 30 seconds from first platelet contact; red arrow indicates direction of flow.

We observed highest platelet capture at 1500 s^{-1} with von Willebrand Factor coating, with fibronectin and fibrinogen being equal and collagen having the least capture. Previous research groups have established that von Willebrand Factor combined with Collagen coatings resulted in enhanced platelet adhesions. This is due to the inherently fast forward rate of von Willebrand Factor and GPIb interaction and its low half-life which disassociates these bonds rapidly.

6.10 Live Platelet Experiments – Shear Microgradients

Experiments showed the importance that shear microgradients have on platelet capture. A channel mold with slightly offset triangular protrusions into the channel was fabricated and resulted in a region of intense shear gradient. When platelets were flowed through the channel, it was seen that a thrombus formed and grew at the point of highest gradient (Figure 44)

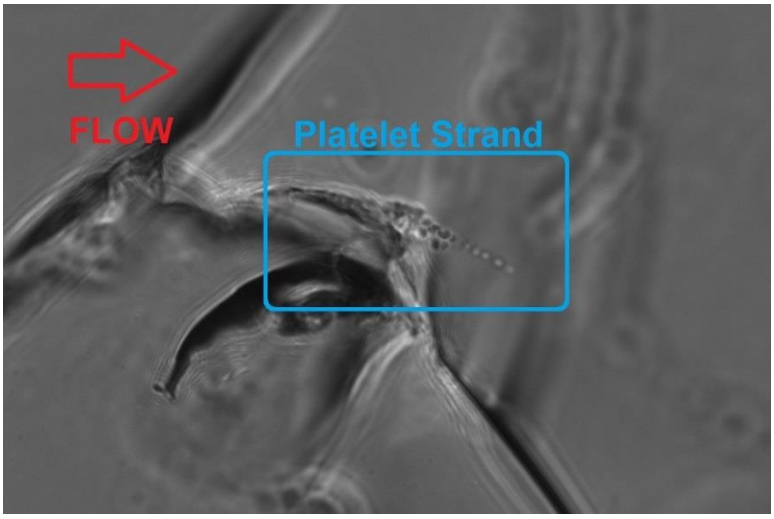

Figure 44 - Platelets aggregating downstream of a triangular protrusion into the channel.

Recreating this situation in COMSOL shows that this corresponds with an area where shear rises from 4000 s^{-1} to over 30,000 s^{-1} before recovering to 4000 s^{-1} (Figure 45). These were preliminary indicators that shear gradients should be pursued.

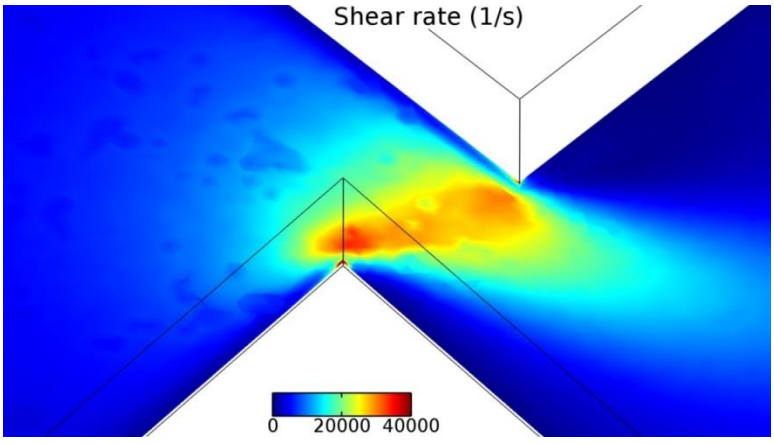

Figure 45 - COMSOL simulation of an offset triangle shear region with the layer shown at the post height (7µm).

6.11 Platelet Force is Myosin Dependent

Microfluidic devices consisting of blocks with microposts were used to make measurements of contractile forces under shear using whole blood. A time lapse of a forming clot is shown in Figure 47A. We found that platelets start gathering at the downstream corners of the block before connecting with the micropost forming a mechanical connection linking them together. An SEM of CPD prepared clots shows membrane tethers adhering several platelets to the structures in Figure 46. Other platelets in different stages of spreading are seen initiating adhesion to the back edge of the microposts. It was evident that different donors have different rates at which platelets bind to the structures. Many factors can influence this, such as the difference in receptor densities for certain proteins on an individual's platelets, gender differences, and activity level prior to blood collection.

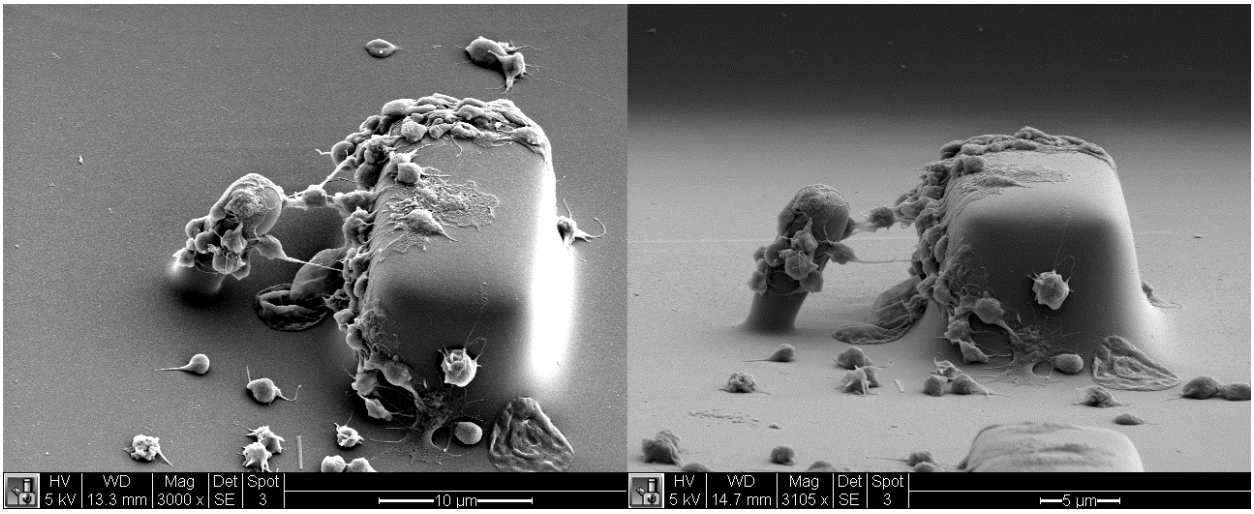

Figure 46 - Two views of a clot show several platelets bridging between the block and micropost after 45 seconds of whole blood perfusion. Micropost bending is an artifact of dehydration of the samples during critical point drying causing volume shrink.

Phase light images were taken every 20 seconds, and a mechanical connection was observed to form between the 20 second and 40 second images. Fluorescent images are taken every 1 second to track the structures as previously described. We found that clots grew in size due to additional platelets aggregating over time. At the same time, under sufficient shear rate loading, the clot also contracts inwards. This type of behavior is seen in the frame at 120 seconds. These opposing effects on the projected area implies that there is a rate with which the clot is growing competing against the inwards contraction or densification of the clot. Therefore, even while the area is increasing, the clot may be aggregating even more platelets than are observed since existing platelets are decreasing their occupied volume. At higher shear rates clots grew at higher rates with some samples leading to rapid occlusion of the channel after 120 seconds.

Donor to donor variability affects this as well, with some donor samples forming clots that reached a maximal size before plateauing while other donor samples grew continuously and without stoppage.

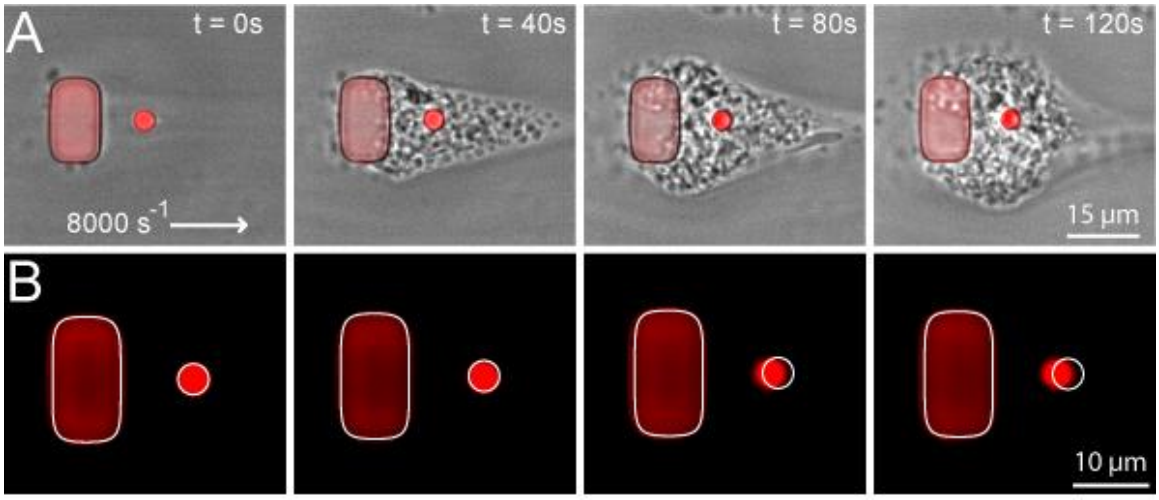

Figure 47 – (A) Time-lapse of platelets sheared at 8000 s^{-1} showing progression of clot formation. Initially some time is required to form a mechanical bridge between the two structures, and eventually the platelet clot retracts inwards. (B) Time-lapse of microposts deflecting towards the block along with an outline of their starting positions in white.

In this set of experiments whole blood was sheared at a physiological rate of 2000 s^{-1} and pathological rate of 8000 s^{-1}, a rate which may be experienced by platelets in highly stenosed vessels. The mechanism for platelet force can be inhibited by incubating whole blood with myosin IIA inhibitor blebbistatin. Force results for both the low and high shear conditions of inhibited and uninhibited platelets are shown in Figure 48A-D.

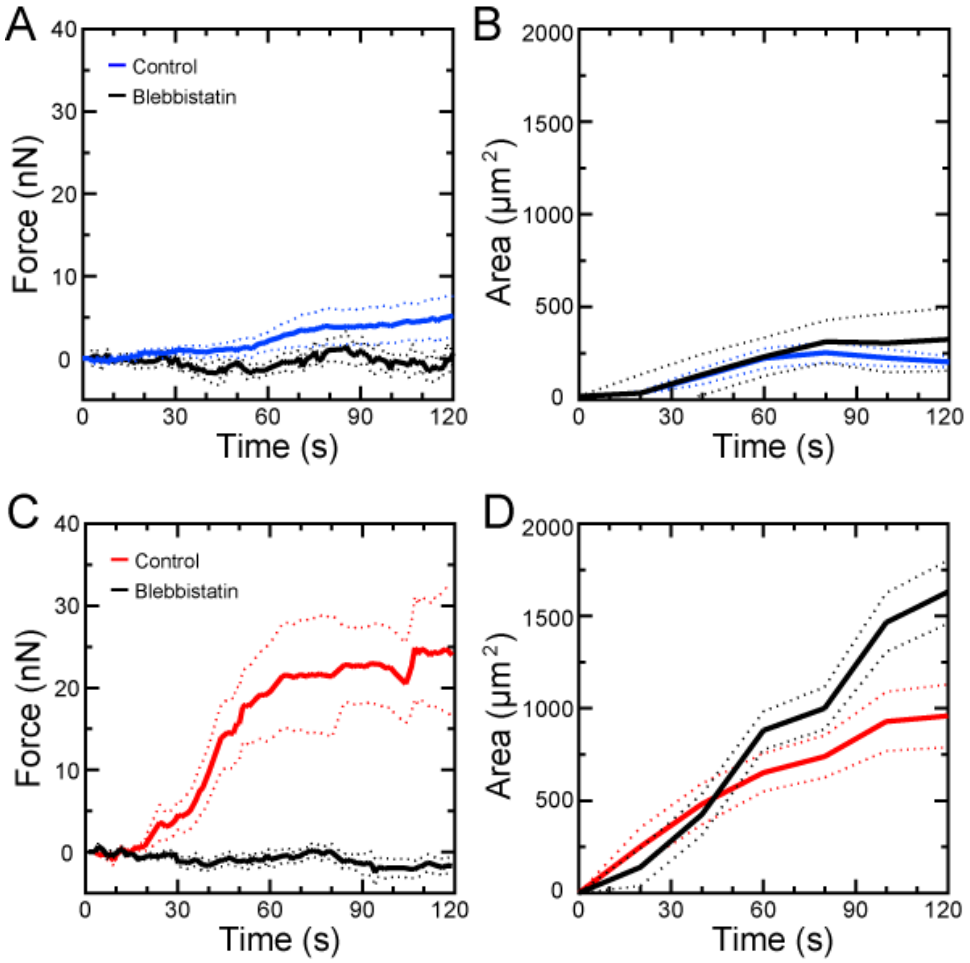

Figure 48 – (A) Control platelets sheared at 2000 s^{-1} had a very low rise in contractile force while blebbistatin treated platelets had a similar lack of force. (B) At 2000 s^{-1} areas for either condition were similar. (C) Control platelets sheared at 8000 s^{-1} show rise in contractility over time while platelets treated with blebbistatin show no such response. (D) Blebbistatin treated platelets had a larger projected area after 120 seconds compared to control platelets. Force and area graphs are an average and standard error of N≥4 sensors per condition across N≥3 independent experiments.

It was found that at low shear rates (2000 s^{-1}) both control and blebbistatin inhibited platelets exhibited similar trends of zero to very low contractile forces. A clot was present as evidenced by the projected area results with no significant difference between the two conditions. At high shear rates (8000 s^{-1}) platelet contractile force is observed to climb rapidly for control platelets whereas blebbistatin inhibited platelets remain at zero forces. This discrepancy confirms that the measured force is a result of myosin IIA action within platelets. We additionally observe with that with either treatment under high shear, that the clots enlarge at a much higher rate than low shear. This is likely because high shear rates promote membrane tether extrusion of existing platelets at a site, which extend into the flow and assist in capturing more discoid platelets. Uninhibited platelets become during this process and contract inwards adhering tightly to each other and decreasing the volume of the clot. Blebbistatin inhibited platelets would be incapable

of inwards contraction, eliminating this clot densification that would be normally seen with the activated control clots and is reflected in the higher area at 120 seconds. One possible explanation is that there is less platelet to platelet entanglement and more interstitial spaces within the clot. This may promote faster disassociation from native plasmin.

6.12 Shear is an Affecter of Platelet Contractility and Area

Shear rates of 2000 s^{-1}, 5000 s^{-1}, 8000 s^{-1}, and 12000 s^{-1} were tested in the microfluidic device by increasing the flow rate through the channels. These experiments were done using substrates that had a range of block to micropost spacing from 6 μm to 15 μm. Data was gathered only from 9 μm, 12 μm, and 15 μm spacing (in equal proportions) as 6 μm spacing typically resulted in a collapsed micropost. Heparinized whole blood was flowed through the device and contractile force and areas were measured for each condition. Results for all four shear rates are shown in Figure 49.

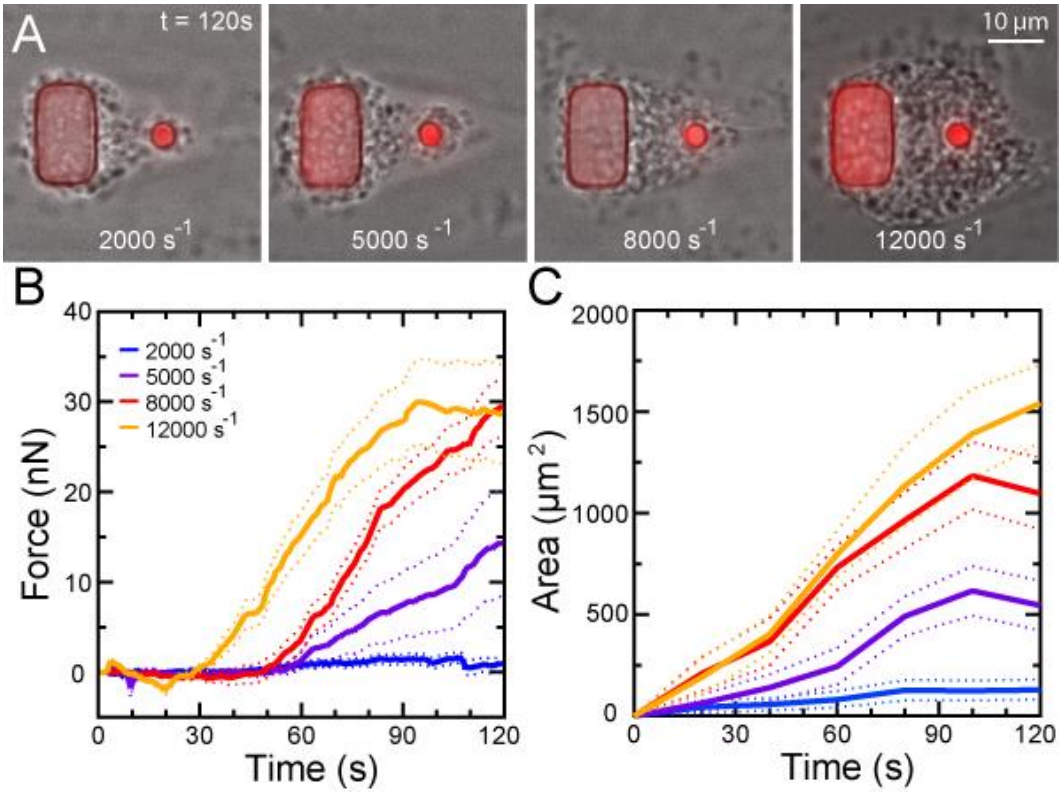

Figure 49 – (A) Combined phase and fluorescent images of platelets grouping at 2000, 5000, 8000, 12000 s^{-1} shear after 120 seconds of continuous blow flow. Higher shear rates aggregated larger groups of platelets. (B) Clot forces show quicker onset and a more rapid climb with increasing shear rate. (C) Higher shear rate also contributed towards a larger projected area. Force and area graphs are an average and standard error of N≥4 sensors per condition across N≥3 independent experiments.

Increasing shears above 2000 s^{-1} decreased the time at which force initiates and has a slight impact on how quickly forces develop. The difference between 8000 s^{-1} and 12000 s^{-1} appears to be primarily in a time-shift towards faster response rather than faster growth. Additionally, the maximal force reached at 120 seconds is similar. This result may imply that these two shear rates led to full activation of platelets but once this occurs, contractile development proceeds at a set rate towards completion. Another important observation is that platelets sheared in a transitional regime between physiological (2000 s^{-1}) and pathological shear (5000 s^{-1}) may then be exhibiting partial activation which is reflected in the slight delay of force onset as well as the slower rate of force growth. The projected areas of each clot also grew with increasing shear rate: 8000 s^{-1} and 12000 s^{-1} were again similar in trend while 5000 s^{-1} was an intermediate between the physiological (2000 s^{-1}) and higher pathological regimes. It is important to note that higher shear rates were due to higher flow rates of whole blood through the device. This increases the rate in which discoid platelets are encountering the forming clot and raises the probability of a platelet aggregating. Similarly, stenosed or narrowed arteries experience higher mass flow rates *in vivo* as they become constricted, which contributes towards increased platelet marginalization towards the luminal surface.

6.13 Platelet Receptors GPIb and $\alpha_{IIb}\beta_3$ are Players in Clot Aggregation and Contractility under Shear

Blocking of GPIb and $\alpha_{IIb}\beta_3$ via antibody incubation is an established method for inhibiting their interactions with VWF and fibrinogen respectively. Whole blood was incubated for 25 minutes with each antibody at room temperature and then sheared through the microfluidic device. Measurements of force and projected area are shown in Figure 50.

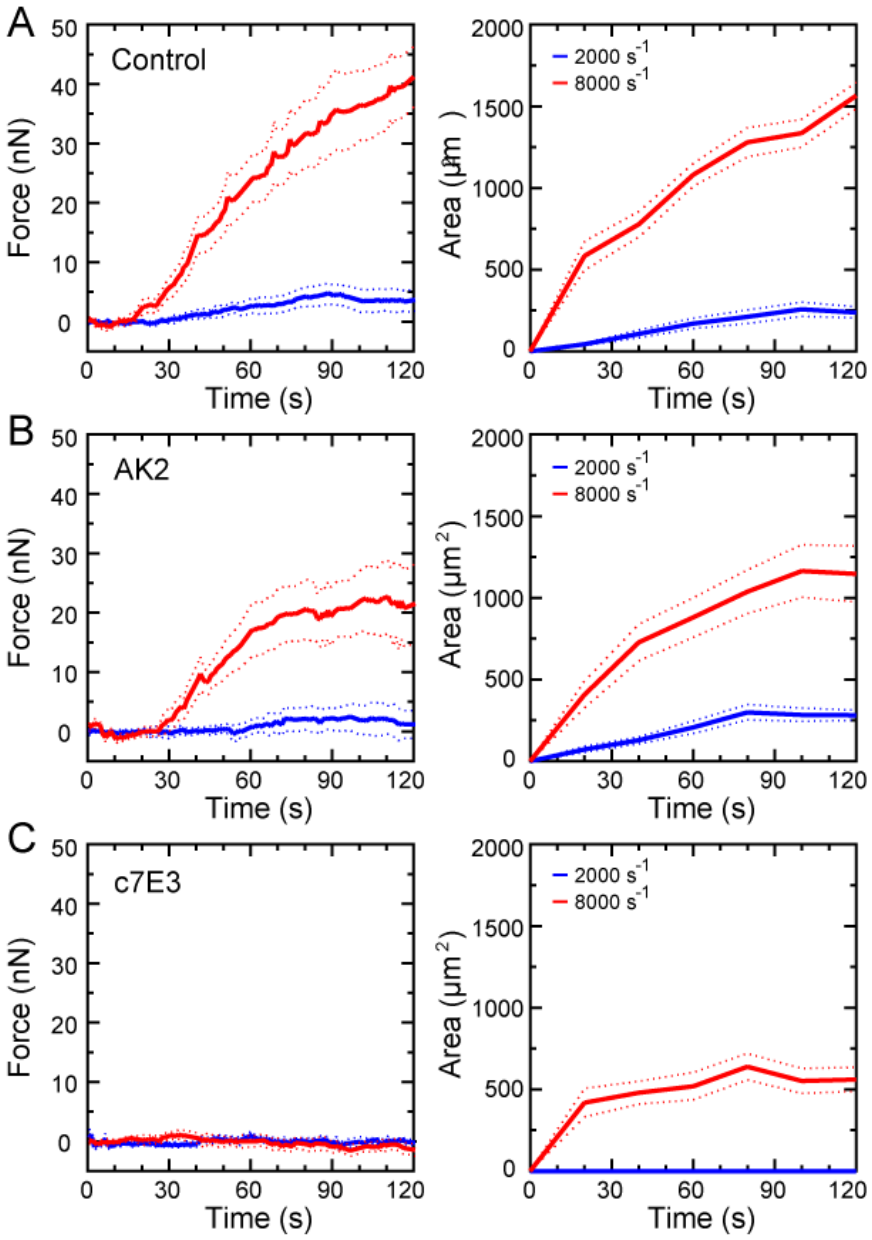

Figure 50 – Platelets incubated with (A) no antibody, (B) GPIb antibody AK2, and (C) $\alpha_{IIb}\beta_3$ antibody c7E3 with measured forces and areas. Suppressed forces and areas were observed for AK2 at high shear rates while at low shear rates there was no significant change. Major suppression of both force and area was seen with c7E3 treated platelets at high shear rates. No adhesion was evident for c7E3 at 2000 s^{-1}. Force and area graphs are an average and standard error of N≥4 sensors per condition across N≥3 independent experiments.

Control platelets under high shear once again show a rapid rise in force and an increase in area compared to low shear platelets. The force onset for this set of three experiments was faster than for previous experiments with variable shear rates. This is most likely due to a switch over to a generation of substrates that had only 9 μm spacing versus a range of measured spacing from 9 μm to 15 μm. Larger spacing requires longer times for the clot to form a mechanical

bridge between the block and micropost meaning a longer delay before forces can start becoming measurable on the sensors.

Platelets inhibited with AK2 antibody for GPIb had a slower rise in force and area when placed under high shear when compared to control. AK2 inhibited platelets under low shear had no significant changes. We expected to observe more inhibition of aggregation as at high shear rates the only established mechanism for receptor based capture is GPIb-VWF. An important consideration is that platelets have a portion of their membrane surfaces hidden within the platelet body in the canalicular system; this effectively shields some portion of surface receptors from the antibody introduced into the fluid until after the membrane expands to reveal them. Incubating whole blood with AK2 at 5 μM may also only be partially blocking the available GPIb receptors on the platelets. These results suggest that transient binding is still occurring from partial blocking, just at a reduced rate compared to controls. Likewise, the force developing at a slower rate and to a lower maximum at 120 seconds may be attributed to this partial blocking. suppression of force and area.

Platelets inhibited with c7E3 antibody for $\alpha_{IIb}\beta_3$ had a complete reduction of forces at high shear level. This suggests that $\alpha_{IIb}\beta_3$ is a necessary component for firm adhesions to the collagen and VWF proteins at the surface. Aggregation was only observed at high shear rates, with extremely low adhesion at low shear rates. The lack of adhesion seen with 2000 s^{-1} sheared c7E3 platelets may potentially be attributed to inefficient $\alpha_{IIb}\beta_3$ binding above 1000 s^{-1} , since this mechanism has been seen to occur insufficiently quickly at high shear. Adding to that, because GPIb-VWF interactions require force to stabilize, the shear rate of 2000 s^{-1} may be insufficient to generate a high enough stress on the bond to allow for bond longevity.

It is anticipated that increasing the antibody concentration of AK2 will lead to a reduction in force and capture which follows with the currently observed trend, while decreasing c7E3 antibody concentration will lead to a recovery of the force curve towards controls. Nonetheless, these results demonstrate the involvement of each receptor in platelet plug formation.

6.14 Platelet shear activation is ADP dependent through $P2Y_{12}$ receptor

An investigation into the degree of activation was done by inhibiting the $P2Y_{12}$ membrane protein which is one of two recognized ADP chemical receptors. Whole blood was incubated with 10 μM of 2-MeSAMP before being flowed through the device at 8000 s^{-1}. Force and area data for this set of experiments is shown in Figure 51.

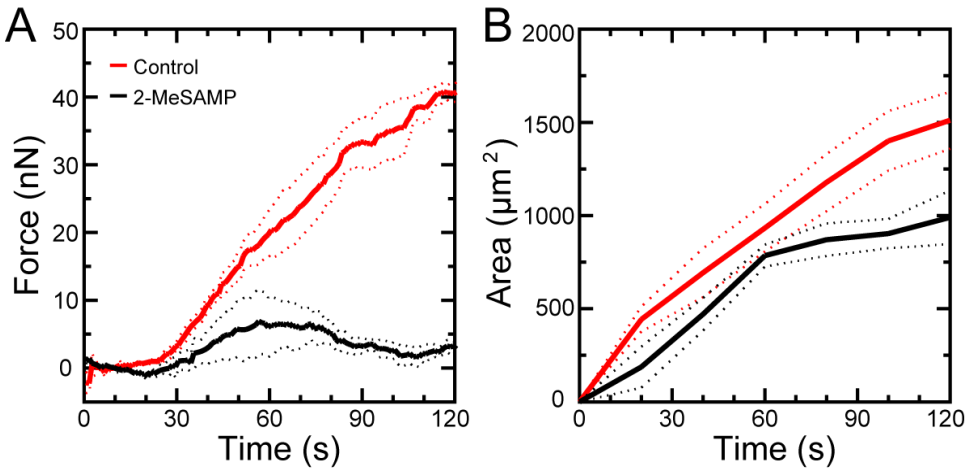

Figure 51 - Platelets incubated with 2-MeSAMP. Control and $P2Y_{12}$ inhibited platelets sheared at 8000 s^{-1} with (A) force and (B) area. Significant suppression of force was observed with 2-MeSAMP. Force and area graphs are an average and standard error of N≥4 sensors per condition across N≥3 independent experiments.

With 2-MeSAMP present, it was seen that forces were largely suppressed when compared to a control sample. A majority of the platelets exhibited zero force generation throughout the time frame, however several clots in one experiment displayed a rise and then drop in platelet force between 30 and 90 seconds. A potential explanation to this phenomenon is that while available surface $P2Y_{12}$ is largely inhibited, shear stresses may be extruding membrane tethers from the platelet surface. This reveals uninhibited membrane previously hidden in the canalicular system. These fresh $P2Y_{12}$ receptors may then receive available ADP and cause contractile shape change. These results largely confirm that shear response is still mediated through ADP driven activation.

If the platelet clot is growing, there is a central core of activated platelets surrounded by a growing shell of partially activated or inactivate platelets. The release of ADP and calcium stores from the platelet core is largely responsible for subsequent capture and activation of shell platelets. With the presence of 2-MeSAMP this effect is suppressed. The overall thrombogenicity of the platelet clot is less and is reflected in the lower clot area at 120 seconds. This was observed in addition to the smaller degree of clot densification in 2-MeSAMP platelets because of activation suppression. These results confirm our hypothesis that platelets are activating to a higher degree with higher shear rates, and that this leads to development and growth of contractile force and size.

7. Conclusions

A variable flow device was designed to simulate physiological shear. Cells were cultured onto glass or silicone microfabricated post array chips that were placed into the device to simulate the working environment of the body. Media is driven across the surface of the chips and this mirrors blood's ability to both induce a force and provide nutrients to the cells. Different shear profiles are introduced through the positioning of a weir in the device to create recirculation and vortices zones with rapid shear changes.

It was demonstrated that with the endothelial shear device, endothelial cells realigned their cytoskeletons with the direction of flow. Next, contractility inhibition with Y-27632 resulted in no cytoskeletal realignment. Y-27632 and Calyculin-A were tested for their ability to modulate endothelial tension, and quantification of myosin phosphorylation confirmed this. Endothelial cells cultured on microposts also showed lower forces with Y-27 and enhanced force with Calyculin-A. Cell-to-cell junctions remodel with force, so measurements of adherens junctions and tight junctions were done to examine how they related to shear-based remodeling. When monolayers were exposed to laminar flow, they contracted more strongly, and with more directionality than static and disturb sheared cells. Junctions likewise changed in parallel. Intercellular force, a metric of overall tension also reinforced with laminar flow. **These results add evidence to the theory of a mechanotransductive model for endothelial shear response and confirms Primary Hypothesis 1: different shear regimes cause mechanotransduction driven cytoskeletal remodeling which affects the protective function of endothelial monolayers.**

Understanding primary hemostasis clot development was a the main goal in the second phase of this research, as shear plays a critical role in controlling platelet adhesion, aggregation, and contractile shape-change which are necessary for clot stabilization. A microfluidic system was created to test for platelet shear response by combining a shear generating obstruction with a flexible micropost sensor. It was discovered that platelets aggregated at the downstream regions of high shear rate and bound to specially designed microstructures, deflecting the micropost and enabling a force measurement. Inhibition of myosin IIA with the use of blebbistatin again showed that this force was imparted by the myosin-actin complex. Increasing the shear rate from physiologic to pathological levels showed that platelet contractility was shear dependent, increasing their forces in response to higher shear rates. It was found that a potential threshold between 2000 s^{-1} and 5000 s^{-1} may exist for rapid platelet contractility, while it was proposed that larger population testing be done to confirm this

finding. Antibody inhibition of surface receptors GPIb and $\alpha_{IIb}\beta_3$ demonstrated that both platelet aggregation and platelet forces need these receptors to function properly. Inhibition of ADP surface receptor $P2Y_{12}$ demonstrated that shear-response was still mediated through ADP activation. **Taken together, these results confirm Primary Hypothesis 2: platelet clot forces and aggregation are shear dependent.**

Our results have implications for the identification and treatment of coagulation disorders by providing a metric with which to diagnose primary hemostasis response, which would be helpful information for caregivers in the field and emergency care settings. By controlling the available integrins within an individual microchannel, it may be possible to quickly discover if a sample of whole blood contains platelets that have reduced or missing complimentary specific receptors, such as with the case of many genetic disorders.

References

1. *Heart Disease & Stroke Statistics*, 2009, American Heart Association.
2. Association, A.H., *Heart and Stroke Facts: 1997 statistical supplement*, 1997, American Heart Association: Dallas, TX.
3. Dai, G., et al., *Distinct endothelial phenotypes evoked by arterial waveforms derived from atherosclerosis-susceptible and -resistant regions of human vasculature.* PNAS, 2004. **101**(41): p. 14871-14876.
4. Wu, C.-C., et al., *Directional shear flow and Rho activation prevent the endothelial cell apoptosis induced by micropatterned anisotropic geometry.* PNAS, 2007. **104**(4): p. 1254-1259.
5. Tarbell, J.M., *Shear stress and the endothelial transport barrier.* Cardiovascular Research, 2010. **87**(2): p. 320-330.
6. Butcher, J.T., et al., *Unique Morphology and Focal Adhesion Development of Valvular Endothelial Cells in Static and Fluid Flow Environments.* Arteriosclerosis. Thromb. Vasc. Biol. , 2004: p. 1429-1434.
7. Ku, D.N., et al., *Pulsatile Flow and Atherosclerosis in the Human Carotid Bifurcation.* Arteriosclerosis, 1985. **5**(3): p. 293-301.
8. Junt, T., et al., *Dynamic visualization of thrombopoiesis within bone marrow.* Science, 2007. **317**(5845): p. 1767-70.
9. Nesbitt, W.S., et al., *A shear gradient-dependent platelet aggregation mechanism drives thrombus formation.* Nat Med, 2009. **15**(6): p. 665-73.
10. Maxwell, M.J., et al., *Identification of a 2-stage platelet aggregation process mediating shear-dependent thrombus formation.* Blood, 2007. **109**(2): p. 566-76.
11. Tovar-Lopez, F.J., et al., *A microfluidics device to monitor platelet aggregation dynamics in response to strain rate micro-gradients in flowing blood.* Lab Chip, 2010. **10**(3): p. 291-302.
12. Davi, G. and C. Patrono, *Platelet activation and atherothrombosis.* N Engl J Med, 2007. **357**(24): p. 2482-94.
13. Gawaz, M., H. Langer, and A.E. May, *Platelets in inflammation and atherogenesis.* J Clin Invest, 2005. **115**(12): p. 3378-84.
14. Kruth, H.S., *The fate of lipoprotein cholesterol entering the arterial wall.* Current Opinions Lipidol, 1997. **8**: p. 246.
15. Zipes, D.P., et al., *Braunwald's Heart Disease*. Vol. 1. 2005, Philadelphia: Elsevier Saunders.
16. Britten, M.B., A.M. Zeiher, and V. Schächinger, *Effects of cardiovascular risk factors on coronary artery remodeling in patients with mild atherosclerosis.* Pathophysiology and natural history, 2003. **14**: p. 415-422.
17. Schneeberger, E.E. and R.D. Lynch, *Structure, Function, and Regulation of Cellular Tight Junctions.* Am. J. Physiol, 1992. **262**: p. L647-L661.
18. Hahn, C. and M.A. Schwartz, *Mechanotransduction in vascular physiology and atherogenesis.* Nature Reviews Molecular Cell Biology, 2009. **10**(1): p. 53-62.
19. Wojciak-Stothard, B. and A.J. Ridley, *Rho GTPases and the regulation of endothelial permeability.* Vascular Pharmacology 2003. **39**: p. 187-199.
20. Dejana, E., M. Corada, and M.G. Lampugnani, *Endothelial cell-to-cell junctions.* FASEB J, 1995. **9**(10): p. 910-8.
21. Langille, B.L., *Morphologic responses of endothelium to shear stress: reorganization of the adherens junction.* Microcirculation, 2001. **8**(3): p. 195-206.
22. Yonemura, S., et al., *alpha-Catenin as a tension transducer that induces adherens junction development.* Nat Cell Biol, 2010. **12**(6): p. 533-42.

23. Liu, Z., et al., *Mechanical tugging force regulates the size of cell-cell junctions.* Proc Natl Acad Sci U S A, 2010. **107**(22): p. 9944-9.
24. Spindler, V., N. Schlegel, and J. Waschke, *Role of GTPases in control of microvascular permeability.* Cardiovasc Res, 2010. **87**(2): p. 243-53.
25. Noria, S., et al., *Assembly and Reorientation of Stress Fibers Drives Morphological Changes to Endothelial Cells Exposed to Shear Stress.* American Journal of Pathology, 2004. **164**(4): p. 1211-1223.
26. Shyy, J.Y.-J. and S. Chien, *Role of Integrins in Endothelial Mechanosensing of Shear Stress.* Circulation Research, 2002. **91**: p. 769-775.
27. Shiu, Y.-T., et al., *Rho Mediates the Shear-Enhancement of Endothelial Cell Migration and Traction Force Generation.* Biophyiscal Journal, 2004. **86**: p. 2558-2565.
28. Fuchs, E. and D.W. Cleveland, *A Structural Scaffolding of Intermediate Filaments in Health and Disease.* Science, 1998. **279**: p. 514.
29. Bray, D., *Cell Movements from molecules to motility*2001: Garland.
30. Helmke, B.P. and P.F. Davies, *The Cytoskeleton Under External Fluid Mechanical Forces: Hemodynamic Forces Acting on the Endothelium.* Annals of Biomedical Engineering, 2002. **30**: p. 284-2296.
31. Tarbell, J.M., S. Weinbaum, and R.D. Kamm, *Cellular Fluid Mechanics and Mechanotransduction.* Annals of Biomedical Engineering, 2005. **33**: p. 1719-1723.
32. Davies, P.F., *Hemodynamic shear stress and the endothelium in cardiovascular pathophysiology.* Nature Clinical Practice Cardiovascular Medicine, 2009. **6**(1): p. 16-26.
33. Albiges-Rizo, C., et al., *Actin machinery and mechanosensitivity in invadopodia, podosomes and focal adhesions.* Journal of Cell Science, 2009. **122**: p. 3037-3049.
34. Mott, R.E. and B.P. Helmke, *Mapping of dynamics of shear stress-induced structural changes in endothelial cells.* Am J Physioll Cell Physiol, 2007. **293**: p. C1616-C1626.
35. Wojciak-Stothard, B. and A.J. Ridley, *Shear stress-induced endothelial cell polarization is mediated by Rho and Rac but not Cdc42 or PI 3-kinases.* The Journal of Cell Biology, 2003. **161**(2): p. 429-439.
36. Li, S., et al., *The role of the dynamics of focal adhesion kinase in the mechanotaxis of endothelial cells.* PNAS, 2002. **99**(6): p. 3546-3551.
37. Ren, X.-D., et al., *Focal adhesion kinase suppresses Rho activity to promote focal adhesion turnover.* Journal of Cell Science, 2000. **113**: p. 3673-3678.
38. Tzima, E., et al., *Activation of integrins in endothelial cells by fluid shear stress mediates Rho-dependent cytoskeletal alignment.* The EMBO Journal, 2001. **20**(17): p. 4639-4647.
39. Tzima, E., et al., *Activation of Rac1 by shear stress in endothelial cells mediates both cytoskeletal reorganization and effects on gene expression.* The EMBO Journal, 2002. **21**(24): p. 6791-6800.
40. Jou, T.S., E.E. Schneeberger, and W.J. Nelson, *Structural and functional regulation of tight junctions by RhoA and Rac1 small GTPases.* J Cell Biol, 1998. **142**(1): p. 101-15.
41. Fabian, L., J. Troscianczuk, and A. Forer, *Calyculin A, an enhancer of myosin, speeds up anaphase chromosome movement.* Cell Chromosome, 2007. **6**: p. 1.
42. Lu, L., et al., *Mechanical properties of actin stress fibers in living cells.* Biophys J, 2008. **95**(12): p. 6060-71.
43. Lemmon, C.A., C.S. Chen, and L.H. Romer, *Cell traction forces direct fibronectin matrix assembly.* Biophys J, 2009. **96**(2): p. 729-38.
44. Barbee, K.A., et al., *Subcellular distribution of shear stress at the surface of flow-aligned and nonaligned endothelial monolayers.* Heart Circ. Physiol., 1994. **268**: p. H1765-H1772.
45. Mammoto, T. and D.E. Ingber, *Mechanical control of tissue and organ development.* Development, 2010. **137**: p. 1407-1420.

46. Jackson, S.P., *Arterial thrombosis--insidious, unpredictable and deadly.* Nat Med, 2011. **17**(11): p. 1423-36.
47. Kroll, M.H., et al., *von Willebrand factor binding to platelet GpIb initiates signals for platelet activation.* J Clin Invest, 1991. **88**(5): p. 1568-73.
48. Reininger, A.J., et al., *Mechanism of platelet adhesion to von Willebrand factor and microparticle formation under high shear stress.* Blood, 2006. **107**(9): p. 3537-45.
49. Savage, B., F. Almus-Jacobs, and Z.M. Ruggeri, *Specific synergy of multiple substrate-receptor interactions in platelet thrombus formation under flow.* Cell, 1998. **94**(5): p. 657-66.
50. Mailhac, A., et al., *Effect of an eccentric severe stenosis on fibrin(ogen) deposition on severely damaged vessel wall in arterial thrombosis. Relative contribution of fibrin(ogen) and platelets.* Circulation, 1994. **90**(2): p. 988-96.
51. Ruggeri, Z.M., et al., *Activation-independent platelet adhesion and aggregation under elevated shear stress.* Blood, 2006. **108**(6): p. 1903-10.
52. Nieswandt, B. and S.P. Watson, *Platelet-collagen interaction: is GPVI the central receptor?* Blood, 2003. **102**(2): p. 449-61.
53. Barg, A., et al., *Soluble plasma-derived von Willebrand factor assembles to a haemostatically active filamentous network.* Thromb Haemost, 2007. **97**(4): p. 514-26.
54. Savage, B., E. Saldivar, and Z.M. Ruggeri, *Initiation of platelet adhesion by arrest onto fibrinogen or translocation on von Willebrand factor.* Cell, 1996. **84**(2): p. 289-97.
55. Mazzucato, M., et al., *Sequential cytoplasmic calcium signals in a 2-stage platelet activation process induced by the glycoprotein Ibalpha mechanoreceptor.* Blood, 2002. **100**(8): p. 2793-800.
56. Kasirer-Friede, A., et al., *Lateral clustering of platelet GP Ib-IX complexes leads to up-regulation of the adhesive function of integrin alpha IIbbeta 3.* J Biol Chem, 2002. **277**(14): p. 11949-56.
57. Kasirer-Friede, A., et al., *Signaling through GP Ib-IX-V activates alpha IIb beta 3 independently of other receptors.* Blood, 2004. **103**(9): p. 3403-11.
58. Siedlecki, C.A., et al., *Shear-dependent changes in the three-dimensional structure of human von Willebrand factor.* Blood, 1996. **88**(8): p. 2939-50.
59. Savage, B., J.J. Sixma, and Z.M. Ruggeri, *Functional self-association of von Willebrand factor during platelet adhesion under flow.* Proc Natl Acad Sci U S A, 2002. **99**(1): p. 425-30.
60. Dayananda, K.M., et al., *von Willebrand factor self-association on platelet GpIbalpha under hydrodynamic shear: effect on shear-induced platelet activation.* Blood, 2010. **116**(19): p. 3990-8.
61. Szanto, T., et al., *New insights into von Willebrand disease and platelet function.* Semin Thromb Hemost, 2012. **38**(1): p. 55-63.
62. Feng, S., et al., *Pathological shear stress directly regulates platelet alphaIIbbeta3 signaling.* Am J Physiol Cell Physiol, 2006. **291**(6): p. C1346-54.
63. Doggett, T.A., et al., *Selectin-like kinetics and biomechanics promote rapid platelet adhesion in flow: the GPIb(alpha)-vWF tether bond.* Biophys J, 2002. **83**(1): p. 194-205.
64. Lam, W.A., et al., *Mechanics and contraction dynamics of single platelets and implications for clot stiffening.* Nat Mater, 2011. **10**(1): p. 61-6.
65. Chantarangkul, V., et al., *Assessment of the influence of citrate concentration on the International Normalized Ratio (INR) determined with twelve reagent-instrument combinations.* Thromb Haemost, 1998. **80**(2): p. 258-62.
66. Franke, R.P., et al., *Induction of human vascular endothelial stress fibers by fluid shear stress.* Nature, 1984. **307**: p. 648-649.

67. Hewett, P.W., *Vascular Endothelial Cells from Human Micro- and Macrovessels: Isolation, Characterisation and Culture*, in *Methods in Molecular Biology, Angiogenesis Protocols*, S. Martin and C. Murray, Editors. 2009, Humana Press. p. 95-111.
68. Alevriadou, B.R., et al., *Real-time analysis of shear-dependent thrombus formation and its blockade by inhibitors of von Willebrand factor binding to platelets.* Blood, 1993. **81**(5): p. 1263-76.
69. Kamiya, A. and T. Togawa, *Adaptive regulation of wall shear stress to flow change in the canine carotid artery.* Am J Physiol., 1980. **239**: p. H14-21.
70. Davies, P.F., J. Zilberberg, and B.P. Helmke, *Spatial Microstimuli in Endothelial Mechanosignaling.* Circulation Research, 2003. **92**: p. 359-370.
71. Helmke, B.P., *Molecular Control of Cytoskeletal Mechanics by Hemodynamic Forces.* Physiology, 2005. **20**: p. 43-53.
72. Lee, J.S.H., et al., *Ballistic intracellular nanorheology reveals ROCK-hard cytoplasmic stiffening response to fluid flow.* Journal of Cell Science, 2006. **119**: p. 1760-1768.
73. Reneman, R.S., T. Arts, and A.P.G. Hoeks, *Wall Shear Stress - an Important Determinant of Endothelial Cell Function and Structure - in the Arterial System in vivo.* Journal of Vascular Research, 2006. **43**: p. 251-269.
74. Malek, A.M., S.L. Alper, and S. Izumo, *Hemodynammic Shear Stress and its Role in Atherosclerosis.* JAMA, 1999. **282**: p. 2035-2042.
75. Wallace, C.S., J.C. Champion, and G.A. Truskey, *Adhesion and Function of Human Endothelial Cells Co-cultured on Smooth Muscle Cells.* Annals of Biomedical Engineering, 2007. **35**(3): p. 375-386.
76. Sniadecki, N.J. and C.S. Chen, *Microfbricated Silicone Elastomeric Post Arrays for Measuring Traction Forces of Adherent Cells.* Methods in Cell Biology, 2007. **83**.
77. Hong, D., et al., *Heterogeneous response of microvascular endothelial cells to shear stress.* Am J Physiol Heart Circ Physiol, 2006. **290**: p. H2498-H2508.
78. del Alamo, J.C., et al., *Anisotropic rheology and directional mechanotransduction in vascular endothelial cells.* PNAS, 2008. **105**(40): p. 15411-15416.
79. Helmke, B.P., A.B. Rosen, and P.F. Davies, *Mapping Mechanical Strain of an Endogenous Cytoskeletal Network in Living Endothelial Cells.* Biophysical Journal, 2003. **84**: p. 2691-2699.
80. Garcia-Cardena, G., et al., *Biomechanical activation of vascular endothelium as a determinant of its functional phenotype.* PNAS, 2001. **98**(8): p. 4478-4485.
81. Yoshigi, M., E.B. Clark, and J.H. Yost, *Quantification of Stretch-Induced Cytoskeletal Remodeling in Vascular Endothelial Cells by Image Processing.* Cytometry Part A, 2003. **55**: p. 109-118.
82. Martin, J.F., et al., *The causal role of megakaryocyte-platelet hyperactivity in acute coronary syndromes.* Nat Rev Cardiol, 2012. **9**(11): p. 658-70.
83. Zar, J.H., *Biostatistical analysis*. 4th ed1999, Upper Saddle River, N.J.: Prentice Hall.
84. Dejana, E., *Endothelial cell-cell junctions: happy together.* Nat Rev Mol Cell Biol, 2004. **5**(4): p. 261-70.
85. Noria, S., et al., *Transient and steady-state effects of shear stress on endothelial cell adherens junctions.* Circ Res, 1999. **85**(6): p. 504-14.
86. Yao, Y., A. Rabodzey, and C.F. Dewey, Jr., *Glycocalyx modulates the motility and proliferative response of vascular endothelium to fluid shear stress.* Am J Physiol Heart Circ Physiol, 2007. **293**(2): p. H1023-30.
87. Rubenstein, D.A. and W. Yin, *Quantifying the effects of shear stress and shear exposure duration regulation on flow induced platelet activation and aggregation.* J Thromb Thrombolysis, 2010. **30**(1): p. 36-45.

88. Johnson, G.J., et al., *Measurement of shear-activated platelet aggregate formation in non-anticoagulated blood: utility in detection of clopidogrel-aspirin-induced platelet dysfunction.* Clin Appl Thromb Hemost, 2012. **18**(2): p. 140-9.
89. Li, M., D.N. Ku, and C.R. Forest, *Microfluidic system for simultaneous optical measurement of platelet aggregation at multiple shear rates in whole blood.* Lab Chip, 2012. **12**(7): p. 1355-62.